National Library of Canada
Acquisitions and Bibliographic Services Branch
395 Wellington Street
Ottawa, Ontario
K1A 0N4

Bibliothèque nationale du Canada
Direction des acquisitions et des services bibliographiques
395, rue Wellington
Ottawa (Ontario)
K1A 0N4

Your file Votre référence

Our file Notre référence

NOTICE

The quality of this microform is heavily dependent upon the quality of the original thesis submitted for microfilming. Every effort has been made to ensure the highest quality of reproduction possible.

If pages are missing, contact the university which granted the degree.

Some pages may have indistinct print especially if the original pages were typed with a poor typewriter ribbon or if the university sent us an inferior photocopy.

AVIS

La qualité de cette microforme dépend grandement de la qualité de la thèse soumise au microfilmage. Nous avons tout fait pour assurer une qualité supérieure de reproduction.

S'il manque des pages, veuillez communiquer avec l'université qui a conféré le grade.

La qualité d'impression de certaines pages peut laisser à désirer, surtout si les pages originales ont été dactylographiées à l'aide d'un ruban usé ou si l'université nous a fait parvenir une photocopie de qualité inférieure.

Canada

ESTIMATION AND CONTROL OF PART WEIGHT AND RELEVANT PROCESS PARAMETERS IN INJECTION MOLDING OF AMORPHOUS THERMOPLASTICS

Alfredo E. Varela

Department of Chemical Engineering
McGill University
Montreal, Canada

March 1996

A thesis submitted to the Faculty of
Graduate Studies and Research
in partial fulfilment of the requirements for the degree of
Doctor of Philosophy

ISBN 0-612-12504-1

ABSTRACT

Injection molding is a cyclic process used for the fabrication of thermosetting and thermoplastic articles. The thermoplastic polymer is melted and injected into the cavity, where it is molded under pressure and ejected after solidification. The amount of polymer mass contained in the cavity is the part weight. The control of part weight is important to ensure quality injection molded parts. The part weight is determined by the state of the polymer at the time the cavity gate freezes. The bulk temperature and the peak cavity pressure at the gate are used to characterize this state.

Measuring internal polymer temperature profiles in the injection mold cavity during molding is extremely difficult. This work presents a method which combines measurements of cavity surface temperatures, cavity pressure, and on-line calculations for estimating temperature profiles inside the cavity. These profiles are then used to estimate the bulk polymer temperature. Fitting the cycle-to-cycle values of bulk polymer temperature and peak pressure to a Tait equation of state yields a model to predict part weights.

The part weight is controlled through the use of a control strategy for the cavity pressure and the part weight model, together with the on-line estimation of the bulk temperature. A self-tuning algorithm with an observer is employed for controlling the cavity pressure time profile to a set point trajectory. The dynamics and control of the bulk temperature are also studied.

RÉSUMÉ

Le moulage par injection est un procédé cyclique utilisé pour la fabrication d'articles thermodurcisseurs et thermoplastiques. Le polymère du thermoplastique est fondu et injecté dans une cavité, où il est ensuite moulé sous pression et éjecté après solidification. La quantité de polymère contenu dans la cavité fixe le poids de la partie. La régulation du poids de la partie est important afin d'assurer la qualité des parties moulées par injection. Le poids de la partie est déterminé par l'état du polymère au temps ou la barrière de la cavité gèle. La température d`ensemble du polymère et la pression maximum de la cavité à la barrière sont utilisées pour caractériser cet état.

La mesure de profils de température du polymère dans la cavité d`injection pendant le moulage est extrêmement difficile. Ce travail présente une méthode qui combine les mesure de températures de surface de la cavité, la pression de la cavité et des calculs en temps reél pour faire l`estimation des profils de température à l'intérieur dans la cavité. Ces profils sont ensuite utilisés pour faire l`estimation de la température d`ensemble du polymère. En adaptant les températures d`ensemble du polymère et les pressions maximum de la cavité de cycle à cycle à une équation d`état Tait produit un modèle pour prédire le poids des parties.

Le poids de la partie est réglé à l`aide une stratégie de contrôle de pression et du modèle de prédiction du pois de la partie combinée avec l'estimation en temps réel de la température d`ensemble du polymère. Un algorithme auto-réglant avec un observateur est utilisé pour ajuster le profil temporel de la pression de cavité à une trajectoire précise. Les variations et le contrôle de la température d`ensemble du polymère sont aussi étudiés.

ACKNOWLEDGEMENTS

This adventure, which involved considerable responsibility for me and my family, would not have been accomplished without the confidence and moral support of my colleagues in Venezuela and friends at McGill University.

I am grateful to my advisors: Dr. Musa R. Kamal and Dr. W. Ian Patterson, for their effort in expending many hours of guidance and productive discussion. From these were born the ideas which helped to overcome many difficulties and complete this research.

I have to acknowledge the invaluable contribution of the personnel in the Electronics Shop, Machine Shop, and Department Storeroom in the Department of Chemical Engineering. I would like to thank Mr. Luciano Cusmich, Mr. Walter Greenland, Mr. Alain Gagnon, Mr. Charles Dolan, and Mr. Jean Dumont, who were always very helpful in difficult moments.

I wish to thank Dr. Mark Weber for his cooperation in proof reading this manuscript and help in the operation of the injection molding machine at the early stages of this work, and to the members of our research group: Dr. Furong Gao, Mehdi Rafizadeh, and Federico Manero, for the productive discussion about injection molding. The encouragement and advice of Dr. Juan H. Vera and Dr. Zhenghe Xu are also appreciated. I should recognize the amicable and professional help of three persons: Imad Ansari, Kenneth Rivkin, and Charles Abrams.

I gratefully acknowledge the financial support of Fundación Gran Mariscal de Ayacucho (FUNDAYACUCHO) through my scholar advisor Peter O'Meara. The completion of the Ph. D. program was possible with the financial support of Universidad de Carabobo, in Venezuela. The rector, Ricardo Maldonado and vice-rectors Asdrúbal Romero and José Botello, put their faith in me in spite of the fiscal circumstances.

This research was supported by McGill University, the Natural Sciences and Engineering Research Council of Canada (NSERC), and the Fonds pour la Formation de Chercheurs et l'Aide à la Recherche (FCAR), Gouverment du Quebec. Dow Chemical Canada supplied the polystyrene resin used in the experiments.

I am indebted to my colleagues of the Department of Chemical Engineering at Universidad de Carabobo for giving me the opportunity to pursue my Ph.D. degree.

To conclude, I would like to acknowledge the moral support of my wife, Trina, and my children: Isabel and Javier, who have borne with me and shared my anguish and uncertainties during my absence from them.

TABLE OF CONTENTS

LIST OF FIGURES

LIST OF TABLES

LIST OF SYMBOLS

Symbol	Definition
C_p	specific heat, Kcal/(Kg °C)
a	cavity centre temperature difference, °C
a_i	parameters in the Tait equation of state, i = 0, 1, 2
$A(z^{-1})$	system numerator polynomial. See Eq. 5.15
A_o	observer polynomial
$B(z^{-1})$	system denominator polynomial. See Eq. 5.15
B	Biot number, $= h y_b / k$
c	parameter of the initial parabolic profile F(y)
c_i	coefficients of the polynomial approximation for λ_n (Eq. 4.8), i=0, 1, 2
d^t	directional vector in parameter estimation algorithm, See Eq.. 4.15
d_i	parameters in the Tait equation of state, i = 0, 1, 2
$F(y)$	parabolic profile at t_{gf}. See Eq.. 4.5
h	heat transfer coefficient from polymer melt to coolant, Kcal/(m^2 °C s)
J	objective function for least squares parameter estimation, °C^2.
k	heat conductivity of polymer melt, kcal/(m s), Eq.. 4.4
k	discrete time index
$K(k)$	gain, see Eq.. 5.21
M	number of measurements at cavity surface from the end of packing
p	cavity pressure, MPa
P	covariance matrix
q	proportionality factor between servo-valve openings. See Eq.. 5.42
$r(t)$	set-point trajectory, MPa
R	slope of the cavity curve during the filling stage, MPa/s
t	time, s
t_{fill}	time at which the polymer stops flowing into the cavity, s
t_{gf}	time at which the gate freezes, s
t_m	time at the measurement m, s
T	polymer melt temperature difference, $= T^* - T_c$
T^*	polymer melt temperature, °C
T_a^*	average cavity polymer temperature, °C, Eq.. 4.12
T_{ai}	average cavity polymer temperature at location i, °C, Eq.. 4.10
T_c	inlet coolant temperature, °C
T_s	cavity surface temperature difference, °C
T_{sw}	period of the square-wave pulse trains, s
u	control signal (supply servo valve opening), %
u_c	opening of the cold-water valve, %
u_r	return servo valve opening, %
u_t	opening of the hot-water valve, control variable, %

u_2	control variable for the cavity polymer control system, Eq.. 6.10, °C
$v(t)$	control signal, %. See Eq.. 5.33
V_c	cavity volume, cm^3
V_m	voltage transmitted by pressure transducer, mV
y	coordinate perpendicular to the large cavity surface, cm.
y_s	half cavity thickness, cm
y_1	dimensionless coolant temperature, Eq.. 6.1
y_2	bulk temperature, Eq.. 6.8, °C
Y	measured polymer-melt surface temperature difference, °C.
W	part weight, g
z	unit forward shift operator; *z-transform argument*

Greek Symbols

Symbol	Definition
α	heat diffusivity of polymer melt, m^2/s
Δt	sampling interval, s
θ	parameter vector, Eq. 5.20
λ	forgetting factor
λ_n	roots of the transcendental equations. See 4.7
μ	a scalar in the parameter estimation algorithm, μ = 1, 1/4, 1/8, ..(See Eq. 4.15)
v	bulk specific volume, cm^3/g.
v_o	bulk specific volume at atmospheric pressure, cm^3/gr
ρ	density of the polymer melt, g/cm^3.
τ	time constant, s
τ_{sp}	time constant for the set-point trajectory, s. See Eq. 5.42
φ	vector of input and output measurements.

ABBREVIATIONS

Symbol	Description
FPE	final prediction error criterion
PI	proportional-integral
PID	proportional-integral-derivative
RSV	return servo-valve
SSV	supply servo-valve
STC	self-tuning control
STCO-SP	self-tuning control with observer starting a predefined screw position
V_N	prediction error criterion

CHAPTER 1

INTRODUCTION

Injection molding is a cyclic process used for the fabrication of both thermoplastic and thermosetting polymer articles. To produce injection molded thermoplastic products, the granular polymer or resin is softened by heating and shearing, formed under pressure in a closed mold, and solidified by cooling. After solidification, the mold opens and releases the product. An injection molding cycle includes four stages: filling, packing, holding, and cooling. Typically, one cycle takes about 10 to 30 seconds. The packing and holding stages allow additional material to flow into the cavity until the gate seals. This compensates for the natural volume reduction during the cooling stage due to shrinkage. When the molten polymer is forced into the cavity, the pressure increases rapidly, in one or two seconds, to a maximum or peak pressure at the end of packing which may range from 20 to 100 MPa.

Automobile parts, electrical appliances, and medical equipment are some of the great variety of products that are manufactured using the injection molding process. For more than 25 years, researchers in the Department of Chemical Engineering at McGill University have conducted research on the modeling and control of injection molding.

1.1 SUBJECT

The present study considers the estimation and control of the bulk polymer temperature in the injection mold cavity, the cavity gate pressure-

time profile, and part weight of amorphous thermoplastics. For simplicity, the first two variables are called the bulk temperature and cavity pressure profile, respectively.

Thermoplastic polymers are classified into semi-crystalline and amorphous materials. Semi-crystalline polymers exhibit abrupt changes in specific volume in the melting region, while amorphous polymers show a transition between a glassy and a rubber-like state at the glass transition temperature. Volume changes at the glass transition temperature are not as abrupt and severe as those observed during melting.

Cycle-to-cycle variations in product properties may occur due to several factors. Disturbances in machine variables cause alterations in the injection temperature, nozzle pressure, and mold temperature. Changes in the filling rate and temperature profile affect the part weight, and induce variations in the molecular orientation developed by amorphous polymers during the filling stage (Dietz et al., 1978). The orientation of chain molecules in the layers close to the cavity wall is high with respect to that of the core (Janeschitz-Kriegl, 1977). Once the gate is frozen, flow into the cavity stops and a relaxation process, which affects orientation and other physical properties (e.g., tensile strength, resilience), starts during the cooling stage.

1.2 IMPORTANCE OF THE SUBJECT

Final properties of the molded article may not be technically acceptable. Defects, weak points, and changes in optical properties may occur in the direction of chain orientation. Therefore, controlling process

variables during the filling and packing stages is necessary to obtain products with specified characteristics.

The importance of controlling material properties within the injection molding cavity has been discussed by Agrawal et al. (1987). Cycle-to-cycle consistency in material properties is an indicator of the success of the injection molding operation in maintaining part quality. Thus, it is desirable to control product properties such as part dimensions and shape, degree of molecular orientation, and residual stress distribution, but this task is difficult as no appropriate sensors are available. The variables selected to be controlled in the present research are: the bulk temperature at the moment the gate freezes, cavity pressure profiles during filling and packing, and part weight.

1.3 OBJECTIVES

The present research is a continuation of the previous work on control of the injection molding process at McGill University. Examples of studies made during the past ten years include: control of the nozzle melt temperature using a thermocouple installed at the screw tip (Patterson et al., 1985); time scheduling control of the hydraulic, nozzle and cavity pressure (Kamal et al., 1987, and Abu Fara, 1988); modeling and control of the mold temperature (Gao, 1989); control of the nozzle melt temperature using an immersed thermocouple (Ruscitti, 1992); and self-tuning control of the cavity pressure profile (Gao, 1993).

The objectives of the present work are:

(1) To develop a method to estimate the bulk temperature in the injection mold cavity, at the moment the gate seals, from pressure and temperature measurements at the cavity surface.
(2) To develop a mathematical model for estimating the part weight based on the bulk temperature and pressure at the moment the gate seals.
(3) To design and implement a strategy for cavity pressure control during the filling and packing stages.
(4) To design and implement a strategy for the control of the bulk temperature and part weight.

1.4 THESIS OUTLINE

Chapter 2 of this thesis gives a brief literature review of the general aspects of the injection molding process, and of the previous work in the control of the melt nozzle temperature, cavity pressure profile, polymer temperature distribution in the cavity, and part weight.

In Chapter 3, the equipment and software used for the control experiments and data acquisition are described. In Chapter 4, an approach for estimating the bulk temperature from measurements at the cavity surface is discussed. The proposed estimation method uses a heat conduction model with a parametric estimation algorithm. The results are used to fit the injection molding data to the Tait equation of state.

Chapter 5 deals with the control of the cavity pressure profile during filling and packing, using the self-tuning algorithm with a recursive on-line identification algorithm for the determination of parameters of a time-varying model.

Chapter 6 presents a cascade control strategy for the bulk temperature. A dynamic relationship between this temperature and the coolant temperature is determined using the step-changes procedure. Chapter 7 contains a discussion of the different control strategies for the part weight. Also, the results of two indirect control strategies are given. Finally, Chapter 8 presents the main conclusions of the present research, suggestions for further research, and claims of original contributions.

CHAPTER 2

LITERATURE REVIEW

This chapter deals with the main features of the injection molding process and the strategies used to control the cavity pressure, melt temperature, and product quality. Considerable research in testing new sensors, prediction of melt properties, and in modeling and control has been carried out at McGill University.

2.1 INJECTION MOLDING PROCESS

A brief description of the process, and the bases for process modeling and control are summarized in the following sections.

2.1.1 General Aspects

Several broad reviews are available concerning the different kinds of equipment used in the injection molding process (Berins, 1992; Whelan, 1984; and Rosato, 1982). Figure 2.1 shows a schematic representation of a reciprocating screw injection molding machine similar to the type of machine used in this study. The major components are the injection unit and the clamping unit. The injection unit includes the hydraulic system, a hopper, and the extruder, which is made up of the barrel and the injection screw. A granulated polymer, fed through the hopper, is melted by heating and shearing, and then pushed by the translating screw into the clamping unit where the molding operation takes place.

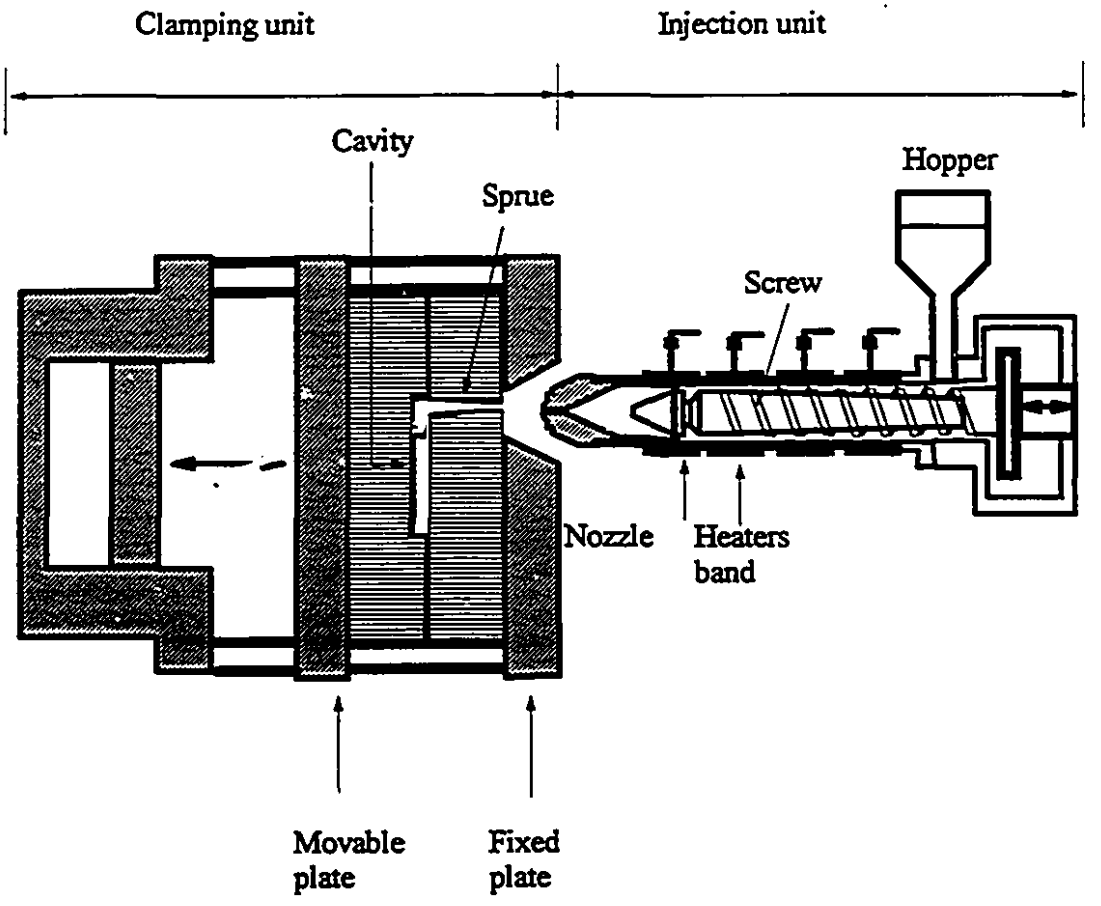

Figure 2.1 Schematic illustration of a reciprocating screw injection molding machine.

Three zones are usually identified in an injection screw: a feed section, a transition section, and a metering section. As the screw rotates, the feed section propels the granulated polymer from the hopper to the compression section. Here, the polymer mass is melted by the heat transferred from barrel heaters and the heat generated due to viscous dissipation. The viscous heating occurs because of the friction generated between the polymer melt and the internal walls of the barrel. The molten polymer continues moving through the transition and metering sections where it is mixed and passes to the front of the screw or the nozzle zone of the barrel. In some screw designs, a check-valve prevents the melt from leaking back down the screw. The screw rotation continues until it reaches a movable limit switch, set at a predefined position, so that a certain mass of the polymer is accumulated in the nozzle. This stage of the process is called the plasticating stage.

Once a sufficient volume of polymer melt is in the nozzle, the injection stage is initiated by closing the mold and moving the barrel forward until the nozzle is connected with the sprue entrance. Hydraulic pressure moves the screw forward, which in turn injects the polymer melt into the cavity through the sprue and runner. Because the temperature of the mold is lower than the polymer melt temperature, the molten polymer starts to solidify immediately on contact with the cavity walls. In the injection stage, the process is governed by flow, solidification, and compression, which determine the melt pressure response in time.

Variations in nozzle pressure and cavity pressure at the gate with time, for the injection molding of polystyrene, are shown in Figure 2.2. Three phases are defined in the injection stage: filling, packing, and holding. After the holding phase, the hydraulic pressure is released to allow the screw to retract for the plasticating stage of the next cycle. Then, the cooling stage

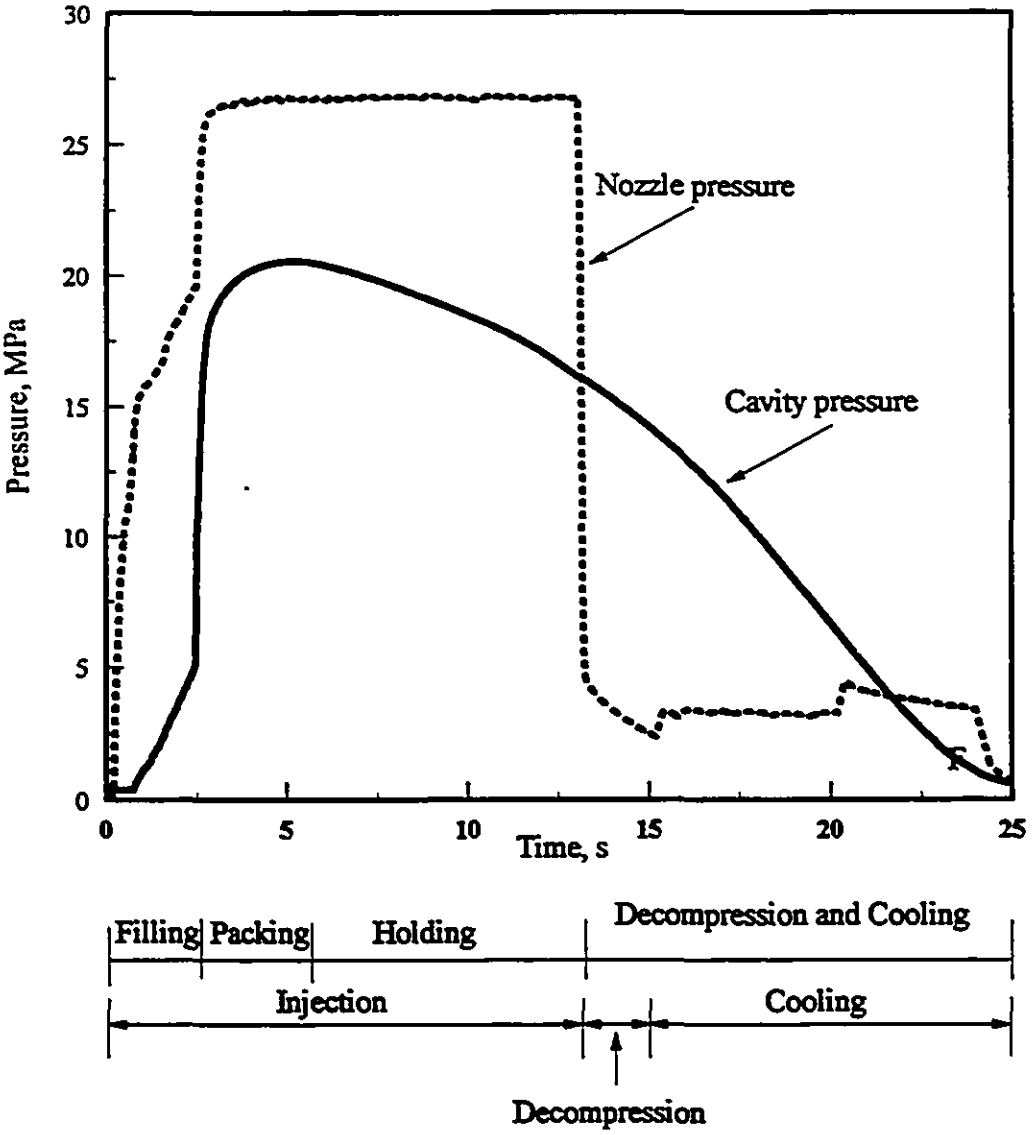

Figure 2.2 Nozzle and cavity pressure profiles showing the cycle stages (Poystyrene 685D from Dow Chemical).

starts when the polymer has filled the cavity, and is continued until the material in the cavity and delivery system has solidified. Finally, the mold is opened and the molded part is ejected.

2.1.2 Material Properties

The melt viscosity is highly dependent on temperature, and changes drastically from the nozzle to the cavity where the temperature decreases close to the glass-transition temperature, T_g, at the end of packing. The melt temperature at the nozzle is approximately 100 °C above T_g. This difference produces a large increase in polymer viscosity in the sprue and in the cavity. As the temperature of the polymer approaches T_g, the viscosity increases rapidly to a value of about 10^{12} Pa.s (Cowie, 1991). Several empirical models have been proposed for the variation of the viscosity of amorphous polymers with temperature. The viscosity can be estimated using the WLF equation (Cowie, 1991) given by

$$\ln\frac{\eta(T)}{\eta_o(T_s)} = \frac{-8.86\,(T-T_s)}{101.6+(T-T_s)} \tag{2.1}$$

where T_s is an arbitrary reference temperature, usually $T_s = T_g + 50$, and $\eta_T(T)$ and $\eta_s(T_s)$ are the zero shear viscosities at temperatures T and T_s, respectively.

The PVT behavior of amorphous polymers can be modeled by the Tait equation of state (Zoller, 1989) which is given by

$$v(T,p) = v_o(T)\left[1 - C\ln\left(1+\frac{p}{D(T)}\right)\right] \tag{2.2}$$

where C=0.0894 is a universal constant, $v_o(T)$ denotes the specific volume at

atmospheric pressure, and $D(T)$, or the Tait function, characterizes the pressure sensitivity of $v(T,P)$. Usually, $v_o(T)$ and $D(T)$ are expressed as

$$\begin{aligned} v_o(T) &= a_o + a_1 T + a_2 T^2 \\ D(T) &= D_o \exp(-D_1 T) \end{aligned} \tag{2.3}$$

The Tait equation can be used to describe both the melt and solid regions for amorphous polystyrene.

Figure 2.3 illustrates the approximate changes in specific volume from the nozzle to the cavity in a PVT diagram constructed using the data for polystyrene reported by Quach and Simha (1971). The state changes are the following: (1) A-B: melt compression at the nozzle, (2) B-C: filling of the sprue and runner, (3) C-D: filling and packing, (4) D-E: holding, and (5) E-F: decompression and cooling. During the injection phase, the melt cushion is almost adiabatically compressed at the nozzle, and the melt temperature increases due to viscous heating (Langecker, 1992). The melt temperature in the cavity drops due to heat exchange between the melt and the cold mold walls.

2.1.3 Process Control

The large number of variables in the injection molding process can be divided into three categories:

(1) Machine parameters which include: cycle time (filling, packing, holding, and cooling times, and clamp opening, clamp closing, and clamp open time), barrel temperatures, coolant temperature, average hold hydraulic pressure, average back pressure, shot size distance, screw rotational speed and ram velocity.

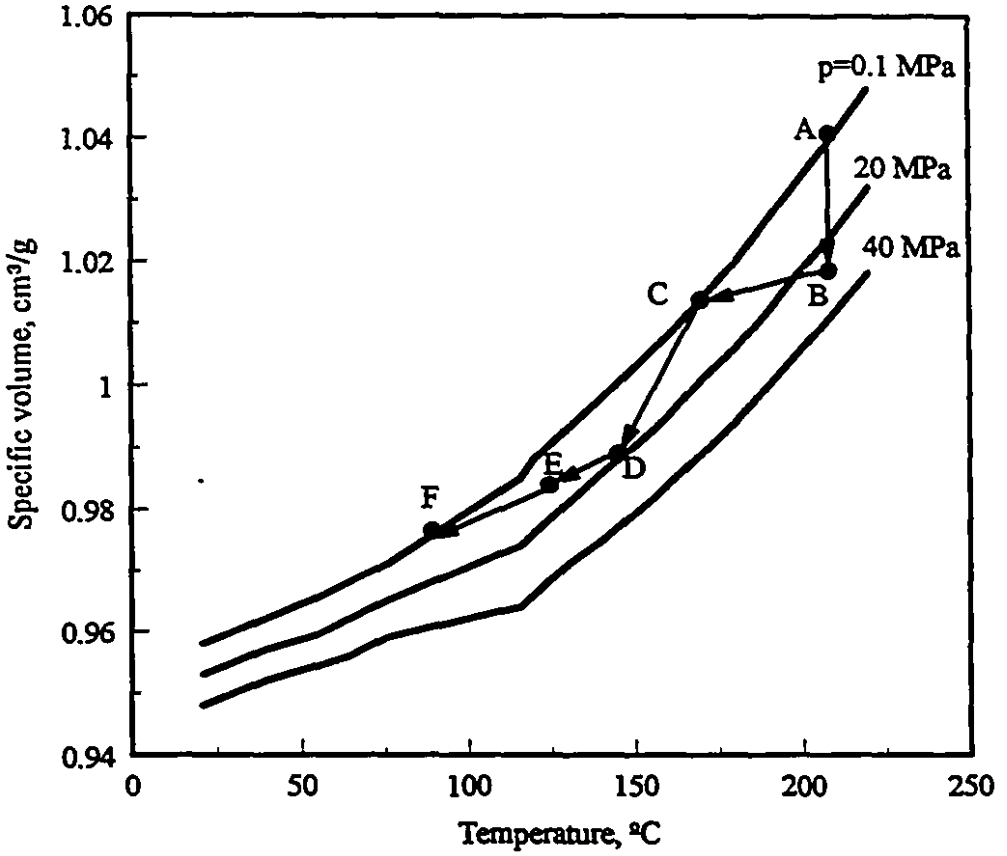

Figure 2.3 PVT diagram for polystyrene showing the approximate changes in specific volumes in the nozzle (A -C) and in the cavity (C-F).

(2) Process variables, e.g., material properties (fillers, regrind, reinforcements), nozzle melt temperature, melt viscosity, nozzle melt pressure, and cavity pressure time profile.

(3) Product properties, e.g., part weight and part dimensions which are usually employed for quality control since it is difficult to measure other properties on-line.

The major goal in the injection molding operation is to maintain product quality from cycle to cycle. Changes in environmental conditions, material contaminants and humidity, machine variations, and fluctuations in properties of the melt injected into the cavity are factors which can cause changes in the injection molding variables, and consequently in product quality. Therefore, it is important to control or compensate some of these variables. Most proposed strategies are intended for control of process variables such as cavity pressure, nozzle melt pressure, and nozzle melt temperature, and machine variables like ram velocity, barrel temperatures, and coolant temperature. An important machine parameter is the ram velocity. According to Turng et al. (1995), control of the ram velocity profile can be used to reduce the maximum injection pressure, maintain a constant velocity at the melt front, and reduce warpage. Strategies for ram velocity control have been evaluated using simulations (Pandelidis and Agrawal, 1988, and Agrawal and Pandelidis, 1988).

The success of a control strategy depends on the sensors, final control elements, and model accuracies. Measuring melt pressure is difficult, but indirect measurements obtained using piezoelectric pressure transducers are suitable (Langecker, 1992). No adequate sensors or techniques are available for the direct measurement of melt temperatures or product properties.

Different models have been proposed to control variations in process variables and product properties. Empirical modeling provides the transfer functions required for the controller design. The dynamic of most processes in injection molding can be described using a transfer function, $G(s)$, which can be expressed as

$$G(s) = \frac{Y(s)}{U(s)} = K\frac{(1+\kappa_1 s)(1+\kappa_2 s)\ldots}{(1+\tau_1 s)(1+\tau_2 s)\ldots} \tag{2.4}$$

where K is the steady state gain, and κ_i and τ_i are time-constants. However, the data used to find the parameters in Equation 2.4 are obtained at a finite sampling time. Therefore, the model is also written in discrete-time domains as

$$\left[1 + a_1 z^{-1} + \ldots + a_{n_a} z^{-n_a}\right] y(k) = \left[b_1 z^{-1} + \ldots + b_{n_b} z^{-n_b}\right] u(k) \tag{2.5}$$

where z is the unit forward shift operator, and $u(k)$ and $y(k)$ are the input and output sequences, respectively.

The following review considers some strategies that have reported experimental data of the control of cavity pressure, melt temperature, part weight, and PVT control. For the different control strategies used in injection molding, the reader is referred to the review article of Agrawal et al. (1987).

2.2 CAVITY PRESSURE CONTROL

As the melt fills the cavity, the flow resistance increases with time; as a result, the cavity pressure rises. At the end of filling when the resistance is

higher, the pressure rises rapidly and reaches a maximum or peak pressure. The sensitivity of the part weight to the peak pressure has been experimentally demonstrated (Sanschagrin, 1983; Harry, 1991). In open-loop operation, the peak pressure is preset using a fixed unloading valve. Cavity pressure control is desirable because the factors mentioned above may introduce variations in the required peak pressure. For example, the melt temperature may change due to inefficient band heaters.

Cavity pressure is controlled by a servo-valve which manipulates the hydraulic pressure applied to the screw. The cavity pressure is measured using a sensor installed flush with the cavity surface near the gate, where rapid variations in pressure can be sensed. The detection of the transition from filling to packing allows the use of different control strategies for each stage. When the cavity pressure reaches a set value, the nozzle pressure is dropped to the dwell or holding pressure for the reminder of the injection time.

Sanschagrin (1983) and Haber and Kamal (1987) have proposed time series models for the cycle-to-cycle dynamics and control of the peak cavity pressure. Control strategies for the hydraulic, nozzle, and cavity pressure-time profiles were proposed initially by Kamal et al. (1987). The dynamic response of the cavity pressure to variations in servo-valve opening (manipulated variable) during filling was modeled as

$$p(t) = K_1 t + K_2\left(1 - e^{-(t-\tau_d)/\tau_p}\right) \tag{2.6}$$

where p is the cavity pressure, K_1 and K_2 are the process gains, and D is the dead time. With a zero-order hold, the discrete transfer function is given as

$$\frac{p(z)}{u(z)} = \frac{b_1 + b_2 z^{-1} + b_3 z^{-2}}{1 + a_1 z^{-1} + a_2 z^{-2}} z^{-k_d} \tag{2.7}$$

where $k_d = \tau_d / \Delta t$, and Δt = sampling interval. For the packing stage, a first-order model was suggested

$$G_p(z) = \frac{p(z)}{u(z)} = \frac{b_1 z^{-1}}{1 + a_1 z^{-1}} z^{-k_d} \tag{2.8}$$

Parameter values found using input-output experiments varied with the degree of filling, so it was concluded that the gain scheduling can achieve stable performance. PI and PID control strategies gave similar experimental results. The results suggest that the controller parameters are related to the material and operational conditions.

To avoid the need for controller tuning, Gao (1993) implemented a self-tuning algorithm (Åström and Wittenmark, 1990). The dynamic relation between the cavity pressure and the opening of the hydraulic servo-valve was defined in discrete-time domains as

$$G_p(z) = \frac{p(z)}{u(z)} = \frac{b_1 z^{-1} + b_2 z^{-2}}{1 + a_1 z^{-1} + a_2 z^{-2}} z^{-k_d} \tag{2.9}$$

where a_i and b_i are parameters, which are estimated by a recursive identification algorithm. Figure 2.4a shows a block diagram of the self-tuning control strategy.

An alternative approach to control the cavity pressure during packing was proposed by Smud et al. (1991). In this approach, the control is carried out using a variable-volume cavity that relies on the manipulation of clamping force. The clamp pressure is regulated through manipulation of the hydraulic pressure line. A cascade control strategy is proposed for machines that do not have clamping force regulation. Figure 2.4b shows a block diagram of this control strategy. The process response data were modeled with a first-order plus dead-time transfer function (see Equation 2.8). Step tests were used to the find model parameters. In the identification process, the time constant varied with the time of application of the step change in clamp force. This control strategy was tested using a PI controller, and the experiments showed a reduction in variations of part thickness. However, no experimental results were reported on the regulation of the cavity pressure profile.

2.3 MELT TEMPERATURE MEASUREMENT AND CONTROL

Nozzle-melt temperature variations significantly affect important variables in the injection molding process. One immediate effect is observed in the viscosity of liquid polymer entering the cavity. Variations in melt temperature also influence the peak pressure, part weight, and part dimensions (Sanschagrin, 1983). Indirect control of the melt temperature is conducted using a closed-control system for the barrel temperature. The melt temperature at the nozzle is different from the barrel temperature (Whelan, 1984).

The temperature profile across any section of the cavity is not uniform due to several factors: (1) laminar flow of the melt prevents convective

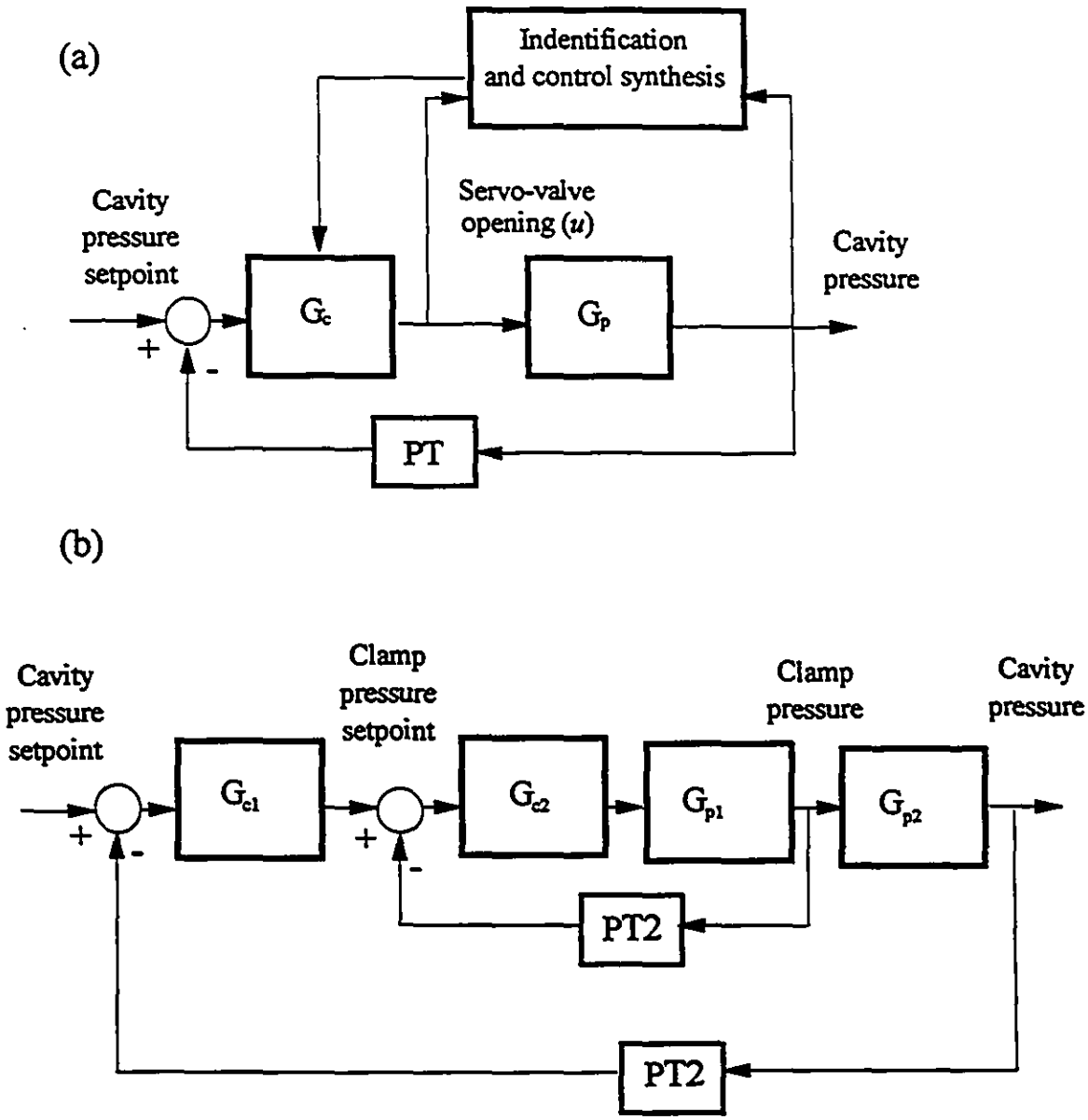

Figure 2.4 Cavity pressure control using: (a) Self-tuning control with servo-valve opening as manipulated variable. (b) Cascade control with clamp force as manipulated variable. PT = pressure transducer, G_c = controller transfer function, G_p = process transfer function.

homogenization, (2) viscous dissipation causes localized heating in high shear rate regions, and (3) the low thermal conductivity of polymers retards the development of uniform temperature profiles. The studies in control of the cavity melt temperature are still in the development stage because no adequate sensors are available. A summary of sensor characteristics for temperature control is given below.

2.3.1 Temperature Sensors

According to McGee (1988), temperature sensors for process control should meet the following requirements:

(1) Unambiguous response with temperature, T. If X, the property being measured (e.g., change in electrical resistance, electromotive force, thermal radiation), depends on T, the response should be as shown in Figure 2.5.

(2). High sensitivity to all temperatures over the desired range. The property being sensed must vary with T enough to be measured with sufficient accuracy (see Figure 2.5). Linear sensitivity is desirable.

(3) Stability. Obtaining reproducible and reliable temperature values over the desired range is very important.

(4) The thermal mass of the sensor should be sufficiently small so that the heat transfer to the sensor is negligible.

(5) Wide range, good mechanical and thermal stability, low cost and fast response. To measure cavity-melt temperatures, the time constant must be in the order of milliseconds.

Temperature sensors have been classified into two categories: immersion and nonimmersion sensors (Leigh, 1988) Immersion sensors include the following devices:

(1) Bimetallic and liquid-filled gauges. These sensors are based on either the thermal expansion of two different metals, or an enclosed liquid. Both kinds are impractical for polymer processing because of slow responses and viscous heating effects.

(2) Resistance temperature detectors (RTD). These consist of thin films of metal deposited on an insulating substrate. The electrical resistance of the metal changes with the temperature. These sensors are not appropriate for high temperatures.

(3) Thermocouples. Two types of thermocouple junctions can be used: grounded or exposed. In the first type, the joint is welded to the metal sheath to improve the speed of response, The reading will be affected by the metal temperature; therefore, exposed junctions are most appropriate for the measurements of melt temperatures. Figure 2.6 illustrates the use of immersed thermocouples to measure internal polymer temperatures in the injection molding cavity.

Nonimmersion sensors.are divided into active and passive systems (Viskanta and Anderson, 1975). Active systems use an external source (light) and the measurement is accomplished by the modulation of this source upon passage through the sample. These include optical systems, called interferometers, which have been used for studies in heat transfer with transparent liquids and gases (Goldstein, 1984). The temperature field within a solid may also be indirectly measured by photo-elastic methods; when

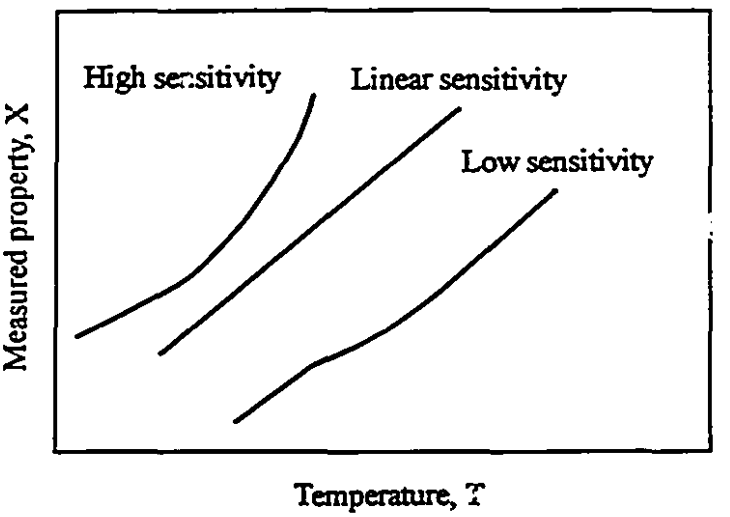

Figure 2.5 Temperature response characteristics.

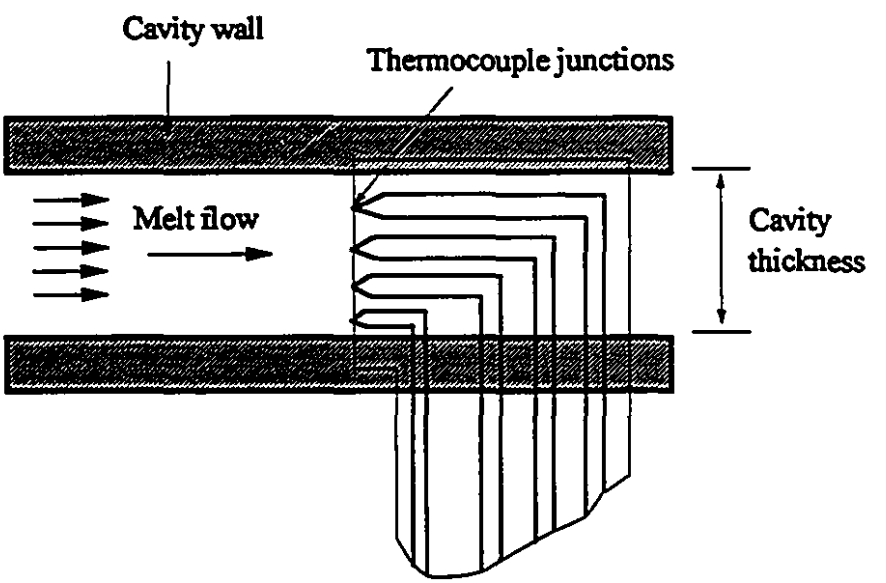

Figure 2.6 Immersed thermocouples for measuring temperature profiles across the cavity thickness.

heated, thermal stresses within the sample change the birefringence. This technique requires a photographic pattern to find the temperature distribution. Infrared pyrometers are passive systems because the temperature is determined from energy emitted by the material.

2.3.2 Melt Temperature Measurement

This section presents a brief review of previous studies on the measurement of the nozzle-melt temperature and the cavity-melt temperature distributions using thermocouples and infrared pyrometers, which are the most commonly used temperature sensors in polymer processing.

2.3.2.1 Thermocouples

Although thermocouples show low sensitivity, the temperature response or generated voltage can be fitted to a linear calibration equation in a wide operating range. Other advantages are low cost, simplicity, and fast response. Several techniques for measuring melt temperature with thermocouples have been proposed. Shen et al. (1992) measured melt temperatures with thermocouples installed in an extruder die, one flush mounted, one immersed at a fixed depth in the melt stream, and an immersed thermocouple with variable depth in the melt stream. The immersed depth variable thermocouple provided better measurement of the polymer temperature. According to these researchers, problems associated with immersed thermocouples are the frictional heating errors, conduction errors, and the intrusive nature of the probes which changes the melt stream flow pattern. Ruscitti et al. (1994) used several NANMAC ribbon thermocouples, which reduce the frictional heating, to measure the surface and internal melt nozzle temperatures.

Thienel and Menges (1978) used immersed thermocouples to measure the temperature at three points inside the cavity, This procedure introduces position errors and gives temperatures affected by viscous heating (Fritch, 1986). Yokoi et al. (1992) reported measurements of temperature profiles using a thin-film thermocouple device installed inside the cavity (see Figure 2.6). However, the solidifying polymer may damage this device during the packing stage. Measurements of polymer temperatures at different locations of the cavity surface using flush mounted thermocouples have been presented by Patterson et al. (1990) and Gao et al. (1993) for polyethylene. Kamal et al. (1991) have presented heat flux data measured at the cavity surface and developed correlations for the heat transfer coefficient as a function of the injection velocity for different resins.

2.3.2.2 Pyrometers

Using pyrometers avoids viscous heating and immersion problems. Fast response and sensitivity are additional advantages of this sensor. Two disadvantages are the nonlinear response and the influence of the temperature of the equipment (Baron, 1994). Several algorithms have been used to infer the temperature profiles from the radiation emitted by transparent glasses (Viskanta, 1975; Viskanta and Anderson, 1975; and Farag and Curran, 1984). The radiation emitted by the medium at different wavelengths is measured with a pyrometer, and the temperature profile along the line of sight is inferred using a mathematical inversion procedure.

This procedure was employed by Rietveld and Lai (1992) in an attempt to infer the cavity-melt temperature profiles using an IR probe installed flush with the cavity surface. The disadvantages of this method are model inaccuracies, lack of data regarding important physical parameters (e.g.,

absorption coefficients), and the non-uniqueness problem involved in the inversion algorithm. Aside from these difficulties, the procedure can only be used with transparent polymers. For a detailed description of the procedure the reader is referred to Viskanta (1975). An algebraic approach based on the work of Farag and Curran (1984) is presented in Appendix A.

A limitation for measuring the temperature of the plastic in the cavity is the low sensitivity of pyrometers at low temperatures in the visible wavelength range. This can be seen when considering the Planck equation for the spectral emissive power of a black body, given as

$$I_b(\lambda) = \frac{C_1 \lambda^{-5}}{e^{C_2/\lambda T} - 1} \tag{2.10}$$

where $I(\lambda)$ = monochromatic emissive power of black body, T = absolute temperature in °K, λ is the wavelength of radiation in μm. C_1 and C_2 are constants with values 3.742×10^8 wμm^4/m^2 and 1.439×10^4 μm°K, respectively. Plots of $I(\lambda)$ vs. $\lambda$from Equation 2.10 are shown in Appendix B for black body radiation in the operating range of polymer temperatures at the nozzle and cavity. The maximum shifts to the right as the temperature decreases. As the temperature to be measured becomes lower, it is necessary to move to longer wavelengths in order to obtain sufficient radiation to drive the detector. The maximum radiating power is obtained at a wavelength λ_m, which is given by Wein's displacement law, which states that

$$T\lambda_m = \text{Constant} \tag{2.11}$$

The constant is 2890 for λ_m in microns and T in °K. For instance, at T = 60°C = 333 °K, the λ_m = 2890/333 = 8.7 μm, which is in the infrared. However,

most polymers transmit radiation at low wavelengths in the visible region. This is seen in data reported by Heiman and Mester (1975) for plastic foils of PVC, PE, and PT, and by Shelby (1991) for a 3.8 mm thick PET sample. As a result, the emitted radiation of polymers at low temperatures is weakly detected by an infrared pyrometer. The minimum temperature sensed by the Vanzetti model LTD pyrometer is 120 °C.

Galskoy and Wang (1978) have found that thin-film thermocouples are more accurate sensors of the cavity melt temperatures than infrared sensors. For this and all the above reasons, pyrometers are not usually employed in controlling the melt temperature.

2.3.3 Control Strategies

Patterson et al. (1985) used a thermocouple installed at the screw tip to measure the melt temperature. A second-order model of the form given below was used for the dynamic response of the melt temperature to heater power input:

$$\frac{T_m(s)}{\Delta H(s)} = \frac{K_m e^{-\tau_d s}}{(1+\tau_{m1} s)(1+\tau_{m2} s)} \tag{2.12}$$

where ΔH = change in heater power input to band heaters, K_m = gain, τ_d = time delay, and τ_{m1}, τ_{m2} = time constants. The identified time constants were as high as 2010 s, which reflect the slow response of the melt temperature.

Ruscitti et al. (1994) used a thermocouple immersed in the nozzle to control the melt temperature. A second-order plus dead-time model was selected for the dynamic of melt temperature, and the manipulated variable

was the total power input to the heater bands in the compression and metering zones. The identified model in the Laplace variable is given as

$$G_p(s) = \frac{K_d e^{-\tau_d s}}{(\tau_1 s + 1)(\tau_2 s + 1)} \qquad (2.13)$$

where $\tau_d = 61.2$, $\tau_1 = 71.4$ s, and $\tau_2 = 713.4$ s. Dahlin and PID controllers were found to be effective in controlling the melt temperature. These values, in comparison with those of Equation 2.12, suggest that the immersed sensor allows faster control of the melt temperature.

2.4 PART WEIGHT AND PVT CONTROLS

Although part weight is not normally shown in product specifications, part weight consistency has been used as an indicator of consistency in other product properties, such as dimensions and optical properties. In comparison with other property measurements, weight measurement can be done with acceptable accuracy and repeatability. Savings in material could also be very significant when one molds millions of small parts. Cycle-to-cycle random process disturbances cause fluctuations in part weight. These disturbances occur during the injection molding process and include:

(1) Changes in the nozzle-melt and mold temperatures
(2) Change in injection-to-pack phase transfer position
(3) Change in the ram injection velocity
(4) Change in back pressure.

Cycle-to-cycle part weight consistency can be maintained by setting the injection and holding times to values which guarantee that the gate seals (gate seal time) before releasing the holding pressure. The gate seal time is found when part weights oscillate around an average value. This procedure avoids large variations in part weight, but it does not avoid small changes due to the process disturbances mentioned above.

Accurate measurements of part weight are difficult to obtain in a short time. The time needed to separate the sprue from the mold, as well as the waiting time until the balance gives a stable reading, are larger than the usual time available for measuring. Therefore, using a model that relates part weight to other measurable process variables is convenient.

Machine variables and process variables have been used for fitting part weight to experimental data. Harry (1991) found that the average cavity pressure near the gate correlates better with part weight than the melt temperature does. Schenker (1993) determined that the temperatures of the mold and the hydraulic oil and the hold pressure have the most significant effect on part weight. Davis and Hudson (1991) fitted the part weight sequence using time-series models (ARIMA), and found that there is a significant trend in part weight during the first 140 cycles in the injection molding process, after which equilibrium is established.

A regression model that considers all possible factors of the part weight variations was used by Srinivasan et al. (1992). The resulting formula relates part weight to set-points for mold temperature (x_1), nozzle-melt temperature (x_2), packing time (x_3) and packing pressure (x_4), and is written as

$$W = \sum_{i=0}^{3}\sum_{j=0}^{3} B_{ij} x_i x_j + B_p x_4 \qquad (2.14)$$

The authors suggested a PI controller for the cycle-to-cycle control of part weight, which was designed without accounting for variations in the melt and mold temperatures (first right-hand terms in Equation 2.14), and considered a cycle as time delay, so that the closed-loop transfer function is given by

$$\frac{W(z)}{W_d} = \frac{B_p z^{-1}\left[K_I + K_P(1 - z^{-1})\right]}{1 - z^{-1} + B_p z^{-1}\left[K_I + K_P(1 - z^{-1})\right]} \qquad (2.15)$$

where W_d is the desired part weight. The part weights showed large cycle-to-cycle variations. The reason is that the properties of the melt in the cavity which are directly related to the part weight were not controlled.

The idea of controlling product properties using the PVT characteristics of the material in the injection molding process is nearly twenty years old (Langecker, 1992). Several authors have described PVT strategies. Most of them are based on the equation of state of Spencer and Gilmore (1949), expressed as:

$$(p + a)(v - b) = RT \qquad (2.16)$$

where p = cavity melt-pressure, T = cavity melt temperature, v = melt specific volume, and a, b, and R are constant parameters. Solving for p, this equation becomes

$$p = xT - a \qquad (2.17)$$

where $x = R/v - b$. Assuming constant specific volume, this equation gives the required melt pressure needed to compensate for variations in melt

temperature.

Different algorithms have been proposed using the PVT behavior of the polymer. In these approaches, simulations using the simple models derived from the conservation equations are employed to estimate the cavity melt properties (e.g., temperature, viscosity) which cannot be measured directly. A part weight control algorithm was implemented by Yakemoto et al. (1993) using:

$$\frac{\Delta W}{W} = \beta \Delta p - \kappa \Delta T \tag{2.18}$$

where W = part weight, T = polymer temperature in the cavity, β = compressibility, and κ = thermal expansion. The polymer temperature is calculated by numerical simulation of a heat conduction model assuming constant initial temperature and neglecting the thermal contact resistance between the polymer and the cavity wall. The algorithm consists of calculating the required packing pressure necessary to have zero weight fluctuations, $\Delta W = 0$, from cycle to cycle.

2.5 PROCESS MODELS

Analytical process models can be derived from the principles of conservation of mass, momentum, and energy (Bird et al., 1960). The solution of these equations is beyond the scope of this work. General solution procedures for the different stages of the process are given by Tadmor and Gogos (1979), Richardson (1989), and Baird and Collias (1995). However, in order to understand the complex interrelation between process variables, the basic models used for simulation will be presented.

A complete mathematical description of all processes involved in the injection molding operation requires analysis of the hydraulic system, extruder (feed, compression, and metering sections), delivery system (sprue and runners), and the mold cavity. This section refers to the molding process taking place in the delivery system and a rectangular cavity only, as shown in Figure 2.7. The flow in the delivery system can be described using the approach of Williams and Lord (1975) for circular channels. Neglecting the acceleration terms and radial and circumferential velocity components, the equation of motion can be simplified to

$$\frac{\partial p}{\partial \zeta} = \frac{1}{r}\frac{\partial}{\partial r}\left(r\eta\frac{\partial w}{\partial r}\right) \tag{2.24}$$

where w = velocity in the axial coordinate, and ζ = axial coordinate. Neglecting axial conduction and radial convection, the equation of energy may be written as

$$\rho C_p w\frac{\partial T}{\partial \zeta} = \frac{1}{r}\frac{\partial}{\partial r}\left(rk\frac{\partial T}{\partial r}\right) + \eta(\dot{\gamma})^2 \tag{2.20}$$

where $\dot{\gamma} = \partial w/\partial r$ is the shearing rate. These equations can be solved using the following boundary conditions

$$\begin{aligned} T(0,r) &= T_1(r) \\ \frac{\partial T}{\partial r}(\zeta,0) &= 0 \end{aligned} \tag{2.21}$$

where $T_1(r)$ is the temperature distribution of the melt entering the sprue. Solving Equations 2.20 and 2.21 numerically yields the required temperature and velocity distribution of the melt entering the cavity.

Many mathematical models have been proposed for the simulations of the polymer flow in the cavity. A model for radial flow in cavities was

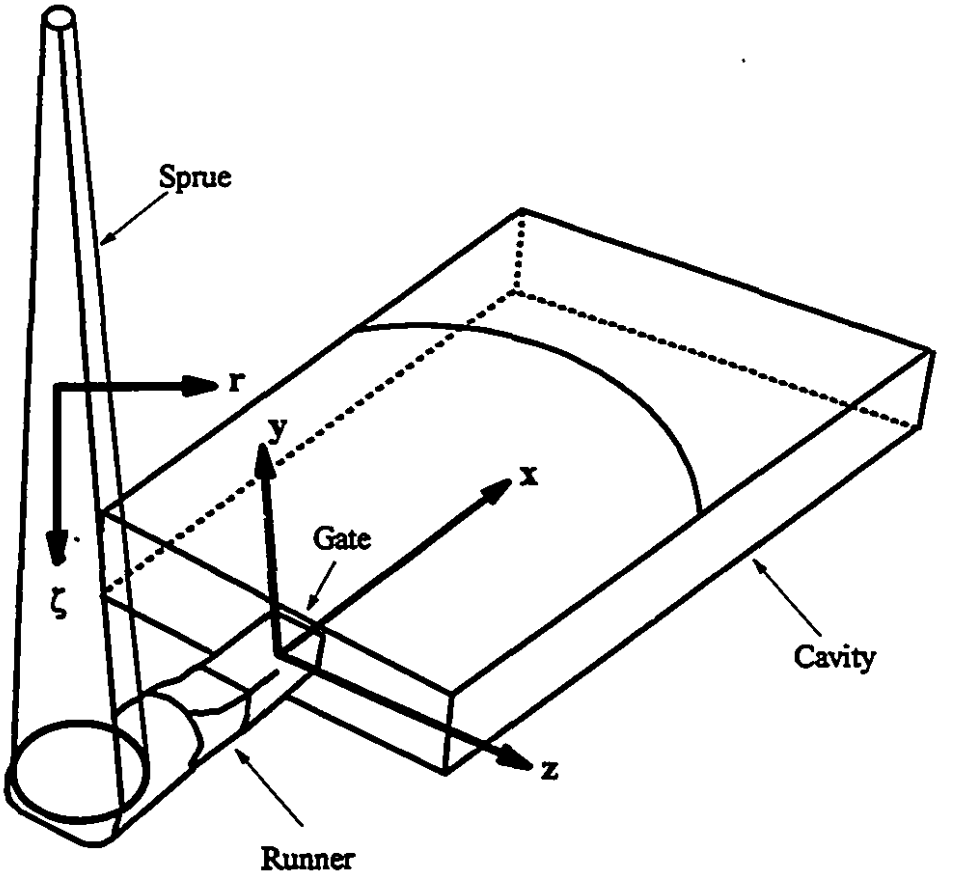

Figure 2.7 Cylindrical and Cartesian coordinate systems for the sprue and cavity.

proposed by Kamal and Kenig (1972). An analytical solution to the transport equations describing polymer flow in a rectangular cavity was presented by Kamal et al (1975). The continuity equation for the rectangular cavity shown in Figure 2.7 is approximated by

$$\frac{\partial \rho}{\partial t} + \frac{\partial}{\partial x}(\rho u) + \frac{\partial}{\partial y}(\rho v) + \frac{\partial}{\partial z}(\rho w) = 0 \tag{2.22}$$

The flow of polymer melt in the cavity has been modeled assuming a one-dimensional stationary process or generalized Hele-Shaw flow (Hieber and Shen, 1980). In this approach, with the pressure variation in the thickness direction being negligible, the components of the equation of motion are expressed by

$$\begin{aligned} 0 &= \frac{\partial}{\partial y}\left(\eta \frac{\partial v_x}{\partial y}\right) - \frac{\partial p}{\partial x} \\ 0 &= \frac{\partial}{\partial y}\left(\eta \frac{\partial v_z}{\partial y}\right) - \frac{\partial p}{\partial z} \end{aligned} \tag{2.23}$$

where η is the viscosity, whose dependence on the shear-rate ($\dot{\gamma}$) and temperature is

$$\eta = \eta(\dot{\gamma}, T) \tag{2.24}$$

and $\dot{\gamma}$ is

$$\dot{\gamma} = \sqrt{\left(\frac{\partial v_x}{\partial y}\right)^2 + \left(\frac{\partial v_z}{\partial y}\right)^2} \tag{2.25}$$

With the assumption that the heat conduction occurs across the cavity thickness only, the energy equation takes the following form:

$$\rho C_p\left(\frac{\partial T}{\partial t}+v_x\frac{\partial T}{\partial x}+v_z\frac{\partial T}{\partial z}\right) = k\frac{\partial^2 T}{\partial y^2}+\eta\dot{\gamma}^2 \qquad (2.1)$$

Equations 2.22 to 2.27 can be solved numerically using appropriate initial and boundary conditions. Solutions to these equations have been presented by Chiang et al. (1991), and recently by Chen and Liu (1994) for the packing stage, including modifications for the two-phase flow. A detailed computer simulation, including factors such as viscoelasticity, fountain flow, crystallization kinetics, and solidification, was presented by Chu et al. (1989) and Chu (1992).

2.6 SUMMARY

A review of some of the studies on control of the cavity pressure and the nozzle melt temperature, and on measurement of the melt temperature, has been presented in the preceding sections. Injection molding is a complex process that involves operations of heat transfer and transport of a polymer in the solid and liquid states. Thus, the simulation and control of this process are still areas of active research interest.

Simplified input/output models do not consider the melt solidification and thermal aspects during filling and packing, but allow for the design and implementation of controllers. The closed-loop control of cavity pressure has shown positive effects in maintaining part weight and part dimensions. Two control variables have been used to manipulate the cavity pressure: the servo-valve opening and the clamp force. Some studies have been concerned with the control of the melt temperature in the nozzle. Controlling the temperature of the plastic in the nozzle is difficult as no appropriate sensors

are available. A procedure for estimating the melt temperature from other measurements in the cavity is necessary. Due to sensor limitations and difficulties of the mathematical models, using infrared pyrometers for measuring melt temperatures in the cavity is not recommended.

Strategies for the control of part weight, using regression models or a PVT relationship, are not implemented under closed-loop control. Therefore, the effects of process variables which affect the cycle-to-cycle variations in part properties were not considered.

CHAPTER 3
DESCRIPTION OF EQUIPMENT AND COMPUTER CONTROL SYSTEM

This chapter presents a brief description of the equipment and software employed in this study. The three essential components of the equipment are: the injection molding machine, interfaces, and a microcomputer. The interfaces allow the transmission of the input /output signals from the sensors to the computer and from the computer to the final control elements (e.g., servo-valves, band heaters, directional control valves).

3.1 INTRODUCTION

The development of more sophisticated measuring devices and faster computers has resulted in the application of complex algorithms to control important factors in the injection molding operation. Extensive literature and technical data regarding injection molding machines are available in such references as Rosato and Rosato (1982), Whelan (1984), and Berins (1991). A major goal of the integration of a microprocessor to an injection molding machine is to maintain part quality consistency. Some advantages of using a microcomputer-based control system are:

(1) Monitoring and recording measurements at different points. For example, a record of the melt temperature, melt pressure, hydraulic pressure, screw position, and screw velocity is useful for analysing operational problems.

(2) Prediction of the melt and product properties for changes in machine settings (e.g., in the barrel and back pressure). This allows preventive corrections from shot-to-shot.

(3) Changing the set-points during the molding operation and flexibility in implementing different control strategies..

Three major levels are recognized in the computer-based control system:

(1) Process instrumentation and process device level, which include the injection molding machine and sensing devices.

(2) Signal transmission system and final control element level (e.g., amplifiers, signal converters, band heaters, and control valves).

(3) Data acquisition and direct digital control level.

3.2 INJECTION MOLDING SYSTEM

Figure 3.1 shows a schematic of the microcomputer-based control system used in this work. The injection molding machine consists of a 68-ton Danson Metalmec reciprocating screw injection molding unit. Table 3.1 gives the main specifications of the injection unit and other equipment. The major components of the system are: (1) hydraulic system, (2) screw and barrel, (3) mold and cooling system, (4) measuring devices, (5) hardware interfaces, (6) computer, and (7) software.

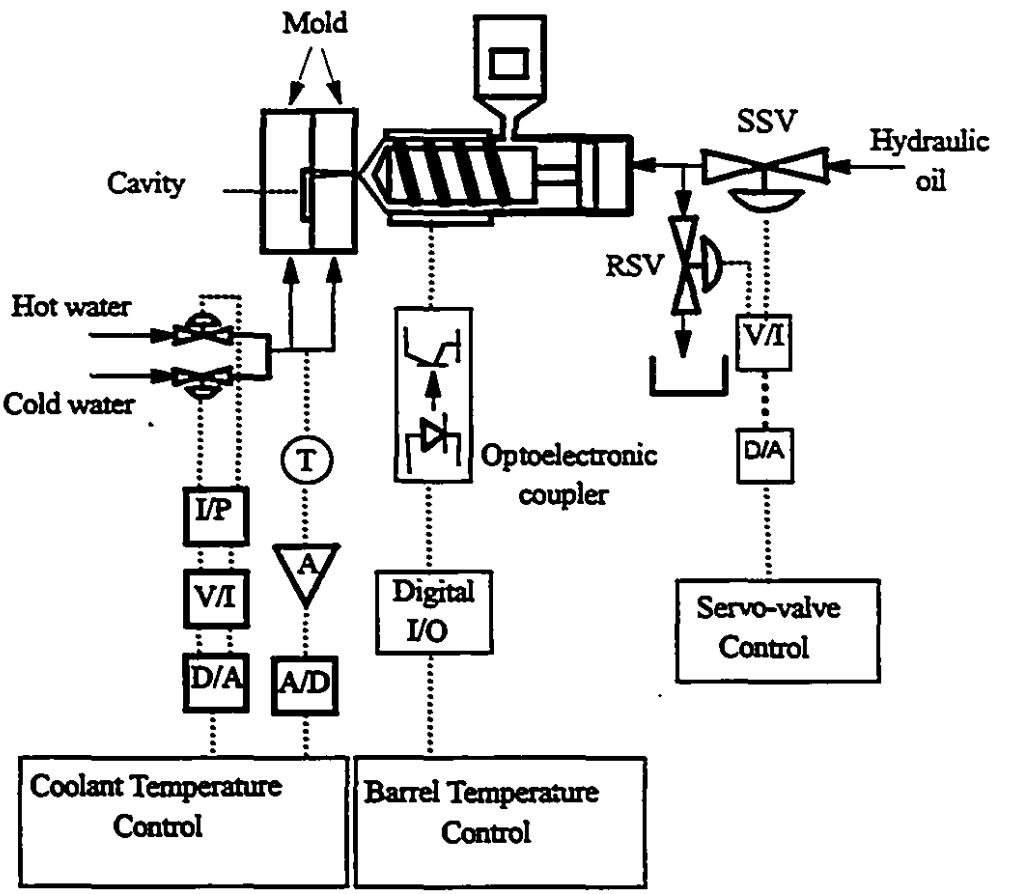

Figure 3.1 Injection molding machine system.

Table 3.1 Specifications of the injection molding unit

Features	Characteristics
Model:	Danson Metalmec 60-SR
Capacity	66.1 g (2 1/3 oz) ps.
Screw diameter:	0.035 m (1.375 inches)
Screw L/D ratio:	15/1
Screw RPM:	40-150
Clamping force	53386 kN (60T)
Hydraulic pump:	Sperry-Vickers Vane Pump
Electric motor:	Power: 14.92 Kw (20 hp), 3 phases, 50 Hz
Servo-valves:	Moog A076-103

3.2.1 Hydraulic System

Directional control valves, or solenoid valves, direct the hydraulic oil for the sequential movements of the barrel and the opening and closing of the mold. The functions of the active directional valves are listed in Table 3.2. During the injection stage, valve S5 enables the flow of hydraulic fluid toward the injection cylinder, as shown in Figure 3.2.

The original design of the hydraulic system was modified (Haber, 1982) to install an electro-hydraulic servo-valve, type A076-103 Moog with a flow capacity of 37.85 l/min at a pressure drop of 6.2 MPa (1000 psi). Another servo-valve was installed (Abu Fara, 1988) to facilitate the cavity pressure control. One is designated as the supply servo-valve (SSV), and is found in the line that transports oil to the injection cylinder. The other is called the return servo-valve (RSV), and is installed in the line that returns oil to the tank, before the heat exchanger. This configuration allows for control of the oil flow to the injection cylinder during a cycle. The maximum injection speed and hydraulic pressure are determined by adjusting the relief-valve RV (see Figure 3.2) which controls the maximum line pressure by diverting a portion of the oil flow to the tank. Computer outputs range from 0V to 5 V dc, corresponding to 0% and 100% servo-valve openings, respectively. To drive the servo-valves, output voltages are converted to currents varying from 0 to 20 mA.

3.2.2 Screw and Barrel

Several factors affect the heat transfer to the polymer, including: (1) the barrel temperature profile, (2) effective heat transfer areas of the barrel and screw, (3) residence time of the plastic in the screw, (4) screw velocity

Table 3.2 Main functions of the directional control valves

Valve	Function
S2	Mold closing
S3	Carriage advances to injection position
S4	Switch to high-pressure (injection)
S5	Screw movement (injection)
S6	Switch to low-pressure (decompression)
S7	Screw return (plastication)
S8	Mold opening
S9	Carriage return

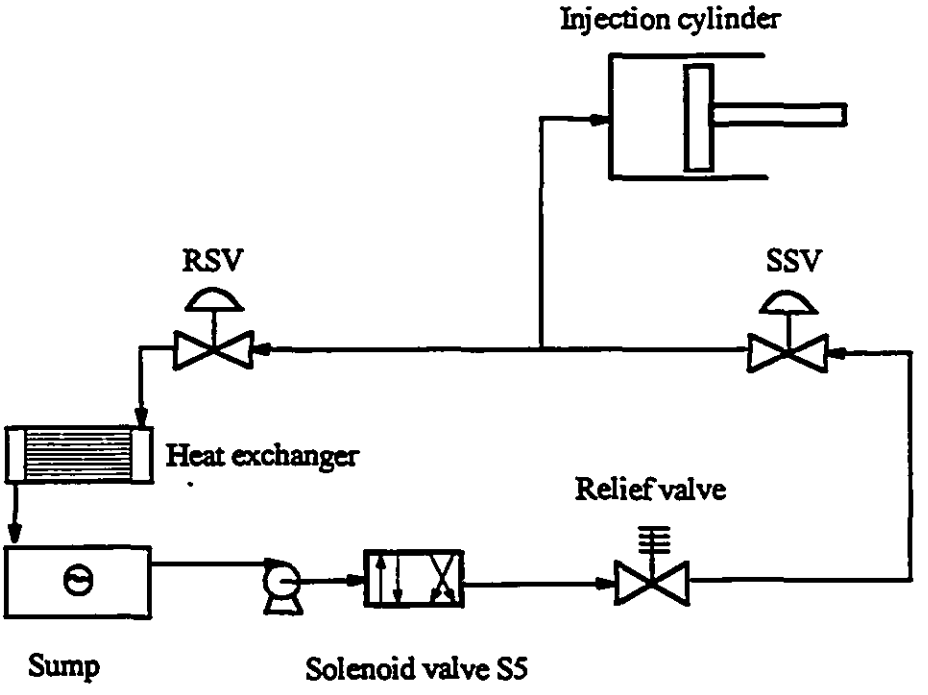

Figure 3.2 Simplified diagram of the hydraulic oil flow system activated by the directional control valve S5.

during injection, and (5) thermal conductivities of the plastic and the barrel and screw materials.

Ruscitti (1992) installed four band heaters to control the temperature of the barrel. Two are in the metering section at the front, one is installed in the transition or compression section, and another in the feed zone at the rear. Figure 3.3 shows the dimensions of the barrel and nozzle. A 220-V ac-voltage source is the main power supply to the band heaters. The power to each band heater is controlled by adjusting the conduction angle of the voltage signal. For an angle $x\pi$ in interval $0 \leq x\pi \leq \pi$, where x is a fraction between 0 and 1, the power transmitted to a band heater is given by

$$P(x) = \frac{V_o^2}{R}\left[\frac{\pi x}{2} - \frac{1}{4}\sin(2\pi x)\right] \tag{3.1}$$

where R is the heater resistance, and V_o is the peak voltage. Gao (1993) designed the heater control system that changes the on-time and off-time periods on each side of the sinusoidal signal (60 Hz).

3.2.3 Mold and Cooling System

Figure 3.4a illustrates the dimensions of the fixed part of the mold. A 3-mm thick rectangular cavity with length 10.1 cm and width 6.5 cm was used in this study. Figure 3.4b shows the sensor locations at the surface of the rectangular cavity. Pressure and temperature sensors are installed flush with the cavity surface of the fixed plate as shown in Figure 3.4c. The dimensions of the sprue and runner, are shown in Figure 3.5a.

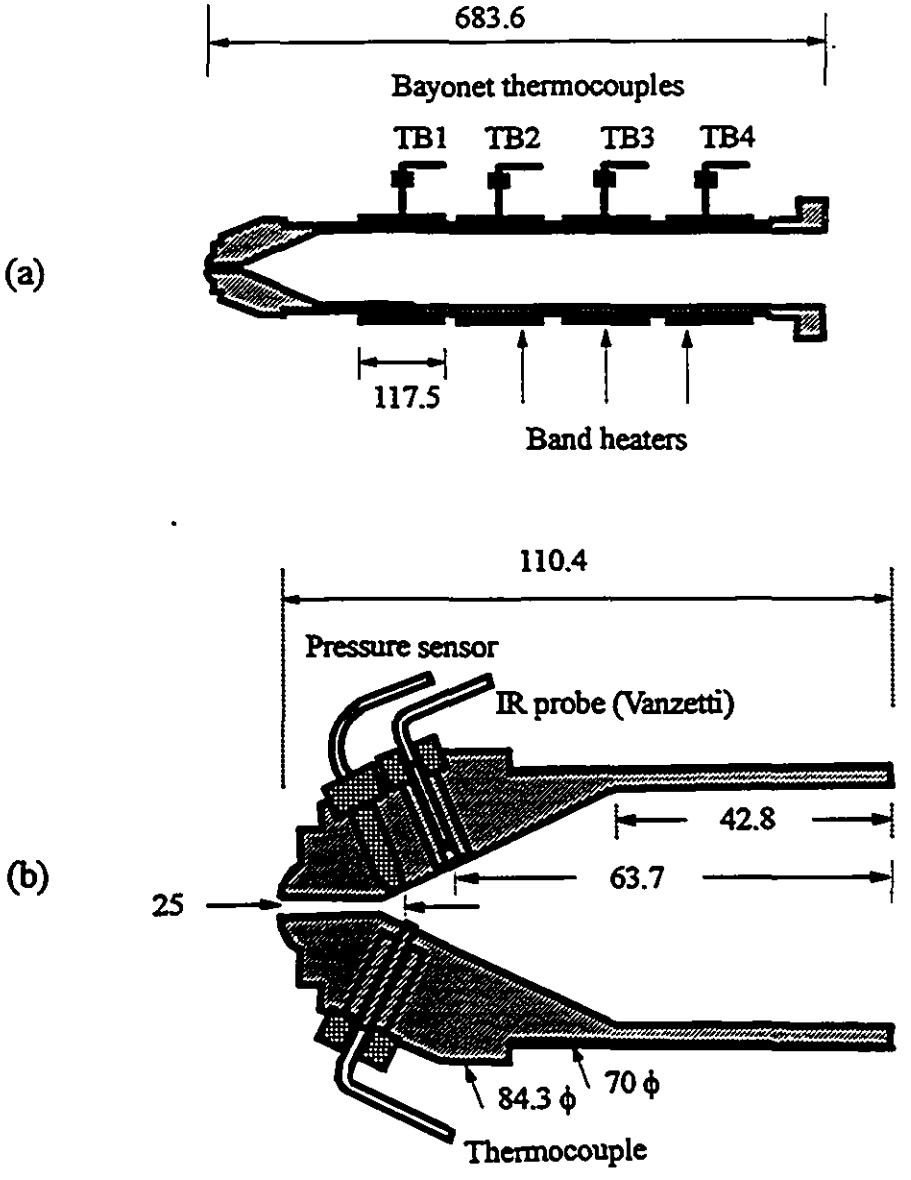

Figure 3.3 Schematics of the barrel (a) and nozzle (b). All dimensions are in mm (Ruscitti, 1992).

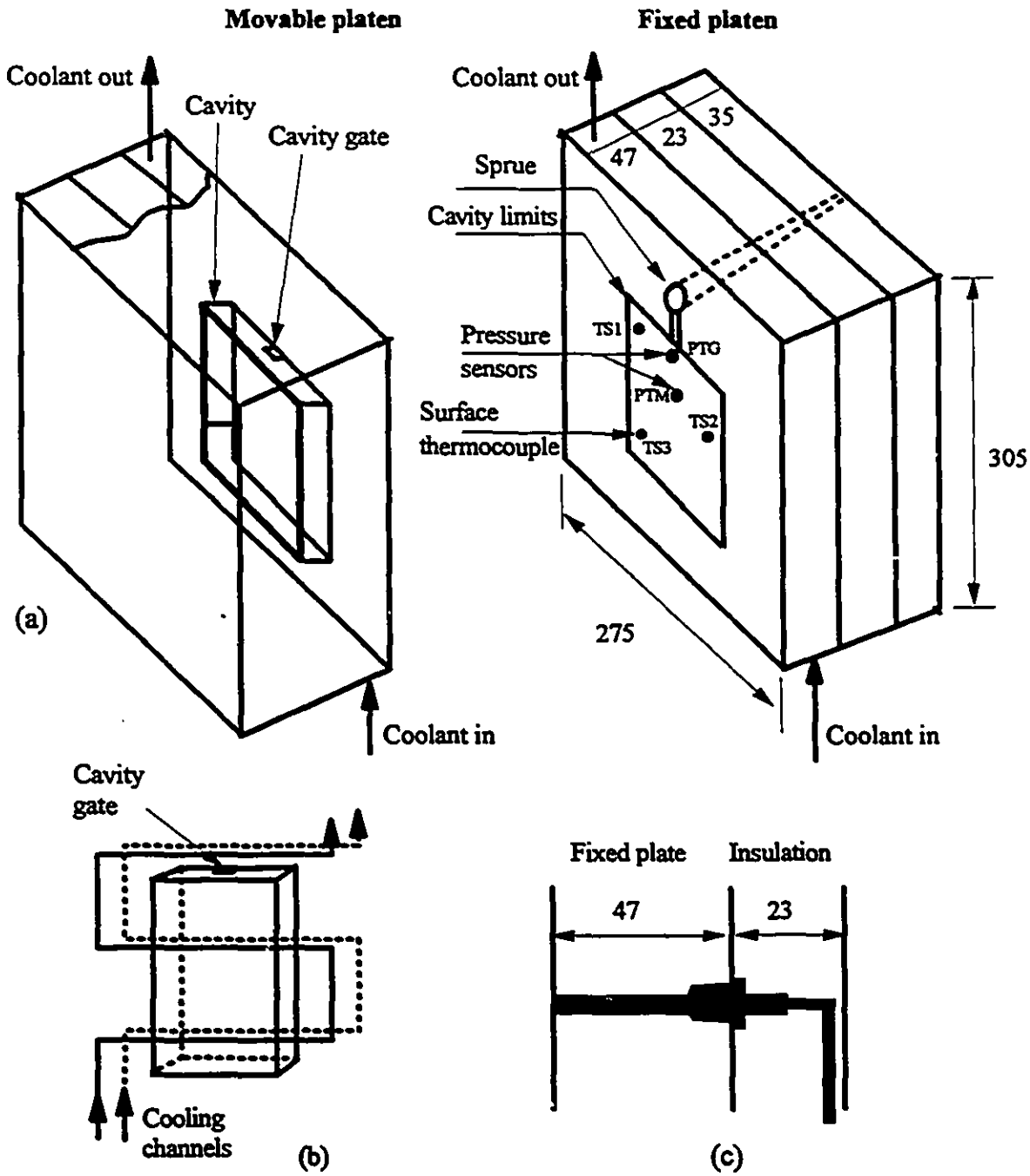

Figure 3.4 Illustration of the mold, cooling channels, and cavity sensors.
(a) Mold dimensions and sensor locations.
PTG, PTM: Pressure transducers, TS: Flush thermocouple.
(b) Cooling channels.
(c) Flush mounted thermocouple.
All dimensions are in mm.

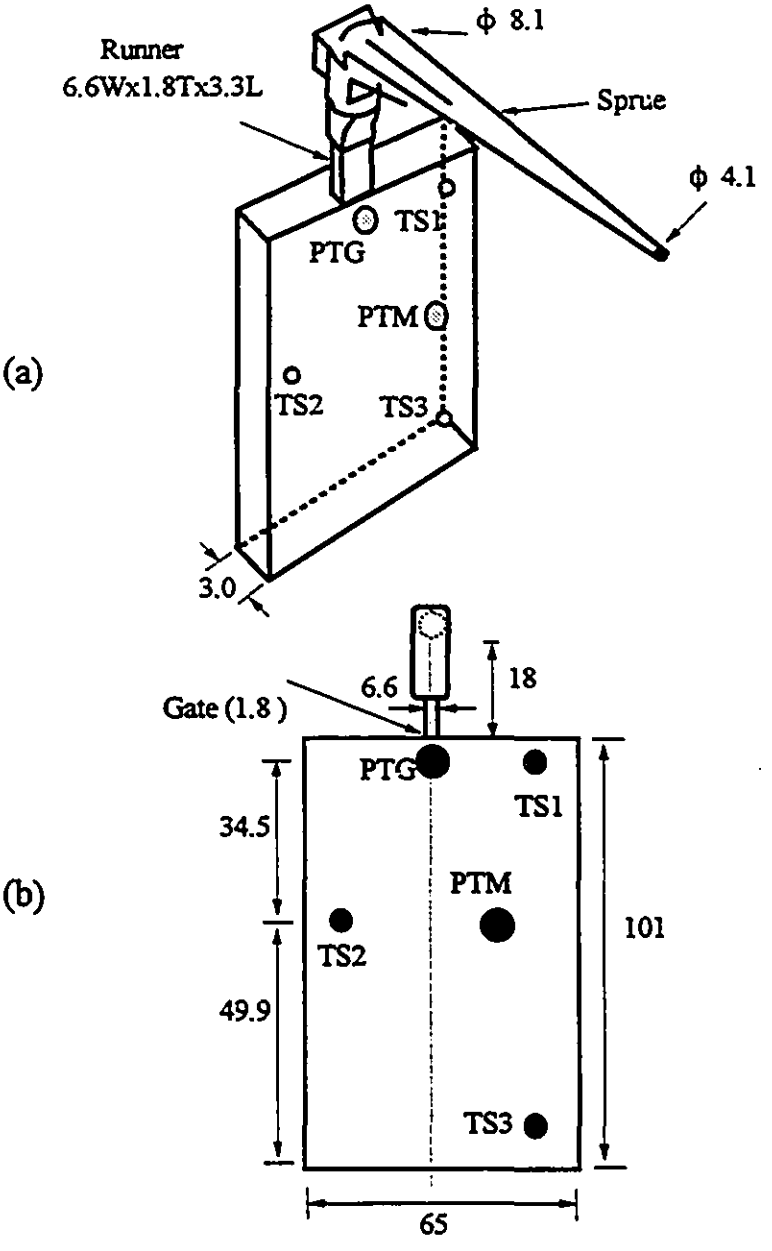

Figure 3.5 (a) Dimensions of the cavity and delivery system.
(b) Sensor locations at the cavity surface.
PT: pressure transducer, TS: surface thermocouple.
All dimensions are in mm.

Coolant water is used to control the temperature of the mold. The coolant temperature is controlled using two electro-pneumatic valves, type 1/2-B-EQ. PCT (Fisher Controls Inc., 1977), for the hot and cold water streams (see Figure 3.1). This system was designed by Gao (1989) and Patterson et al. (1990). The computer sends signals varying from 0V to 5 V dc, which are transmitted to the control valves as a current (4-20 mA) by a voltage/current (V/I) converter. A current-to-pressure transducer (I/P) converts the currents into the pneumatic signals (3-15 psig) that drive the control valves.

3.2.4 Installed Sensors

A variety of sensors are installed in different sections of the hydraulic system (Abu Fara, 1988), the barrel (Ruscitti, 1992), and the cavity and cooling system (Gao, 1993). These sensors deliver the analog signals required for process control and monitoring. The sensors are divided into: (1) temperature sensors, (2) pressure transducers, and (3) the screw position and velocity sensor.

Temperatures at different locations are measured using type E thermocouples and a Vanzetti infrared pyrometer. Table 3.3 summarizes the characteristics of the temperature sensors used in this study. An amplifier with reference junction compensation and an input-output gain of 10mV/1 °C transforms the thermocouple signals into voltages varying between 0 and 5 V, corresponding to temperatures from 0°C to 500 °C. The barrel temperature is measured with four grounded type E thermocouples, one in the melt section (TB1), one in the transition section (TB2) and two in the metering zone at the rear (TB3, TB4). Three type E grounded thermocouples are used to measure the inlet coolant-temperature and the temperature of the hot and

Table 3.3 Temperature sensors in the barrel, mold cavity, and cooling system

Acronym	Location
TB1,TB2,TB3,TB4	Mid-section of each heater (metal temperature) from the nozzle zone to the rear (see Figure 3.3a)
TN	Nozzle (flush mounted)
TV	Nozzle (Vanzetti IR pyrometer)
TS1	Cavity surface near the gate
TS2	Middle cavity surface
TS3	Cavity surface near the end of the cavity
TH	Hot water
TC	Cold water
TM	Coolant (Mixed water)

cold water streams. Three type E thermocouples (NANMAC pencil-probe-eroding type E), TS1, TS2, and TS3, measure the temperature of the polymer at the cavity surface. Figure 3.5(b) gives the rela ive positions of the thermocouple-tips and pressure-transducer diaphragms at the cavity surface.

Table 3.4 summarizes the characteristics of the sensors used to monitor the pressure of the polymer in the cavity at the gate (PTG), at the cavity middle (PTM), and at the nozzle (PTN). The cavity pressure transducers are installed flush with the surface. Another sensor (PTH) measures the hydraulic pressure in the injection cylinder. The input-output calibration equations are given as

$$p = g V_m + \Phi \tag{3.2}$$

where p = pressure, g = gain, V_m = pressure transducer output for 10 Vdc excitation voltage, and Φ = offset. The gains and offsets are shown in Table 3.4 for each pressure transducer. Appendix A-1 presents calibration curves for the gate and nozzle pressure transducers which were obtained using a dead weight tester and 10 Vdc excitation voltage. Offset errors are attributed to the analog-to-digital signal converter (Ogata, 1995), and temperature changes (Dynisco, 1988).

The screw position and velocity are determined by a transducer from Temposonics (Model 011012070208). The input-output calibration equations for the screw position (S in cm) and screw velocity (dS/dt in cm/s) are given as

$$S = 3.05V_{sd} + 4.27\ , \quad \frac{dS}{dt} = 2.03V_{sv} - 3.00 \tag{3.3}$$

where V_{sd} and V_{sv} are the output voltage for the displacement and velocity measurements, respectively.

Table 3.4.Pressure transducers

Sensor	Location	Range	Parameters of calibration equation	
			g, mV	Φ, MPa
PTG New York LTD GP-50 Model 132 S/N:154622	Cavity gate	0-34.473MPa (0-5000 psi)	1.025	- 0.216
PTM Dynisco PT435A-3M S/N:290264	Cavity middle	0-27.579MPa (0 - 4000 psi)	0.632	- 1.221
PTN Dynisco PT435A-10M S/N:160039	Nozzle	0-68.946 MPa (0-10000 psi)	2.054	- 0.507
PTH Dynisco 432A-1M S/N:10423	Injection cylinder	0-6.895 MPa (0-1000 psi)	1.651	- 0.340

3.2.5 Hardware Interface and Computer

The microcomputer used to control the injection molding process is an IBM-compatible-PC ALR-486DX machine. Figure 3.6 shows a simplified diagram of the interfacing system. The temperature and pressure signals are amplified to 0-5 V dc. Two differential amplifiers (A-100 and A-200) transform the signals from the pressure transducers. The analog signals are supplied to two high-level voltage panels (Analog Devices, STB-HL02). Two data-cards from Analog Devices (RTI-220) convert these signals to numeric form. The digital input/output signals are delivered through a digital I/O card from Analog Devices (RTI-217). Table 3.5 gives the main features of the interfaces and termination cards.

3.3 SYSTEM SOFTWARE

Software for data processing and control applications was developed by Fusser (1992) and Gao et al. (1992) and implemented under the QNX 4.1 Operating System (Quantum Software Systems Ltd., 1992). It is used for both on-line and off-line applications. Off-line applications are employed for system communication, debugging, use of utility routines, compilation, linking, and creation of executable files.

On-line application programs were developed in the C language (WATCOM, 1991). Programs and routines have been developed to enable several functions, the most important being: (1) system start-up, (2) data acquisition start-up and shut-down, (3) memory manipulation, (4) data exchange between external input/output devices, (5) use of a real-time processor, and (6) processing of source programs.

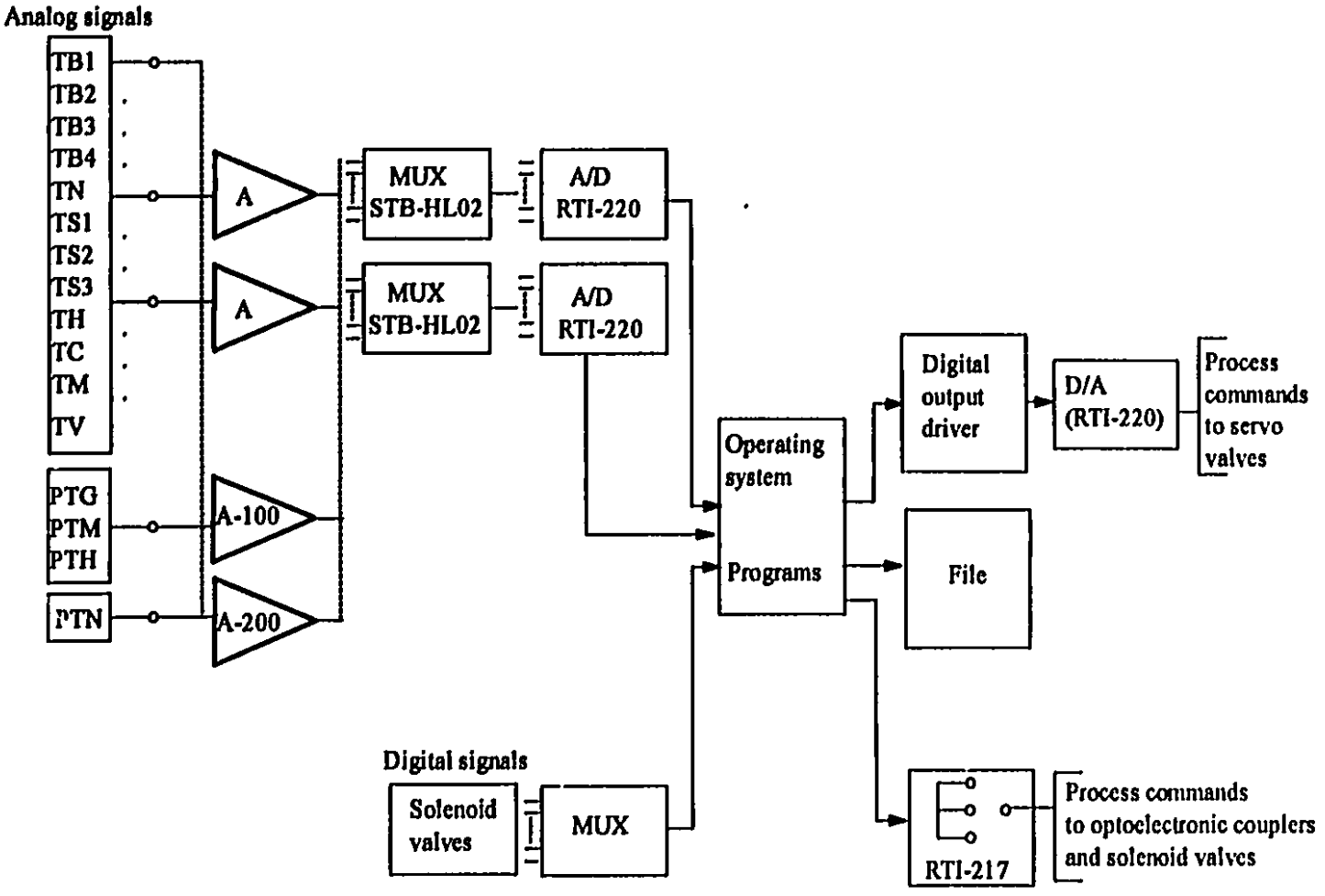

Figure 3.6 Illustration of the digital input-output signal processing.

Table 3.5 Main features of the interfaces and termination cards

	Number of units	Characteristics
Interface cards STB-HL02	2	
Analog input channels	16	single-ended
Analog output channels	4	-
Termination cards :		
RTI-220	2	
Input: Number of channels		16(64 max.)
A/D resolution	-	12 bits
A/D conversion time	-	25 µs
Voltage range	-	±5V or 0-5V
Output: Number of channels		16(max.)
D/A resolution		12 bits
Settling time		16µs
Voltage range		±5V @ 5mA
RTI-217	1	
Number of channels	32	programmable in four 8-bit ports as input or output

The software for real-time control of the injection molding machine comprises a set of programs which are coordinated by the QNX operating system. Table 3.6 lists these programs and their corresponding tasks. The operating system assigns permission for program execution based on time of the request occurrence and on the requested program priority relative to other pending requests.

Processes are programmed instructions transformed by the computer's central processing unit (CPU) so as to use the computer resources most effectively. The QNX operating system and WATCOM C-library provide various routines for activation of real time multitasking applications. These routines are processed through the QNX kernel (1992) and enable:

(1) Inter-process communication: three types of communication are handled by the kernel: messages, proxies, and signals. Routines in the C language for message passing are: *Send*() for sending data, *Receive*() for receiving data, and *Reply* () for replying to processes that have sent data.
(2) Process scheduling.
(3) First-level-interrupt handling: the kernel receives hardware-interrupt request before any driver or system manager.

The other important function of the kernel is process scheduling. Application programs can be activated using three scheduling methods:

(1) FIFO scheduling, in which the activation request is placed into a waiting queue on the priority basis and first-in-first-out principle.

Table 3.6 Programs for real-time control of the injection molding machine

Program	Task
imm†	Operator-system communication
barreltemp†	Barrel temperature display
statdip2†	Cycle time display
variable:	Activation of control programs:
1. *var_const.c*‡	1. *pcontrol* (*p_const.c*)
2. *var_pt.c*	2. *pcontrol* (*pcont1.c* or *pcont2.c*)
3. *var_pwt.c*	3. *pcontrol* (*pcon_pwt.c*)
moldtemp.control:	Coolant/bulk temperature control:
1. *mt_const.c*‡	1. coolant temperature control
2. *mt_tavg.c*	2. step tests in coolant temperature
3.*mt_pt.c*	3. cascade control of the bulk temperature
tcontrol	Change pointers of the bulk temperature
1. *tcont_pt.c*	1. for the bulk temperature control task (*mt_pt.c*)
2. *tcon_pwt.c*	2. for the cavity pressure control task (*pcon_pwt.c*)
tavg	Bulk temperature estimation
pcontrol:	Manipulation of servo-valve openings
1. *p_const.c*	1. open loop
2. *p_ssv.c*	2. cycle-to-cycle variation of servo-valve opening
3. *p_dynam.c*	3. dynamic of the cavity pressure
4. *pcont1.c*	4. pressure control using a first-order model
5. *pcont2.c*	5. pressure control using a second-order model
6. P_tav_tc.c	6. dynamic of the bulk temperature
7. *pcon_pwt.c*	7. pressure control using algorithm PWT control
heater‡	Control of the barrel temperatures
cycle‡	Control of the injection molding cycle sequence
rti217‡	Activation of solenoid valves
sadc‡	Data acquisition for slowly varying signals
sadcbufw‡, *sadcsave*‡	Digital input data (slow varying signals)
fadc	Activation of:
1. *fadc_.c*‡	*pcontrol*, *fadcbufw* and *fadcsave*
2. *fadc_pt*	*pcontrol*, *tcontrol*, *fadcbufw* and *fadcsave*
fadcbufw‡, *fadcsave*‡	Digital input data (rapidly varying signals)

†Programs developed by Fusser (1992).

‡ Programs developed by Gao (1993).

(2) Round-robin scheduling in which the activation request is placed into a waiting queue on the last-in-first-out principle.

(3) Adaptive scheduling, in which a process will decay in priority if it consumes too much of the processor time before blocking

In QNX, the priority must be between 1 (lowest) and 29 (highest for super-user) or 19 (highest for non-super user).

An efficient QNX routine for process creation is *spawn* (). This creates a new process as a child of the calling process. The software used to control the injection molding machine has been developed using the function *spawn* () with FIFO and round-robin scheduling policies. The software includes an interface and a series of sequential application programs in a multitasking environment.

3.3.1 Software Interface

Figure 3.7 illustrates the main processes in the software interface. Program *imm* opens the files: *statdip2*, *barreltemp*, and *variable*, which are given the lowest priority with the round-robin scheduling policy. Programs *statdip2* and *barreltemp* allow:

- Visualization of set-points for the barrel temperatures
- Visualization of the barrel temperature measurements
- Visualization of the stages and elapsed time of each cycle
- Modification of set-points for the barrel temperatures, cycle times, and sampling intervals

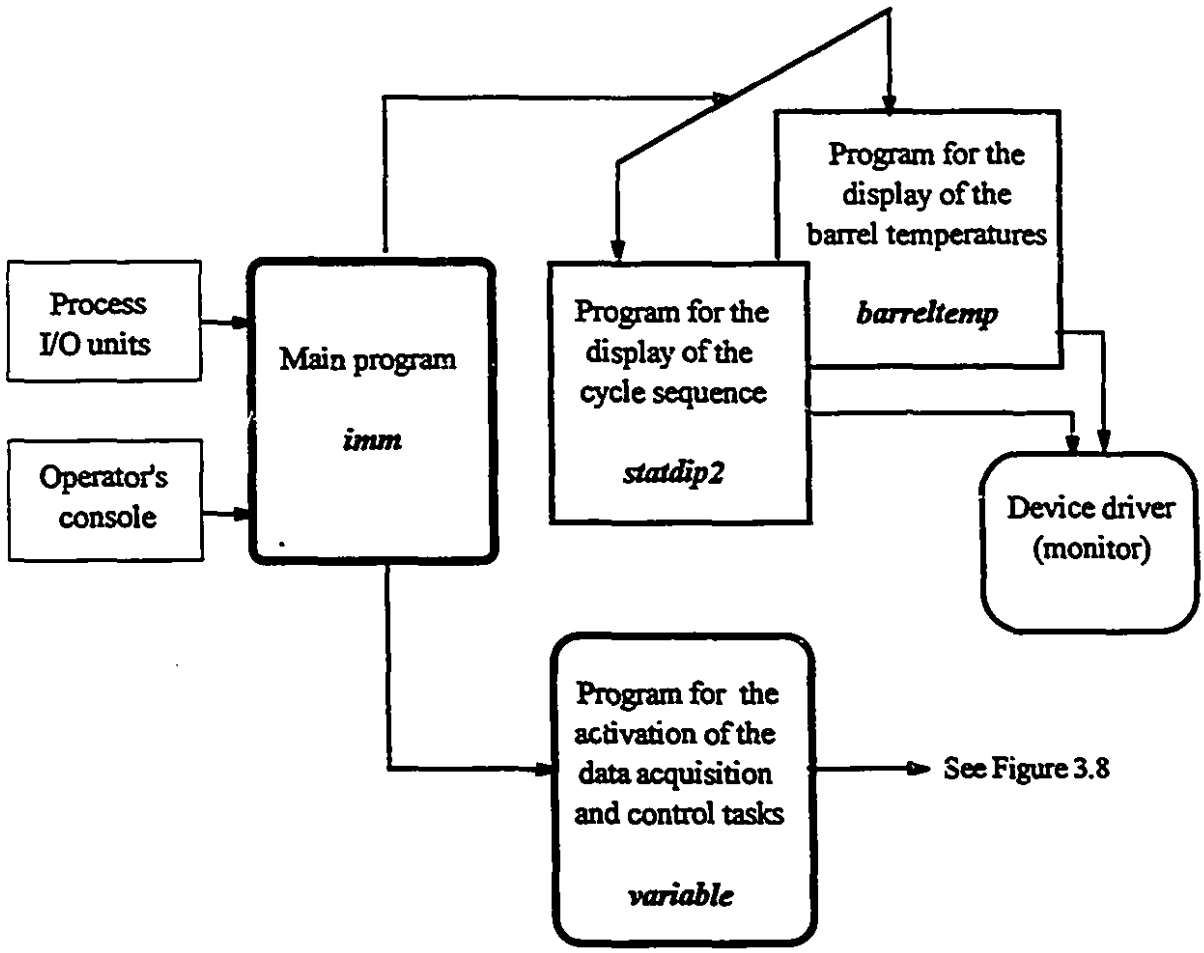

Figure 3.7 File structure showing the main activation programs.

- Selection of the machine operation in automatic, semi automatic, or manual modes

Program *imm* starts file *variable*, which opens the applications for data processing and control of the injection molding process.

3.3.2 Applications Programs

Program *variable* opens application programs for data acquisition and control as shown in Figure 3.8. Task *tcontrol* can be omitted by changing the source code for files *variable* and *fadc*. Programs *variable*, *moldtemp.control*, *tcontrol*, *pcontrol* and *fadc* are common names given to executable files resulting from compilation of different source codes (see Table 3.6).

The highest priority belongs to process *cycle*, which controls the machine sequencing using interrupt routines. Process *fadc* is given the next highest priority, and it allows the following:

(1) Obtaining the system interval timer and time-of-day data. The minimum timer interval is 10 milliseconds.
(2) Activation of the digital input driver and execution of software interrupt for the rapidly varying signals (i.e., cavity and nozzle pressure, surface temperatures).
(3) Building a digital input table for the rapidly varying signals.
(4) Activation of processes *pcontrol* and *tcontrol* (optional) using the C-library routine *Trigger*().

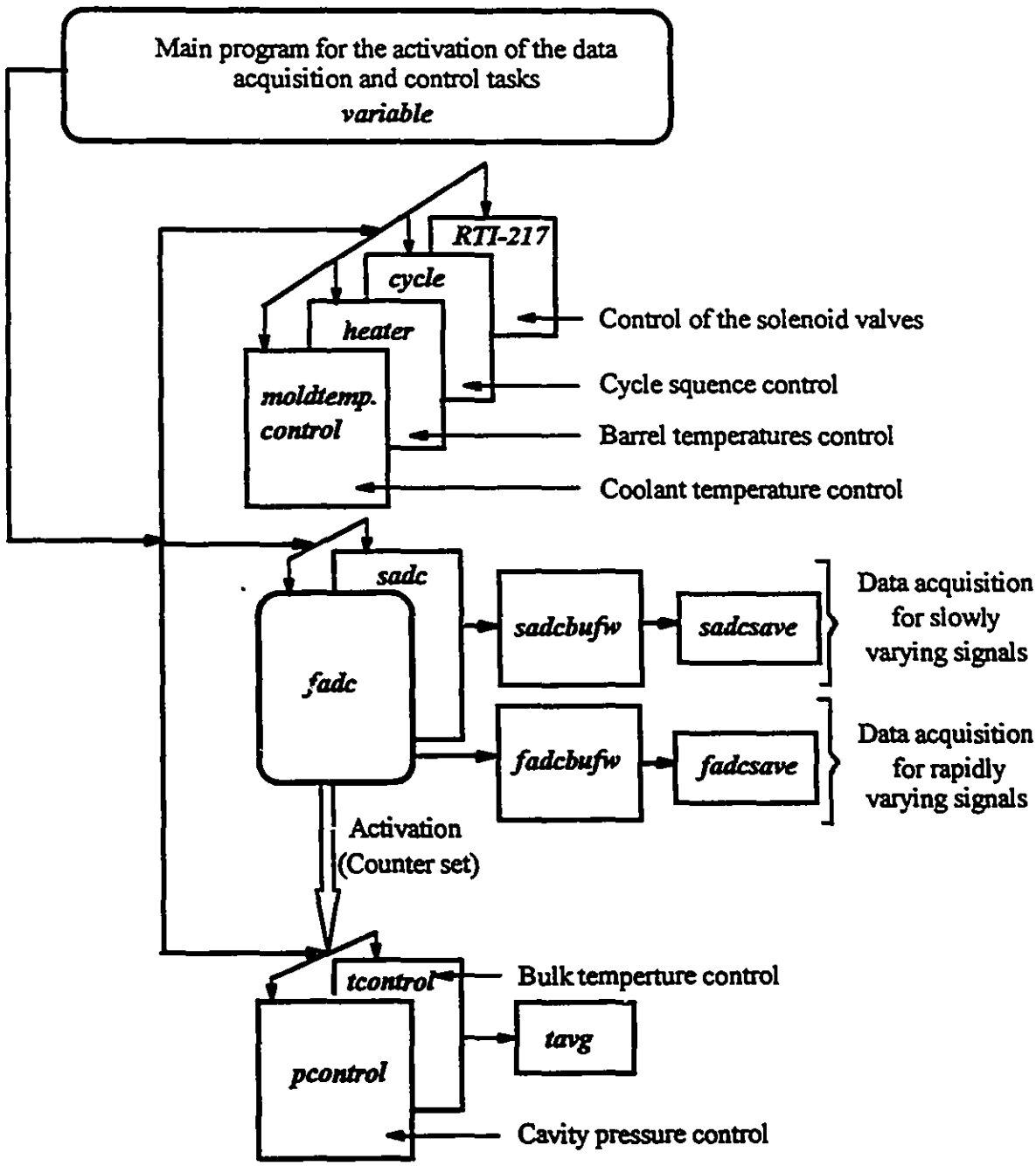

Figure 3.8 File structure showing programs for operation and control of the injection molding system.

3.4 MATERIAL AND MACHINE SETTINGS

Commercial injection molding grade polystyrene (Styron 685D, from Dow Chemical) was used in this study. The manufacturer provided the property data shown in Table 3.7. The settings for an open-loop operation of the injection molding machine consist of the following main components:

1. Coolant temperature set-point.
2. Temperature set-points for each zone of the barrel (TB1, TB2, TB3, TB4).
3. Servo-valve opening.
4. Time for each period of a cycle: injection, decompression, cooling, and open time.

The definitions and events occurring during each period are given as follows:

1. Injection: The time during which the hydraulic pressure is directed into the injection cylinder.
2. Decompression: A short interval used to reduce the melt pressure at the nozzle prior plastication. It is usually set at 1 or 2 s.
3. Cooling: Period given to the molded part after decompression.
4. Open time: Mold opening, part ejection, extruder retraction, and mold open time.

Table 3.7 Properties of polystyrene 685D from Dow Chemical

Property	ASTM Method	Units
Yield tensile strength	D638	56.5 MPa
Ultimate tensile strength	D638	56.5 MPa
Ultimate elongation	D638	2.4 %
Tensile modulus	D638	3350 MPa
Deflection temperature (annealed) @ 1.82 MPa	D648	103 °C
Vicat softening point	D1525 (rate B)	108 °C
Melt flow rate	D1238 (cond. G)	1.6 g/10 min
Specific gravity	D792	1.04

CHAPTER 4
ESTIMATION OF BULK TEMPERATURES AND PART WEIGHT FROM SURFACE TEMPERATURE MEASUREMENTS

4.1 INTRODUCTION

Three aspects of the injection molding process are of particular interest for control purposes. These are: (1) machine parameters (e.g., screw speed, back pressure, coolant temperature, barrel temperatures, cycle time); (2) process parameters (cavity pressure and temperature, nozzle pressure and temperature); and (3) quality of the molded part (dimensions, weight, strength).

Understanding the relationships between the process parameters and product quality is important for controlling production within stringent tolerance limits. The equations that describe these relationships are very complex; therefore, most work on injection molding control has focused on controlling either the cavity gate pressure (Kamal et al., 1987; Patterson et al., 1993; Smud et al., 1991), or the machine parameters such as ram velocity (Pandelidis and Agrawal, 1988). Bourdon (1991) has suggested linear regression models for statistical control of product quality. Srinivasan et al. (1992) used linear models of the holding pressure to control the part weight. Yakemoto, et al. (1993) employed the Spencer and Gilmore (1949) equation of state in estimating the part weight with parameters calculated by fitting PVT equilibrium data.

To improve product quality control, it is desirable to measure and control temperatures and pressure profiles of the polymer in the cavity. Thienel and Menges (1978), molding high impact polystyrene, used a floating thermocouple in the cavity, but this procedure has location problems and is subject to errors due to heat conduction along the thermocouple wires. Recently, Yokoi et al. (1992) reported measurements of temperature profiles obtained with a thin film thermocouple device installed inside the cavity. However, the solidifying polymer may damage this device during the packing stage. Also, this sensor is designed to be used only in molds of rectangular shape.

Because of these limitations, temperature profiles of the polymer in the cavity must be estimated. Most of the research in this area has attempted to predict the polymer-cavity temperatures either by solving the heat and momentum equations (Dupret and Vanderchuren, 1988), or by using factorial models (Richard et al., 1994). The latter are obtained from a variety of measurements, including melt nozzle temperature, nozzle pressure, cavity pressure, barrel temperatures, coolant temperature, ram velocity, and the properties of the cavity gate pressure curve.

This chapter presents a methodology to estimate the bulk temperatures inside the cavity from surface temperature measurements in combination with a heat conduction model (Varela et al, 1995). Data obtained from the analysis of the polymer surface temperature and pressure profiles are used to find parameter values of a part weight model that can be used for control purposes. The proposed treatment is valid for amorphous polymers, since the effect of latent heat of crystallization is not included in the analysis.

4.2 TEMPERATURE PROFILE MODEL

A thin rectangular cavity is considered (see Figure 4.1a) in which both the heat generation due to viscous dissipation and transport by convection occur during filling and packing. The middle plane of the cavity is at y=0 and the cavity surface is at $y = y_s$. Assuming that the polymer flow is one-dimensional and heat conduction in the x and z directions is negligible, the equation of energy balance can be written as

$$\rho C_p\left[\frac{\partial T^*(x,y,t)}{\partial t} + u_x\frac{\partial T^*(x,y,t)}{\partial x}\right] = \frac{\partial}{\partial y}\left[k\frac{\partial T^*(x,y,t)}{\partial y}\right] + \mathrm{H}_c + \Omega_v \qquad (4.1)$$

where ρ is the polymer density, C_p the specific heat, T^* the temperature of the polymer, k the thermal conductivity, H_c the latent heat (for a crystalline polymer), and Ω_v the heat generation due to viscous effects. With very thin cavities, other factors must be considered since filling behavior is dependent on cavity size.

The polymer stops flowing into the cavity at the time the gate freezes. Once the gate freezes, conduction is the dominant heat transfer mechanism. Temperature gradients along the part are small compared to those through the thickness; therefore, a one-dimensional model is a reasonable approximation to describe the melt temperature variations. The energy equation under these conditions becomes:

$$\rho C_p\left[\frac{\partial T^*(y,t)}{\partial t}\right] = \frac{\partial}{\partial y}\left[k\,\frac{\partial T^*(y,t)}{\partial y}\right] + \mathrm{H}_c + \Omega_v . \qquad (4.2)$$

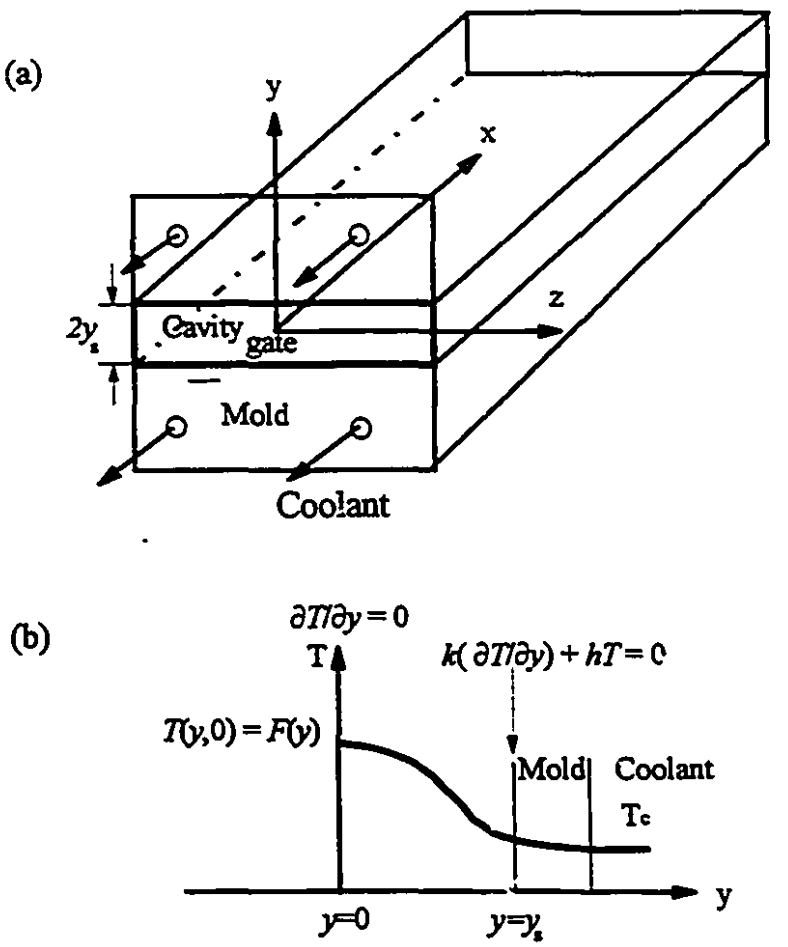

Figure 4.1 Schematic of the mold cavity showing :
(a) Coordinate system
(b) Initial and boundary conditions of the heat conduction model.

The boundary conditions are

$$\frac{\partial T^*}{\partial y} = 0 \quad \text{at } y = 0, \ t > 0$$
$$k\frac{\partial T^*}{\partial y} + h(T^* - T_c) = 0 \quad \text{at } y = y_b, \ t > 0 \tag{4.3}$$

where T_c is the coolant temperature and h the heat transfer coefficient from the polymer to the coolant.

4.2.1 Heat Conduction Model

Two properties of the cavity gate pressure curve are defined during the packing stage: the time at the end of packing (t_{peak}), and the time at which the gate freezes (t_{gf}). To derive a model describing the heat transfer during the post-packing stage, the following assumptions are made:

(1) Heat conduction in both the z and x directions is negligible.
(2) The coolant temperature (T_c) is constant.
(3) A parabolic temperature profile, $F(y)$, exists at $t=t_{peak}$ when the polymer stops flowing into the cavity. This is based on data reported for polystyrene (Yokoi et al., 1992).
(4) The pressure is uniform across the cavity thickness.
(5) The thermal diffusivity, $\alpha = k/(\rho C_p)$, and the Biot number, $B = hy_s/k$, are independent of temperature and pressure.
(6) Latent heat (H_c) and viscous heating effects (Ω_v) are negligible. Latent heat is only important with crystalline polymers.

Using these assumptions and replacing $T(y,t) = T^*(y,t) - T_c$ in Equations 4.2 and 4.3, the model describing the problem is:

$$
\begin{aligned}
\rho C_p \frac{\partial T(y,t)}{\partial t} &= k \frac{\partial^2 T(y,t)}{\partial y^2} && \text{at } t>0,\ 0<y<y_s \\
T &= F(y) && \text{for } t=0,\ 0 \le y \le y_s \\
\frac{\partial T}{\partial y} &= 0 && \text{at } y=0,\ t>0 \\
k\frac{\partial T}{\partial y} + hT &= 0 && \text{at } y=y_s,\ t>0
\end{aligned}
\tag{4.4}
$$

where $F(y)$ is the initial temperature profile at $t=t_{gf}$. Figure 4.1b displays the initial and boundary conditions of the heat conduction model

For the initial parabolic profile

$$F(y) = a - cy^2 \tag{4.5}$$

where a is the melt temperature at the cavity center, an analytical solution to this problem is available (Carslaw and Jaeger, 1959) as

$$T(y,t) = 2\sum_{n=1}^{\infty}\left[\frac{Ba\lambda_n^2 - cy_s^2[\lambda_n^2(B+2)-2B]}{\lambda_n^2(\lambda_n^2+B^2+B)\cos(\lambda_n)}\cos\left(\frac{\lambda_n y}{y_s}\right)\exp(-\lambda_n^2\alpha t/y_s^2)\right]. \tag{4.6}$$

B is the Biot number, $B = hy_s/k$, α the heat diffusivity, $\alpha = k/(\rho C_p)$ and λ_n are the positive roots of the transcendental equations

$$\lambda_n \tan(\lambda_n) = B \qquad n = 1,2,3,\ldots. \tag{4.7}$$

To avoid a lengthy iterative solution of the simultaneous Equations 4.6 and 4.7, the first six roots of Equation 4.7 were approximated as a second order polynomial function of B,

$$\lambda_n = c_{0n} + c_{1n}B + c_{2n}B^2, \qquad n = 1,2,..,6. \tag{4.8}$$

Limiting the summation to six terms does not affect the results significantly

as the relative errors of the estimated surface temperatures are less than 0.5%. Table 4.1 gives the coefficients for these equations. This approximation allows the direct substitution of Equation 4.8 into Equation 4.6.

4.2.2 Cavity Surface Temperature

At $y = y_s$ and $t = 0$, Equation 4.5 yields $c = (a - Y_o)/y_s^2$ where $Y_o = T^*(y_s,0) - T_c$. Y_o is the measured surface temperature difference at the time the gate freezes. Substituting c and y_s into Equation 4.6 yields the solution for the polymer surface temperature:

$$T_s(t,\theta) = 2\sum_{n=1}^{6}\left[\frac{2a(B-\lambda_n^2) + Y_o[\lambda_n^2(B+2) - 2B]}{\lambda_n^2(\lambda_n^2 + B^2 + B)}\exp\left(-\frac{\lambda_n^2 \alpha t}{y_s^2}\right)\right], \tag{4.9}$$

where $\theta = [a \;\; B]^T$ is the vector of parameters.

4.2.3 Average and Bulk Temperatures

For a small cavity, the average temperature at one location can be calculated from the temperature profiles across the cavity thickness. From the integral of the temperature profile, the average temperature T_{ai} at each location can be expressed as follows:

$$T_{ai} = \frac{1}{y_s}\int_0^{y_s} T(t,y)dy \;, \; i = 1,2,3\,. \tag{4.10}$$

Substitution of Equation 4.6 into Equation 4.10 leads to Equation 4.11 for the average temperature.

Table 4.1 Polynomial fit to roots of Equation 4.7

$$\lambda_n = c_{on} + c_{1n}B + c_{2n}B^2$$

c_{on}	c_{1n}	c_{2n}
1.170621	0.035448	-0.000970
3.6907396	0.082940	- 0.002166
6.5061000	0.094721	- 0.002280
9.5061511	0.088302	- 0.001991
12.590277	0.077017	- 0.001477
15.709745	0.065987	- 0.001110

$$T_{a_i} = 2\sum_{n=1}^{6}\left[\frac{2\alpha(B-\lambda_n^2) + Y_o[\lambda_n^2(B+2) - 2B)]}{\lambda_n^3(\lambda_n^2 + B^2 + B)} \tan(\lambda_n)\exp\left(-\frac{\lambda_n^2 \alpha t}{y_s^2}\right)\right]. \quad (4.11)$$

Therefore, with three temperature sensors, the bulk temperature in the cavity may be estimated as

$$T_b^* = \frac{1}{3}(T_{a1} + T_{a2} + T_{a3}) + T_c. \quad (4.12)$$

The addition of T_c is necessary to obtain the melt temperature because T_{a1}, T_{a2}, and T_{a3} are temperature differences. Cycle-to-cycle data of T_b^* and peak pressure are used for parameter estimation.

4.3 ESTIMATION OF BULK TEMPERATURES

The parameters of the heat conduction model can be calculated using transient temperature measurements at selected locations on the cavity surface. Each surface thermocouple (see Figure 3.5) gives a vector of the surface temperature measurements $Y^*(t_m)$, which is used with the measured coolant temperature T_c to obtain the data of temperature differences $Y(t_m) = Y^*(t_m) - T_c$. Because of measurement error and the assumptions used to derive the model, the predictions of $T_s(t_m)$ using Equation 4.9 will not fit the experimental values, and the errors are described by the differences

$$\varepsilon(t) = Y(t_m) - T_s(t_m, \theta), \quad m = 1,2,3,\ldots,M \quad (4.13)$$

where M is the number of measurements. The parameter vector θ can be calculated by finding the minimum of an objective function, $J(\theta)$, which is the sum of the squares of the deviations of the measured temperatures $Y(t_m)$ from

their estimates $T_s(t_m, \theta)$,

$$\min \quad J(\theta) = \sum_{m=1}^{M} \left[Y(t_m) - T_s(t_m, \theta) \right]^2 \tag{4.14}$$

4.3.1 Parameter Estimation Method

The basic approaches for the determination of the model parameters in algebraic models are the following: direct search and gradient methods. Direct search methods are attractive because they do not require the calculation of the derivatives $\partial J(\theta)/\partial \theta i$, but they only converge in well-conditioned parameter optimization problems. Well-conditioned problems are those in which the Hessian matrix ($\nabla^2 J$) is positive-definite for any valid parameter values. In this category, the best-known algorithms are attributed to Hooke and Jeeves (1961), Rosenbrock (1960), and Powell (1964). Gradient methods have proved successful in difficult and well-conditioned problems (Seinfeld and Lapidus, 1974). Detailed discussion of the theory of nonlinear estimation can be found in Walsh (1975) and Armitano et al. (1989).

The basis for the application of these algorithms is as follows. Given an estimate θ^i, a new solution θ^{i+1} is generated so that the objective function J decreases sufficiently to achieve a convergence. The formula used to find the new solution is

$$\theta^{i+1} = \theta^i + \mu^i d^i \tag{4.15}$$

where d^i is a vector oriented to reduce the objective function; μ^i is a scalar chosen between 0 and 1, and it defines the size of the step in the searching direction. Equation 4.15 is applied iteratively until a certain convergence

criterion is satisfied.

Several methods have been used to determine the direction d^i. The Newton direction is obtained from the approximation of the objective function $J(\theta)$ by a Taylor series:

$$J(\theta) = J(\theta^i) + \nabla J(\theta^i)(\theta - \theta^i) + \frac{1}{2}[\theta - \theta^i]^T \nabla^2 J(\theta^i)[\theta - \theta^i] + O\|\theta - \theta^i\|^2 \qquad (4.16)$$

where θ^i is the most recent estimate of the parameter vector. For solutions close to the optimum, the term $O\|\theta-\theta^i\|^2$ can be neglected; the differentiating Equation 4.16 with respect to θ and using the optimal criterion $\partial J(\theta)/\partial\theta = 0$, yields the Newton direction

$$\theta^{i+1} - \theta^i = d^i = -[\nabla^2 J(\theta^i)]^{-1} \nabla J(\theta^i). \qquad (4.17)$$

The Newton direction does not guarantee convergence unless the estimate θ^i is close to the minimum. In addition, this approach requires the calculation of the second derivative of J or the Hessian matrix ($\nabla^2 J$). This matrix may contain elements close to zero (singularities), which lead to numerical problems in calculating the inverse $(\nabla^2 J)^{-1}$. In iterations with a Hessian matrix which is numerically singular, this problem can be avoided using the Cauchy direction, written as

$$d^i = -\nabla J(\theta^i) \qquad (4.18)$$

The algorithm consists of the repetitive application of Equation 4.15 as summarized in the following steps:

(1) Guess the initial values $\theta_1, \theta_2, \ldots, \theta_n$

(2) Evaluate the gradient ∇J and the Hessian matrix ($\nabla^2 J$), then select the direction d^i as follows:

(a) If the Hessian matrix is nearly singular, chose the Cauchy direction $d^i = -\nabla J(\theta^i)$ and continue with Step (3).

(b) Otherwise, calculate the Newton direction $d^i = -[\nabla^2 J(\theta^i)]^{-1}\nabla J(\theta^i)$. A decrease in the objective function is guaranteed if this direction satisfies the condition $[\nabla J(\theta^i)]^T d^i \leq 0.1\|\nabla J(\theta)\|^2$, where the norm is defined as $\|\nabla J(\theta)\|^2=[\nabla J(\theta^i)]^T[\nabla J(\theta^i)]$. For the case where this condition is not satisfied, the Cauchy direction is used to update the parameter estimates.

(3) Chose the maximum positive scalar $\mu^i \in \{1, 1/2, 1/4, \ldots\}$ so that $J(\theta^i+\mu^i d^i)-J(\theta^i)\leq -0.1\mu^i[\nabla J(\theta^i)]^T d^i$, and form the updated estimate of the θ_i using Equation 4.18.

(4) Continue $|J(\theta^{i+1})-J(\theta^i)|/|J(\theta^i)| \leq \delta$ until, where δ is a predetermined tolerance (a small positive number).

The step (2b) is suggested by Armitano et al. (1989) because the Newton method converges with a reduction in the objective function that is proportional to the second norm of the gradient. This algorithm is used to find estimates of parameters of the surface temperature model given by Equation 4.9. Using these parameter estimates, Equation 4.11 and 4.12 allow the calculation of the average and bulk temperatures.

4.3.2 Average and Bulk Temperatures

The parameters in Equation 4.9 are the cavity center temperature, a, and the Biot number, $B = hy_c/k$. Thus, the gradient of J and the Hessian matrixes for $\theta^i = [\, a \; B \,]$ are:

$$\nabla J(\boldsymbol{\theta}) = \begin{bmatrix} \frac{\partial J}{\partial a} \\ \frac{\partial J}{\partial B} \end{bmatrix}, \quad \nabla^2 J(\boldsymbol{\theta}) = \begin{bmatrix} \frac{\partial^2 J}{\partial a^2} & \frac{\partial^2 J}{\partial aB} \\ \frac{\partial^2 J}{\partial aB} & \frac{\partial^2 J}{\partial a^2} \end{bmatrix} \tag{4.19}$$

Derivatives of J are obtained from Equation 4.14 as

$$\begin{aligned}
\frac{\partial J}{\partial a} &= -2\sum_{m=1}^{M}\left[T_s(t_m,\theta) - Y(t_m)\right].\frac{\partial T_s(t_m,\theta)}{\partial a} \\
\frac{\partial J}{\partial B} &= -2\sum_{m=1}^{M}\left[T_s(t_m,\theta) - Y(t_m)\right].\frac{\partial T_s(t_m,\theta)}{\partial B} \\
\frac{\partial^2 J}{\partial a^2} &= -2\sum_{m=1}^{M}\left[T_s(t_m,\theta) - Y(t_m)\right].\frac{\partial T_s^2(t_m,\theta)}{\partial a^2} - 2\sum_{m=1}^{M}\left[\frac{\partial T_s(t_m,\theta)}{\partial a}\right]^2 \\
\frac{\partial^2 J}{\partial B^2} &= -2\sum_{m=1}^{M}\left[T_s(t_m,\theta) - Y(t_m)\right].\frac{\partial T_s^2(t_m,\theta)}{\partial B^2} - 2\sum_{m=1}^{M}\left[\frac{\partial T_s(t_m,\theta)}{\partial B}\right]^2 \\
\frac{\partial^2 J}{\partial a \partial B} &= -2\sum_{m=1}^{M}\left[T_s(t_m,\theta) - Y(t_m)\right].\frac{\partial T_s^2(t_m,\theta)}{\partial a \partial B} - 2\sum_{m=1}^{M}\frac{\partial T_s(t_m,\theta)}{\partial a}\frac{\partial T_s(t_m,\theta)}{\partial B}.
\end{aligned} \tag{4.20}$$

Equation 4.9 allows derivation of the surface temperature derivatives which are given by Equations 4.21 and 4.22.

$$\frac{\partial T_s(t_m,\theta)}{\partial a} = \sum_{n=1}^{6}\frac{2(B-\lambda_n^2)}{\lambda_n^2(\lambda_n^2+B^2+B)}.\exp\left(-\frac{\lambda_n^2 \alpha t_m}{y_s^2}\right)$$

$$F_n = \frac{2a(B-\lambda_n{}^2 + Y_o[\lambda_n{}^2(B+2) - 2B]}{\lambda_n{}^2(\lambda_n{}^2+B^2+B)} \tag{4.21}$$

$$E_n = \exp\left(-\frac{\lambda_n{}^2 \alpha t}{y_s{}^2}\right)$$

$$\frac{\partial T_s(t_m,\theta)}{\partial B} = \sum_{n=1}^{6}\left[E_n\frac{\partial F_n}{\partial B} + F_n\frac{\partial E_n}{\partial B}\right]$$

$$\delta_n = \lambda_n^2(\lambda_n^2 + B^2 + B)$$

$$\zeta_n = \lambda_n\frac{\partial \lambda_n}{\partial B}$$

$$\eta_n = 2\zeta_n(\lambda_n^2 + B^2 + B) + \lambda_n^2(2\lambda_n\zeta_n + 2B + 1) \qquad (4.22)$$

$$\frac{\partial F_n}{\partial B} = \frac{1}{\delta_n}\Big[2a(1-2\zeta_n) + Y_o[\,2\zeta_n(B+2) + \lambda_n^2 - 2\,] - 2a(B-\lambda_n^2) + Y_o[\,\lambda_n^2(B+2) - 2B\,].\eta_n\Big]$$

$$\frac{\partial E_n}{\partial B} = -2\zeta_n\exp\left(-\frac{\lambda_n^2\alpha t_m}{y_s^2}\right)\frac{\alpha t_m}{y_s^2}$$

Application of the algorithm to estimate the heat conduction parameters requires data of surface temperature-time and pressure-time profiles for each cycle. Once these data are collected, the following steps will yield the average ($T_{a\ell}$) and bulk (T_b^*) temperatures:

(1) Estimation of parameters (a_1, a_2, a_3) and (B_1, B_2, B_3) of the surface temperature profile model, Equation 4. 9, for all cycles in the interval $[0, (t_{gf} - t_{peak})]$ using the gradient method described above.

(2) Calculation of the average temperatures $T_{a\ell}$ at the three sensor locations at $t = t_{gf}$ for all cycles using Equation 4.11.

(3) Calculation of the bulk temperature T_b^* using Equation 4.12.

4.4 PART WEIGHT MODEL

The part weight can be calculated (Varela et al., 1966) by

$$W = \frac{V_c}{v(p,T_b^*)}, \tag{4.23}$$

where V_c is the cavity volume; $v(p, T_b^*)$ is the average specific volume evaluated at the time when the gate seals, and p and T_b^* are the pressure and bulk temperature, respectively. Since the polymer occupies the whole cavity when the gate freezes, the ratio of the cavity volume (V_c) to the sample weight (W) gives a measurement of the specific volume for the molded part.

The specific volume data are fitted to the Tait equation, which is appropriate for amorphous polymers in the melt and the glassy states (Zoller, 1989). This equation is written as

$$v(p,T_b^*) = v_o(T_b^*)\left[1 - C\ln\left(1 + \frac{p}{D(p)}\right)\right] \tag{4.24}$$

where $v_o(T_b^*)$ is the specific volume at atmospheric pressure, which is generally expressed by the polynomial

$$v_o(T_b^*) = a_0 + a_1 T_b^* + a_2 (T_b^*)^2 \tag{4.25}$$

There is no theoretical basis for selecting an appropriate model of D. In the conventional form of the Tait equation of state. D depends on temperature only: $D(T) = D_o\exp(-D_1 T)$. However, at the transition between the glass and liquid states, D also depends on pressure (Quach and Simha, 1971). Preliminary results showed that it is a decreasing function of p. The

expression selected for D is

$$D(p) = \frac{d_0 + d_1 p}{1 + d_2 p}. \tag{4.26}$$

Analysis of the cavity pressure curves with the application of the methodology for estimating the average temperatures from surface temperature profiles, for each cycle, yields p, v, and T_b^*. Fitting these data to the Tait equation gives the parameters a_o, a_1, a_2, d_o, d_1, and d_2. The estimated parameters, bulk temperatures, and peak pressure are then used to calculate part weight by applying Equations 4.23-4.26.

4.5 EXPERIMENTAL CONDITIONS

Preliminary experiments with different injection times showed that a minimum injection time of 13 s was required to have the gate seal before releasing the holding pressure. The injection time includes the filling, packing, and holding stages. The time settings for the decompression and cooling stages were 10 and 2 seconds, respectively. Sampling periods of 0.04 s and 0.20 s were employed in the injection and cooling stages, respectively. Tables 4.2 and 4.3 summarize the conditions employed during the various experiments.

The experimental conditions used to estimate parameters of the part weight model are shown in Table 4.2. They were selected to create significant variations in peak pressure, bulk temperature, and part weight, to calculate parameters of the part weight model. Variations in machine parameters such as coolant temperature, barrel temperature near the nozzle, and supply servo-valve opening yielded the required data for parameter estimation.

Table 4.2. Experimental conditions for parameter estimation

Experiment	Barrel temperature set-points (°C)	Range of Coolant Temperature (°C)	Range of servo-valve opening (%)
P-1	250/220/200/190	45-48	50 to 75, square wave with 10 cycles period.
P-2	280/220/200/190	42-48	50 to 75, square wave with period of 10 cycles

Table 4.3 Experimental conditions for validation of part weight model

Experiment	Barrel temperature set-points (°C)	Range of Coolant Temperature (°C)	Range of servo-valve opening (%)
V-1	250/220/200/190	43-48	50 to 75 opening every 5 cycles
V-2	280/220/200/190	40	50
V-3	290/220/200/190	40	50

Figure 4.2 shows the cycle-average coolant temperature (not controlled) for Experiment P-1. Step changes between 50% and 75% in the supply servo-valve opening were used for Experiments P-1 and P-2, as shown in Figure 4.3a. Table 4.3 presents machine parameters for experiments conducted to validate the part weight model. The supply servo-valve opening was set at 50% with pulses at 75% every five cycles in Experiment V-1, and fixed at 50% in Experiments V-2 and V-3. Figure 4.3b shows cycle-to-cycle servo-valve settings for Experiment V-1.

4.6 RESULTS AND DISCUSSION

Typical variations of pressure over time at the gate, middle cavity, and nozzle, and of cavity surface temperatures are shown in Figures 4.4 and 4.5, respectively. The differences between the cavity gate pressure and middle cavity pressure, shown in Figure 4.4, suggest that the polymer starts to solidify inside the cavity before it does near the gate. As shown in Figure 4.5, there are differences in the rate of cooling and surface temperature profiles among the measurements at the three sensor locations. These are due to unbalanced cooling in different portions of the molded part, and to the earlier solidification of the polymer at sensor location TS3 (see Figure 3.5).

4.6.1 Gate Seal Time

In this work, the gate seal time is determined by maintaining the injection time until the cavity pressure is not affected by the release of the hydraulic pressures at the end of the holding stage. At the gate seal time, solidification of the polymer in the sprue and runner may occur. The nozzle and cavity pressure time profiles were measured for injection times from 10s

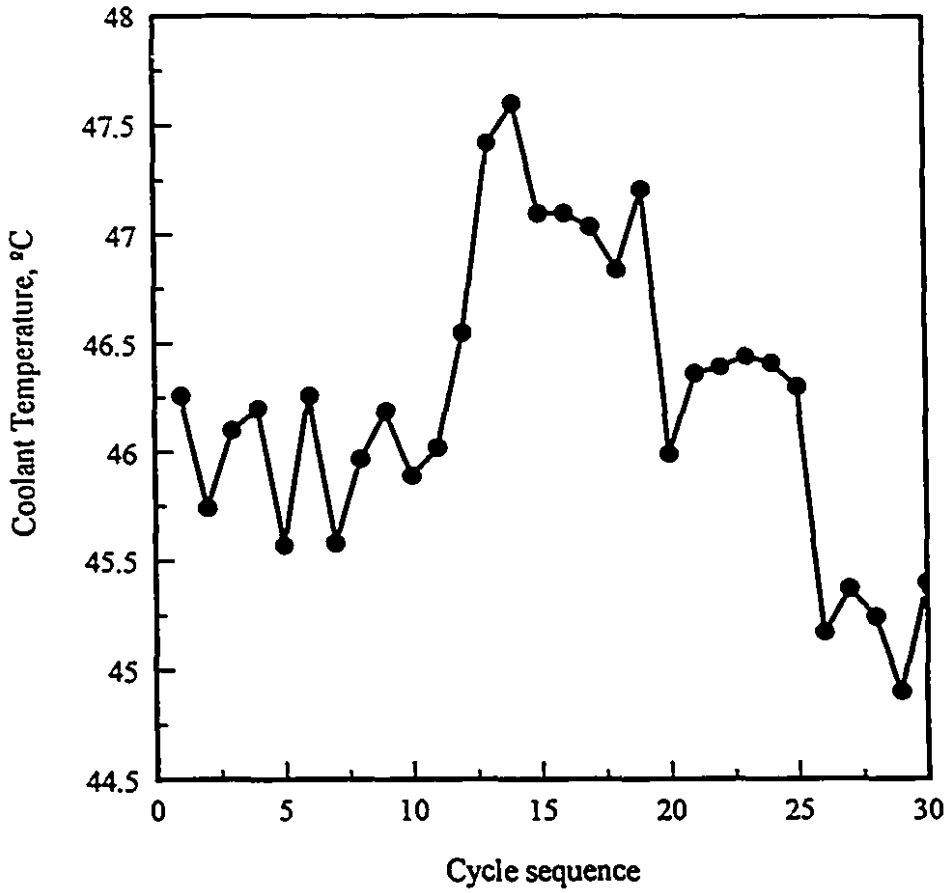

Figure 4.2 Cycle-to-cycle variations in the inlet coolant temperature for Experiment P-1.

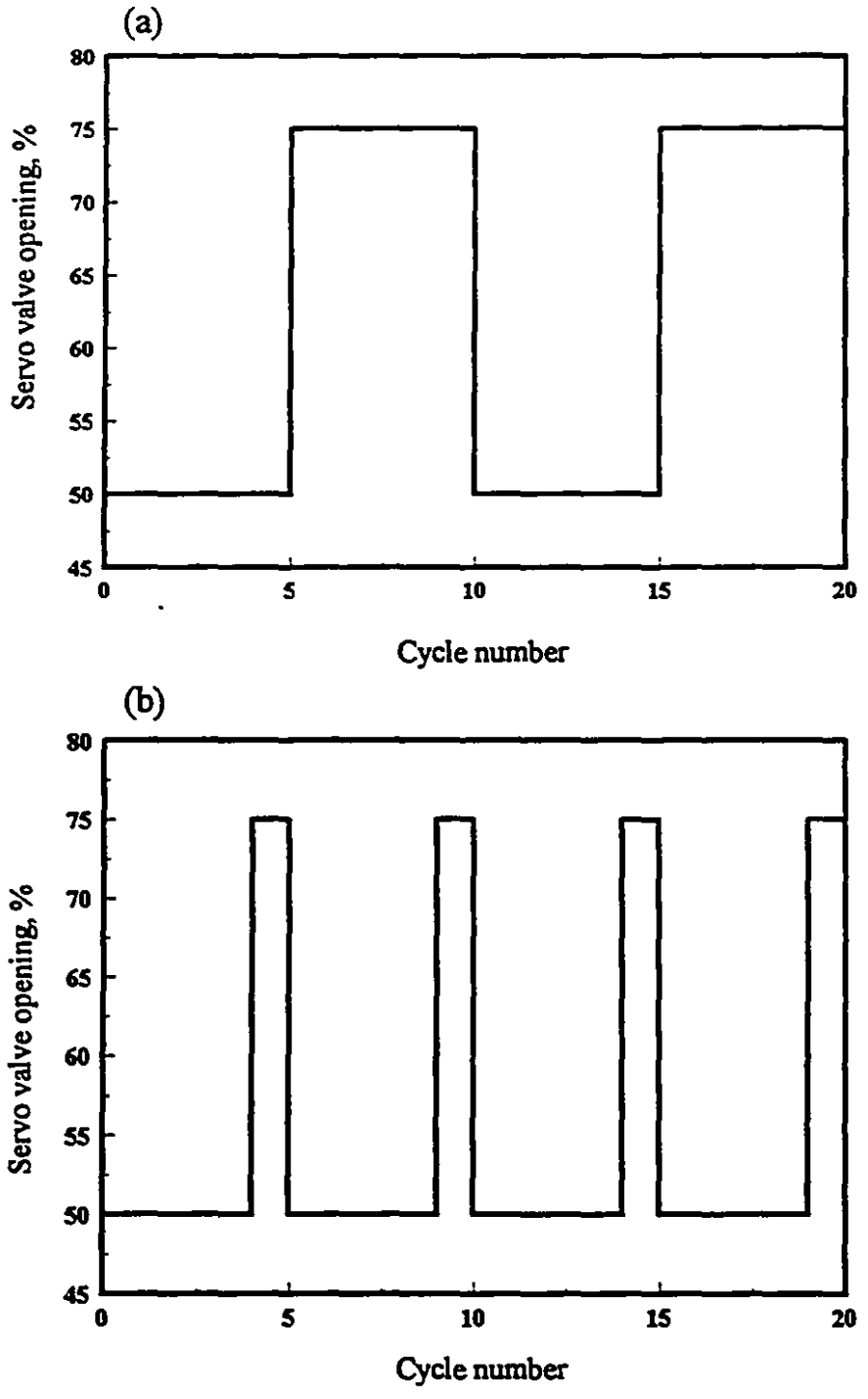

Figure 4.3 (a) Changes in supply servo-valve opening in Experiments P-1 and P-2.
(b) Changes in supply servo-valve opening in Experiments V-1.

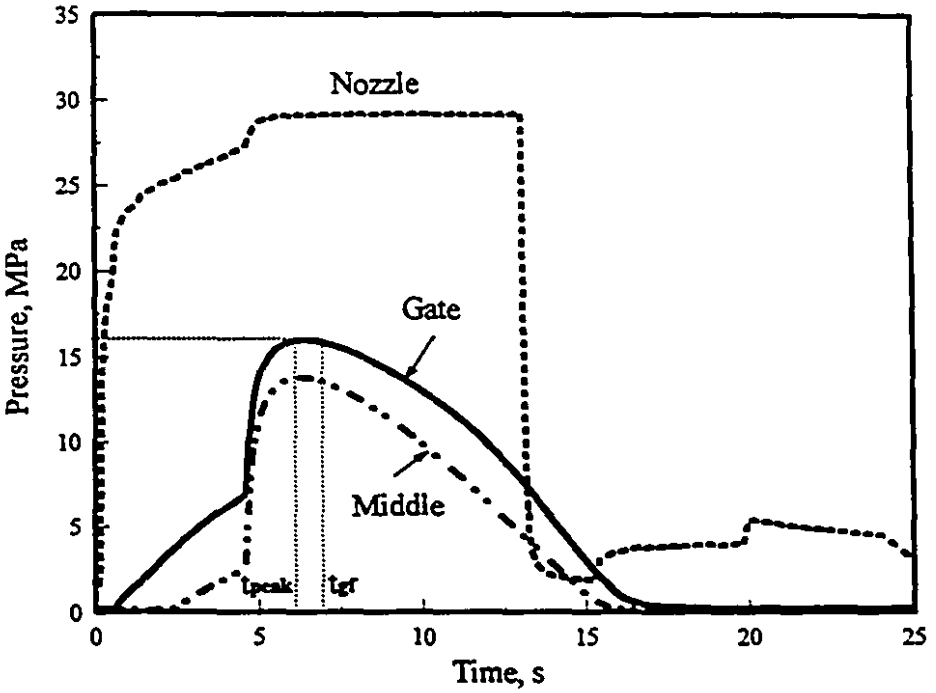

Figure 4.4 Nozzle, mid-cavity, and cavity gate pressure in cycle 1 . for Experiment P-1.

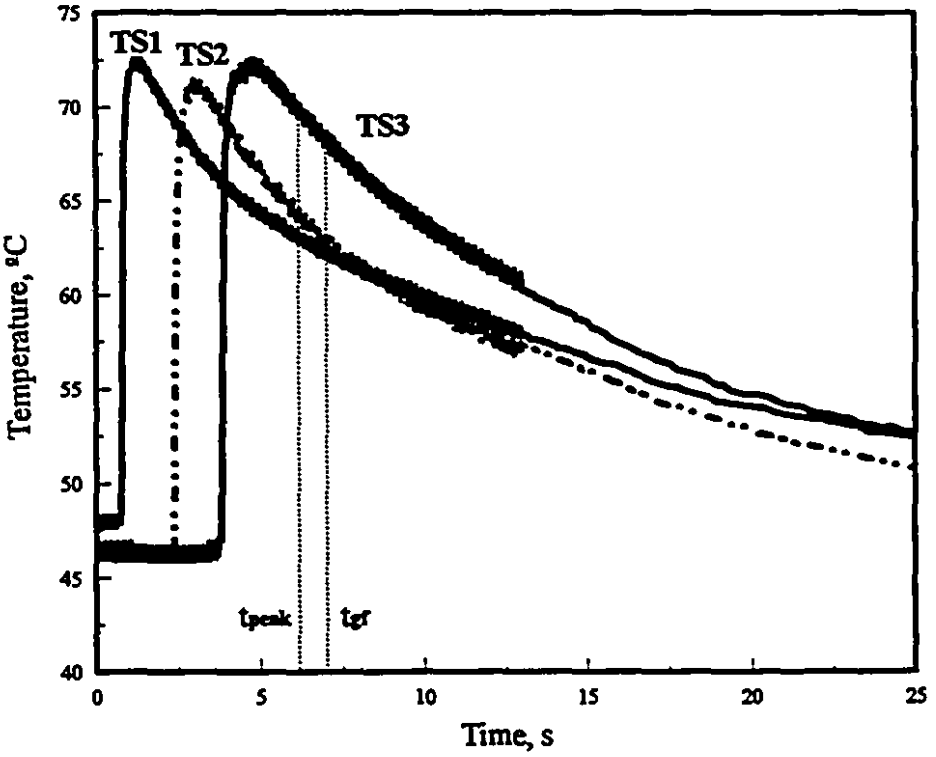

Figure 4.5 Melt surface temperature profiles at three sensor locations in cycle 1 for Experiment P-1.

to 16s. Figures 4.6a and 4.6c show that the gate seals for injection times of 13s and 16s, respectively. On the other hand, the gate does not seal for an injection time of 10 s, as seen in Figure 4.6b. This is shown by the fact that the nozzle and cavity pressure drop simultaneously at the end of holding. Consequently, the injection time was set at 13 s in the experiments for the analysis and control of part weight.

4.6.2 Bulk Temperatures

A thermal diffusivity value of 6.6×10^{-8} m^2/s (Rudd, 1989) was used in calculating the parameters for the temperature profile model. Figure 4.4 shows that the interval (t_{peak}, t_{gf}) for polystyrene is very short. However, the proposed methodology is applicable for longer periods. For example, if t_{gf} is taken as the time the cavity gate pressure drops 1.38 MPa (200 psia) below the peak value, the estimated surface temperatures agree with the measured values, as shown in Figures 4.7 and 4.8. The results of the estimated cavity center temperatures and heat transfer coefficients are compared with values reported in the literature in Appendix C. This confirms the adequacy of the proposed methodology for estimation of cavity polymer temperatures.

The mean absolute errors between the measured and calculated surface temperature, for the three sensor locations, were less than 0.3 C, and the standard deviations were less than 0.2 C. The thermal properties of the polymer may change if cavity pressure drops significantly. Therefore, the gate seal time (t_{gf}) was selected as the point at which the cavity gate pressure drops by about 0.069 MPa (10 psia). With this criterion, the intervals (t_{peak}, t_{gf}) were found to vary from 0.4 to 0.6 s. Using higher pressure drops to define the time the gate seals yields longer cooling times.

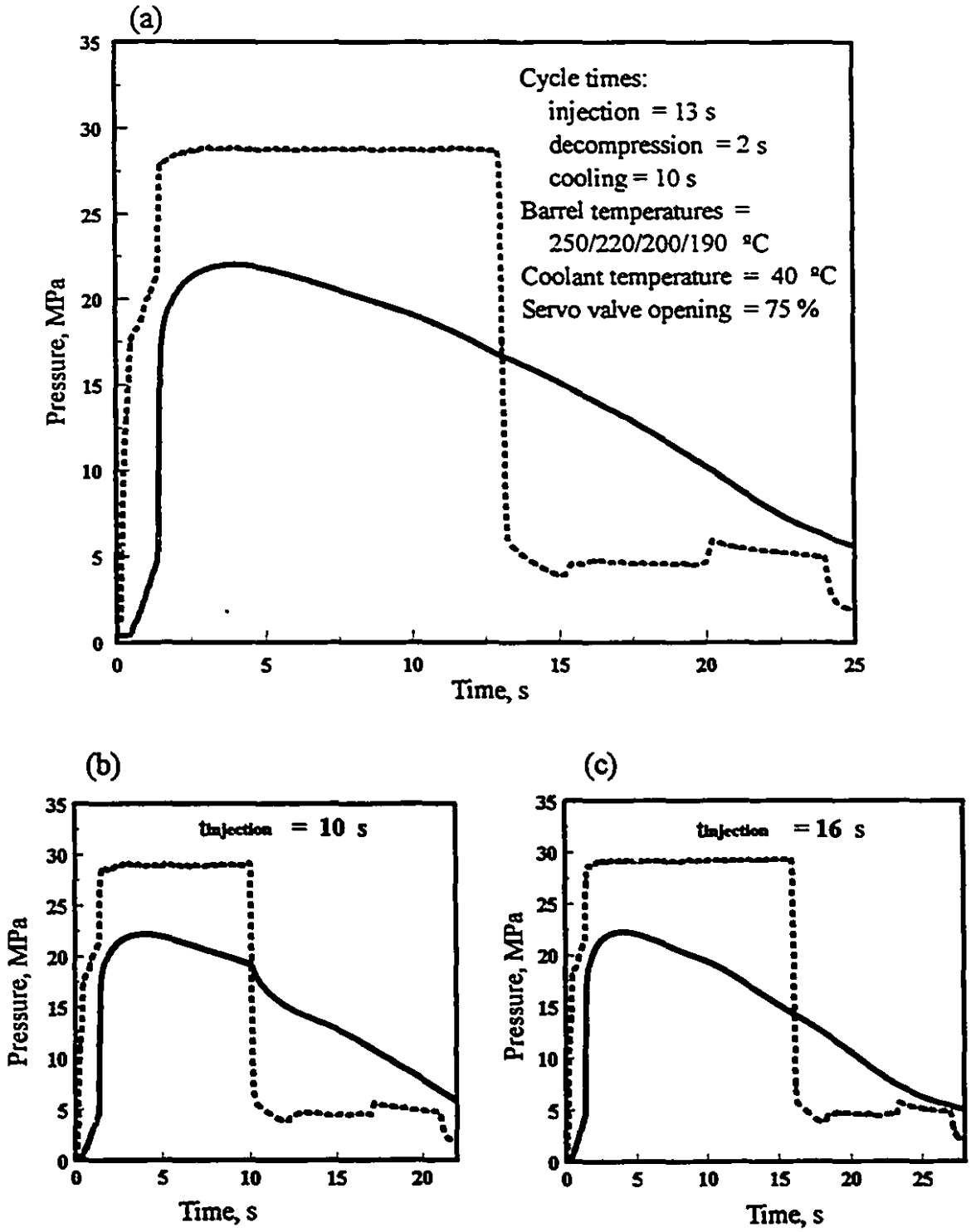

Figure 4.6 Nozzle and cavity gate pressure profiles for three injection times.

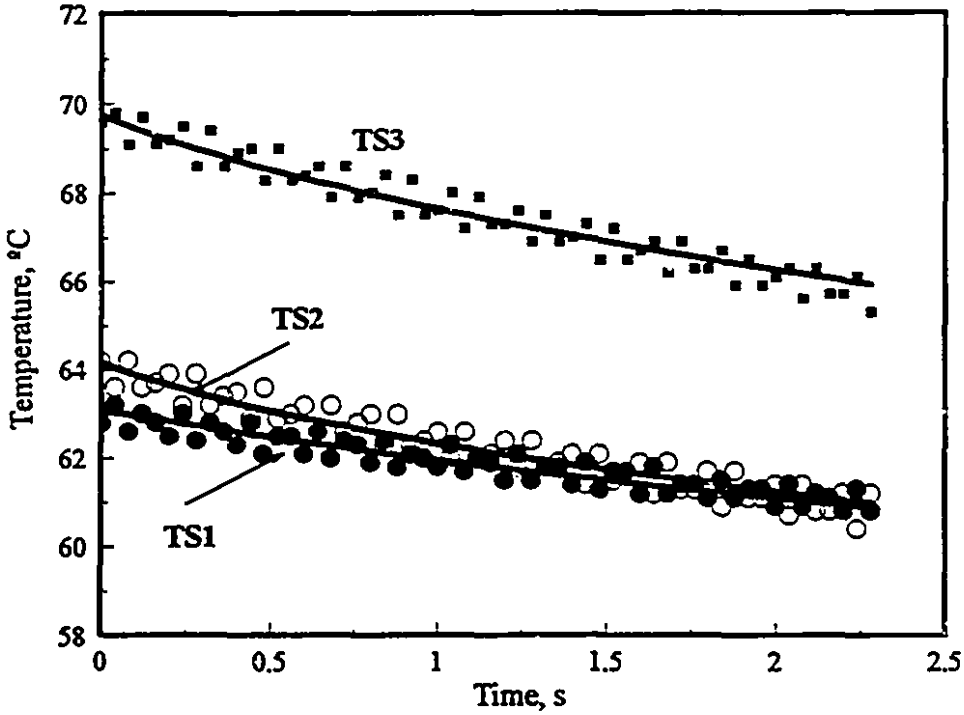

Figure 4.7 Measured and estimated polymer surface temperature at three sensor locations in cycle 1 of Experiment P-1.

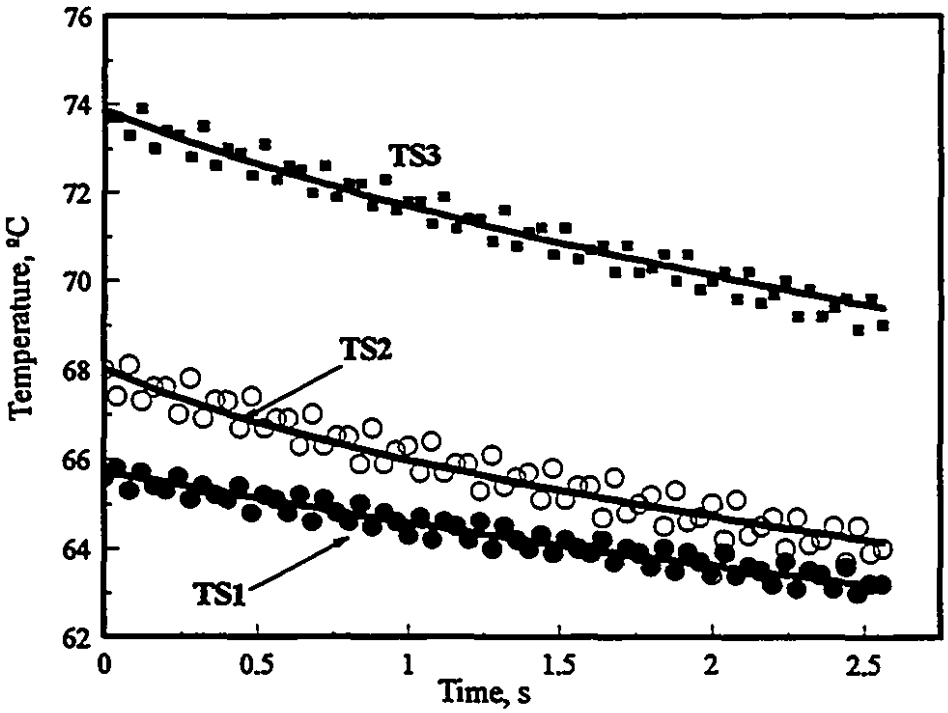

Figure 4.8 Measured and estimated polymer surface temperature at three sensor locations in cycle 30 of Experiment P-1.

Figures 4.9 and 4.10 show cycle-to-cycle variations in peak pressure and bulk temperatures for Experiments P-1 and V-1. In Figure 4.9, changing the supply servo-valve opening in a square wave sequence produces large variations in peak pressure and bulk temperatures in cycles 1 to 12. The temperature and pressure drop simultaneously, but the subsequent variations are lower as the system approaches a steady oscillating condition. Failure of the supply servo-valve to maintain the specified opening resulted in short shots for cycles 10 and 11. When the coolant temperature and servo-valve opening are held constant as in Experiment V-1, Figure 4.10, temperature and pressure change in opposite directions during the first 10 cycles, after which both increase.

4.6.3 Part Weight

The molded part is separated from the runner and sprue by cutting each sample through the gate along the upper edge of the molded piece (see Figure 3.5). An electronic balance, METLER PJ4000 with a precision of 0.0001g, was used to weigh the parts. Graphs of part weight for Experiments P-1 and V-2 are shown in Figures 4.11 and 4.12, respectively. In Experiment V-2, with the fixed servo-valve opening, the standard deviation of part weight was 0.0570 g. The high variation in weight during early cycles occurs because the temperature of the melt injected into the cavity is higher than those of the subsequent cycles. In consequence, more polymer mass enters the cavity.

In the estimation of part weight with Equations 4.23 and 4.24, p is taken to be the peak pressure measured with the pressure transducer flush with the cavity surface near the gate; T_b^* is the estimated bulk temperature of the polymer in the cavity. Measuring the average cavity pressure is difficult because of the effect of the solid skin on sensor readings. This is

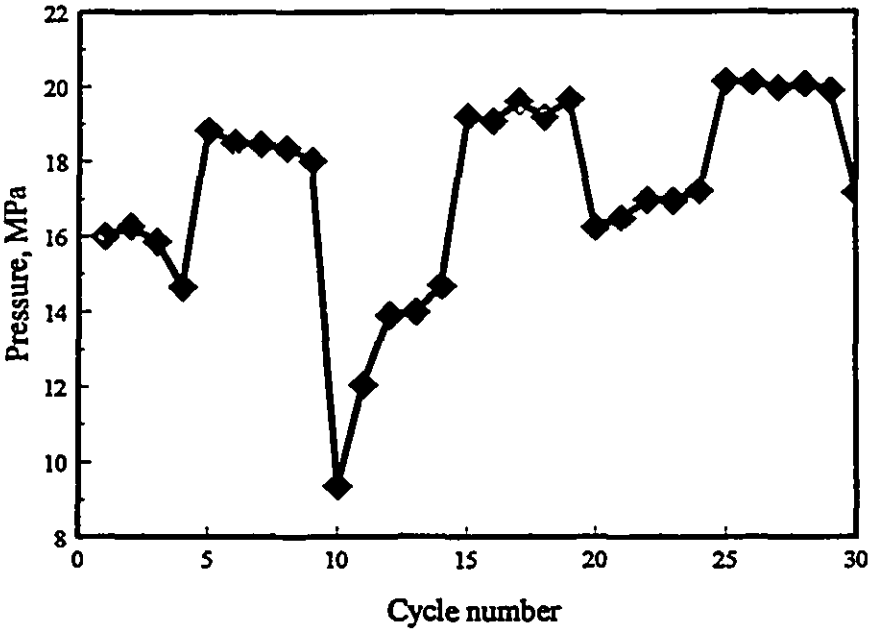

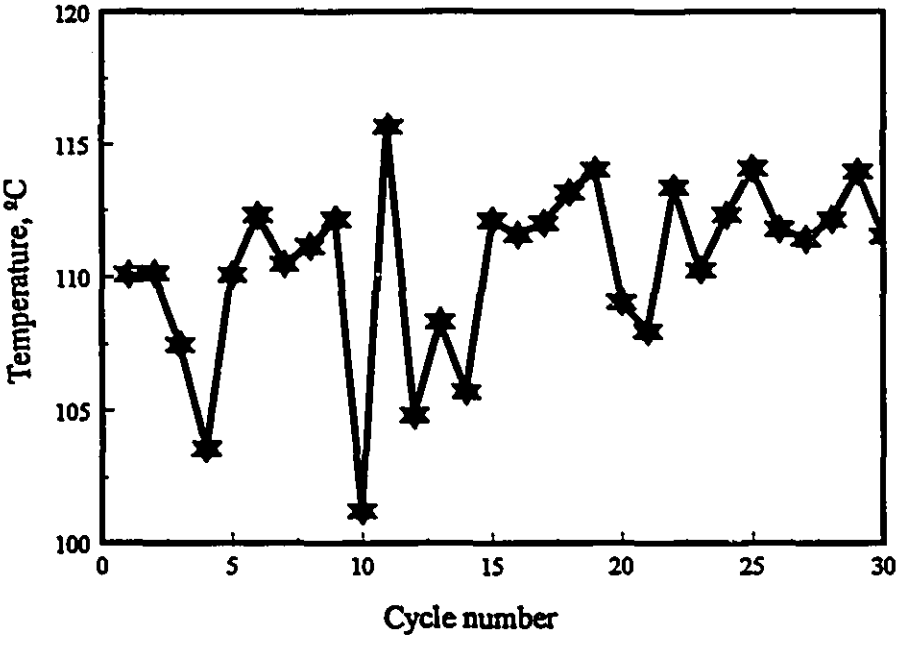

Figure 4.9 Variations in peak pressure and bulk temperature for Experiment P-1.

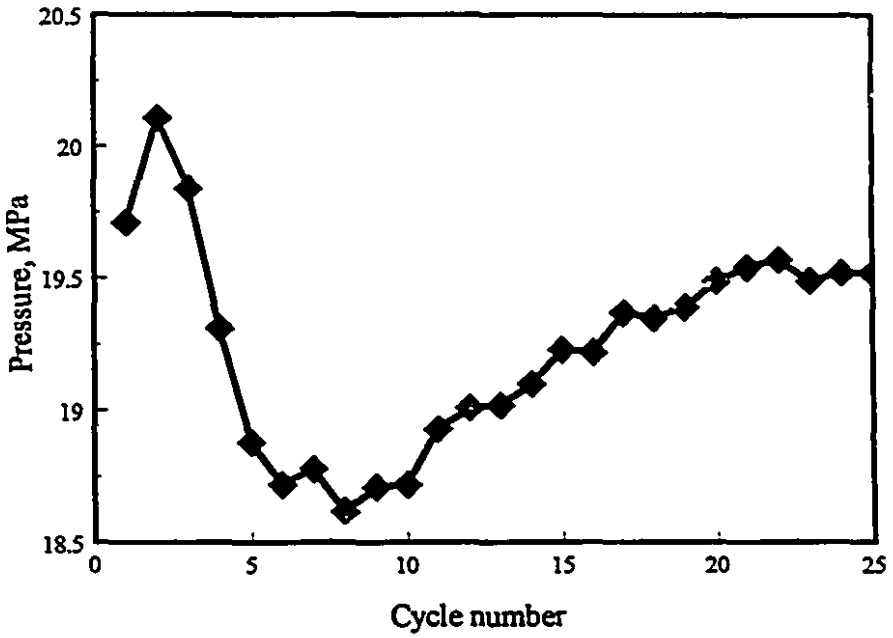

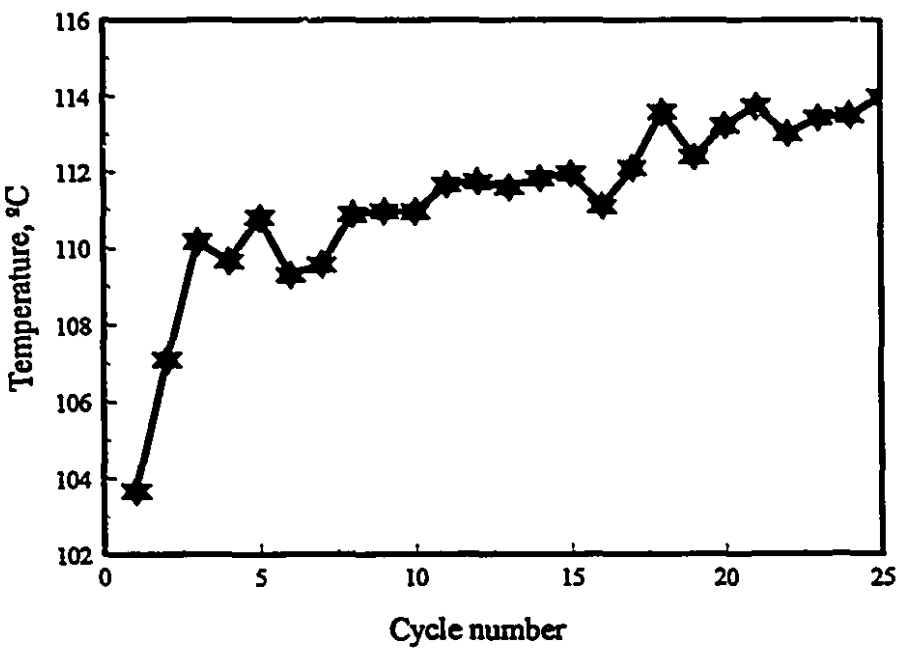

Figure 4.10 Variations in peak pressure and bulk temperature for Experiment V-1.

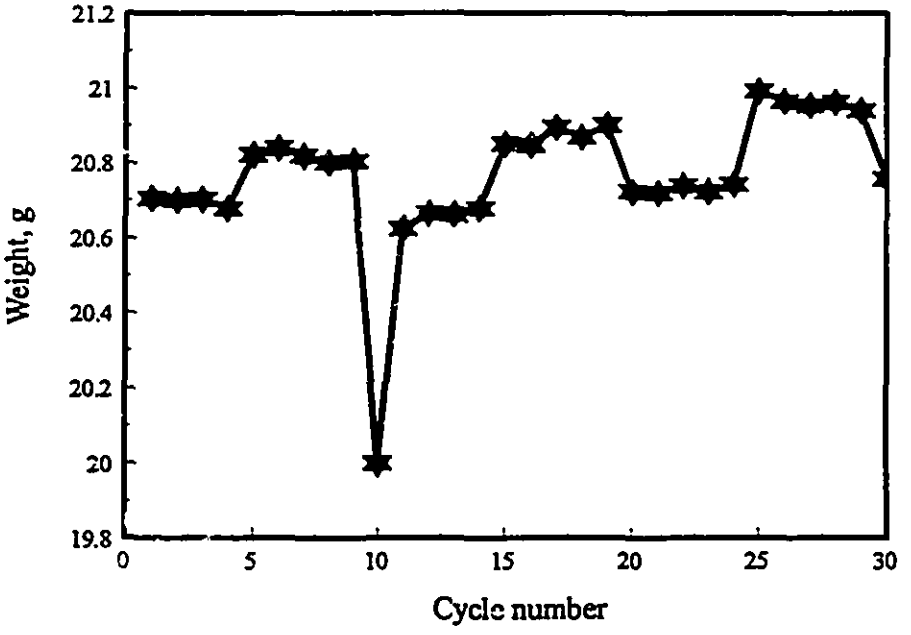

Figure 4.11 Variations in part weight for Experiment P-1.

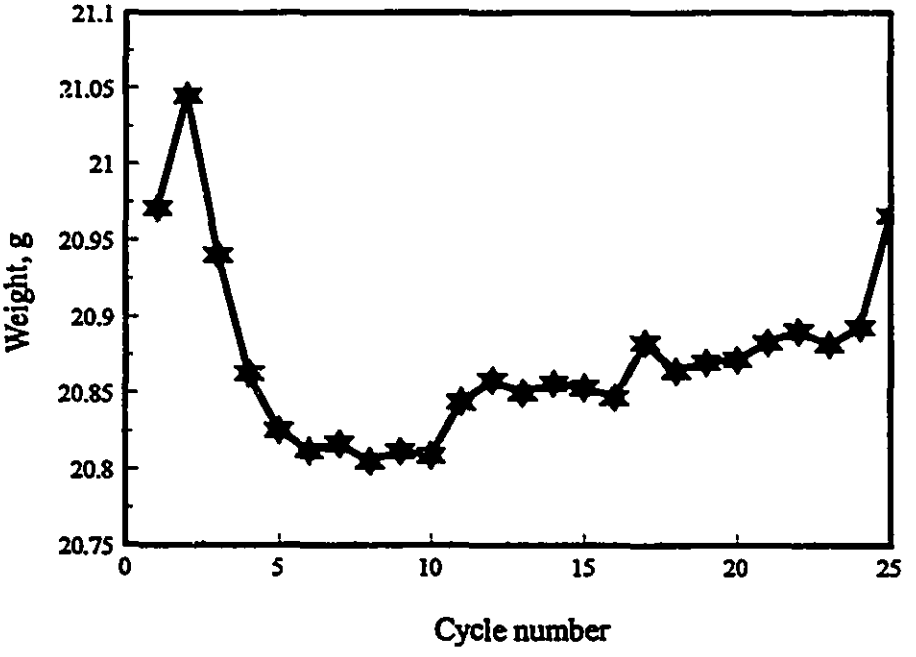

Figure 4.12 Variations in part weight for Experiment V-2.

illustrated by the appreciable difference between the pressure at the gate and at the cavity center, shown in Figure 4.4. Therefore, the pressure at the gate gives a better measurement of the average cavity pressure, since solidification occurs later at the gate than at other positions in the cavity.

Parameters $a_o, a_1, a_2, d_o, d_1,$ and d_2 given in Table 4.4 were estimated using PvT_b^* values from Experiments P-1and P-2. The estimated parameters were substituted into Equations 4.24 and 4.25 to find v, which in turn was used to calculate the part weight according to Equation 4.23. Part weight values thus estimated are very close to the measured values, as can be seen in Figure 4.13. Part weights predicted by the model and those obtained in Experiments V-1, V-2 and V-3 are shown in Figure 4.14.

Model predictions of part weight are generally very good; the mean absolute error with respect to measured values was 0.02 g. They differ from experimental values in the first five cycles of each experiment when the delivery system and cavity walls are cool, and the melt at the nozzle is at a higher temperature than those of subsequent cycles. The high variations in part weight in Experiment V-3, even with a constant servo-valve opening and controlled coolant temperature, were associated with greater temperature variations in the nozzle.

Figure 4.15 depicts a three-dimensional diagram derived from T_b^*Wp data for Experiments P-1 and P-2. This plot shows the effect of variations in bulk temperature and peak pressure on part weight; it suggests that part-weights show low fluctuations for peak pressure around 22 MPa and bulk temperatures of 115°C. High peak pressures are associated with high injection rates, which cause higher bulk temperatures because the injection times are shorter. The bulk temperature ranges from 112 °C to 118 °C. The

Table 4.4 Parameters of the Tait equation of state

C = 0.0894 (from Zoller, 1989)

a_o = 0.8614 cm^3/g

a_1 = 1.604×10^{-3} (cm^3/g) $°C^{-1}$

a_2 = -6.530×10^{-6} (cm^3/g) $°C^{-2}$

d_o = 1.517×10^5 MPa

d_1 = -6.187×10^3

d_2 = 18.22 MPa^{-1}

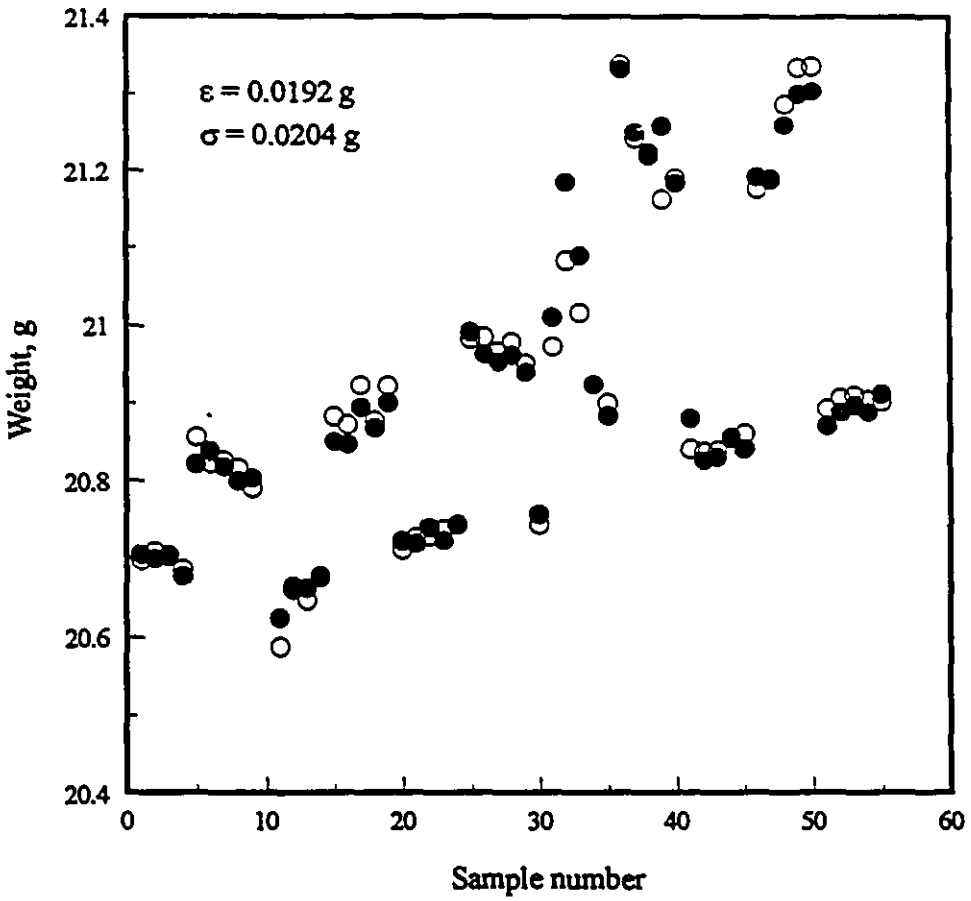

Figure 4.13 Fitting pWT_b^* data to Tait equation for Experiments P-1 and and P-2. Measurement (○), estimation (●). ε and σ are the mean and standard deviation of the absolute errors.

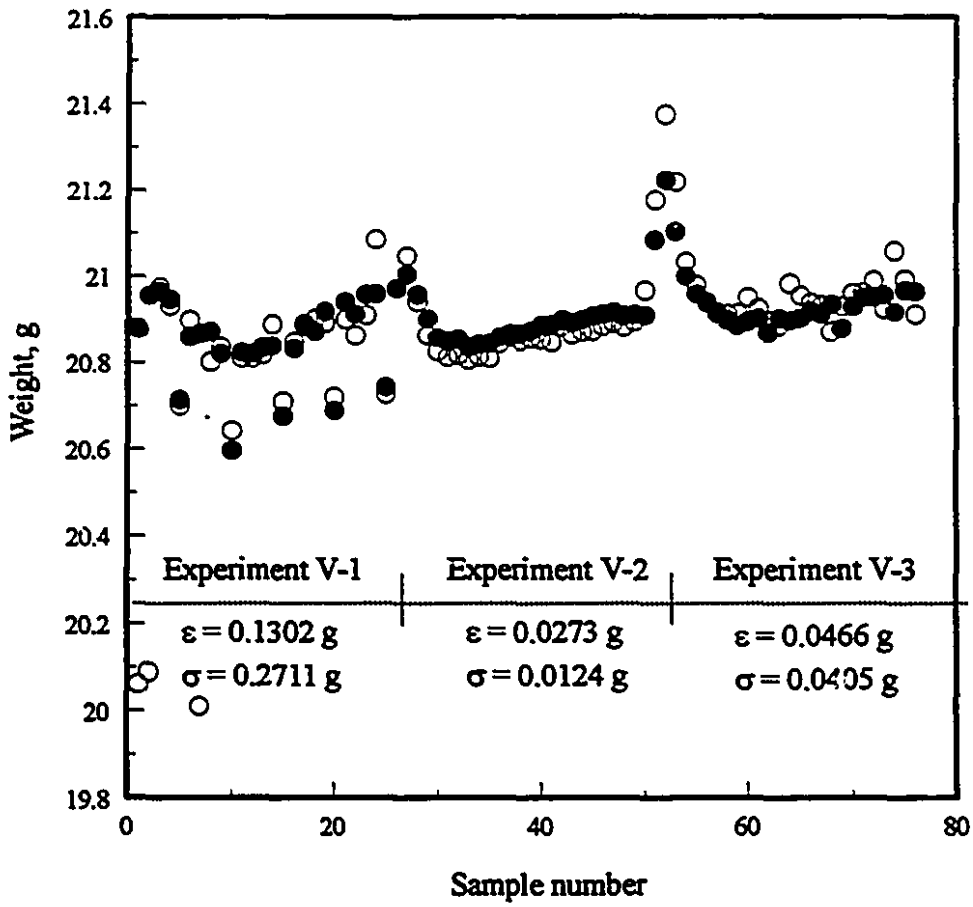

Figure 4.14 Model validation with data of Experiments V-1, V-2, and V-3. Measurement (○), estimation (●). ε and σ are the mean and standard deviation of the absolute errors.

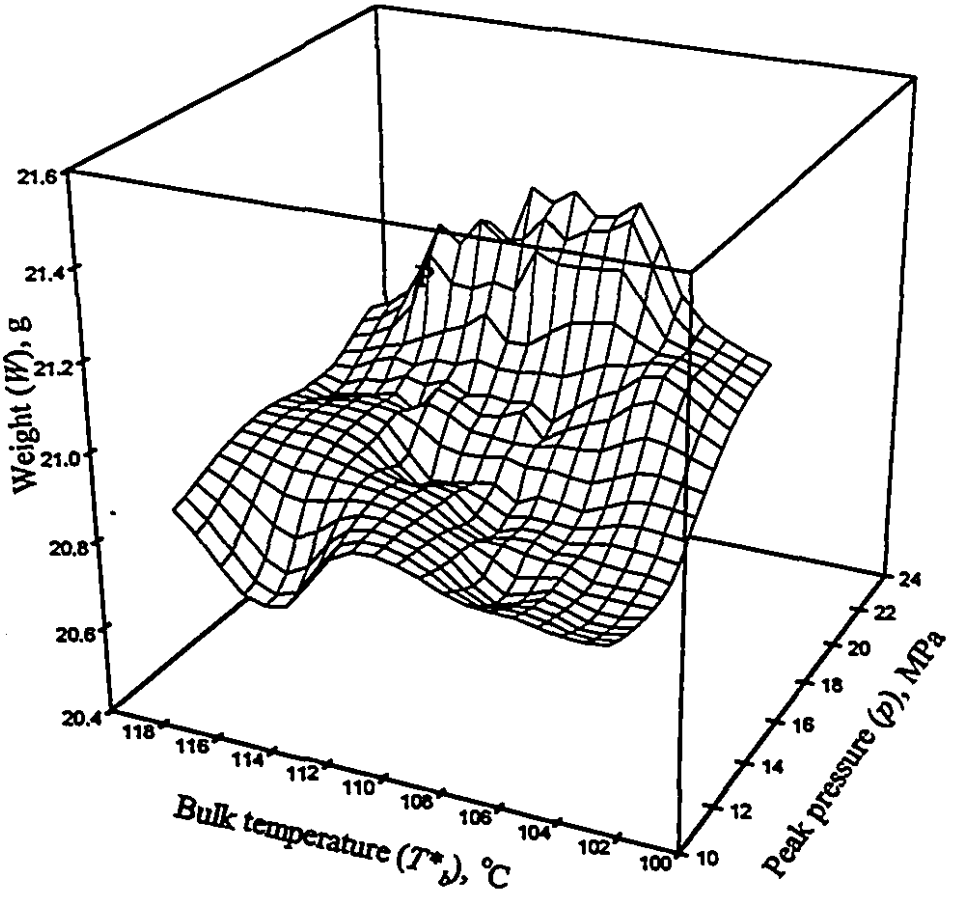

Figure 4.15 pWT^*_b three-dimensional molding diagram from data of Experiments P-1 and P-2.

depressions observed in the Figure at low temperatures may be attributed to measurement errors in the peak pressure and in the bulk temperature estimation, as well as incomplete mold filling caused by a malfunction of the servo-valves.

4.7 SUMMARY

A practical methodology for estimating bulk temperatures in the injection molding cavity and part weight has been developed. This methodology is based on solving the heat transfer problem in the injection molding cavity at the end of the packing stage. A parabolic profile was assumed and found suitable for polystyrene. The proposed approach may be used for on-line estimation of temperature profiles of the polymer in the cavity, part weight, and in constructing pWT_b^* diagrams. The results of the models used to estimate surface temperatures and weights of the molded parts are in good agreement with experimental data.

CHAPTER 5
CAVITY PRESSURE CONTROL

5.1 INTRODUCTION

The cavity pressure experienced during injection molding is a primary factor affecting the final part quality. The idea behind using control strategies for the hydraulic or cavity pressure is to maintain the melt-flow into the cavity at a constant pattern. Changes in the flow pattern produce cycle-to-cycle fluctuations in bulk temperature and cavity pressure. These variations may cause warpage due to residual stresses, as well as significant changes in the physical properties of parts with tight tolerance limits.

Several algorithms have been proposed to control the pressure in different sections of the injection molding process. Kamal et al. (1987) have presented a comprehensive study on the application of PI, PID, and Dahlin algorithms for the cavity pressure control, as well as in the nozzle and injection cylinder. Costin et al. (1987) used the self-tuning algorithm to control the hydraulic pressure profile with respect to the ram position. Gao (1993) used the same technique to control the cavity pressure with respect to the injection time during the filling and packing stages. Chiu (1991), Smud (1991), and Srinivasen et al. (1991) have used other adaptive control algorithms.

Controlling the pressure in cavities with small gates and runners during the injection molding of an amorphous polymer is difficult. This is due to the fact that the process is usually fast (the filling and

packing stages in this work take about three seconds), time-varying, and nonlinear. In addition, during the packing and holding stages the response to changes in the manipulated variable, usually the servo-valve opening, diminishes when the melt starts to solidify. Thus, considering the time-varying characteristics of the filling and packing stages, a self-tuning-control (STC) strategy was selected to control the cavity pressure profile at a specified trajectory.

5.2 CAVITY PRESSURE DYNAMICS

Dynamic models which may include shear thinning, viscoelastic, and thermal behaviour are usually written as a system of coupled partial differential equations of momentum and energy balances. As discussed in Section 2.2.2, numerical and analytical methods have been used extensively to solve these equations. In this area, the work of Lord and Williams (1975) and Kamal and Lafleur (1982) is particularly significant. Numerical simulations which include the hydraulic system have been presented by Rafizadeh et al. (1995). Simple models based on force and mass balances have been proposed by other researchers (Shankar and Paul, 1982, Chiu et al., 1991 and Wei et al.1994). These consider relationships between the hydraulic pressure and the input signal to the supply servo-valve.

The work in this chapter attempts to use a simple model with time-varying coefficients to account for the transient and complex processes experienced during the filling and packing stages. Kamal et al (1987) and Gao (1993) have discussed the occurrence of parameter variations with identification models. Adaptive control algorithms are

therefore effective approaches to regulate the cavity pressure profile.

5.2.1 Deterministic Model

An illustration of the process is given in Figure 5.1, where u is the control variable, the servo-valve opening, and p_h, p_n, and p refer to the hydraulic, nozzle and cavity gate pressure, respectively. Time- pressure profiles obtained in a dynamic experiment, for the injection molding of polystyrene, are shown in Figure 5.2. Here, the servo-valve opening was changed in a square-wave pulse train between 0.5% and 75%. At short times and for each step change, the curves of the hydraulic and cavity pressure may be interpreted as responses of the system to a fixed input, the supply servo-valve opening. The following derivation assumes that the polymer has already filled the delivery system, sprue, and runner. The hydraulic oil pressure response to a fixed servo-valve opening (u) is assumed to be described by a first- order model:

$$\tau_h \frac{dp_h}{dt} + p_h = K_h u \tag{5.1}$$

The increase in pressure during the experiment suggests that the process gain changes with time. The following assumptions are used to derive a simple dynamic model for the controller design:

(1) The frictional force opposing screw movement is negligible.
(2) The acceleration of the actuator-screw assembly is proportional to the hydraulic pressure gradient, dp_h/dt.
(3) The polymer does not leak back through the injection valve.
(4) The polymer flow in the nozzle and runner is isothermal.

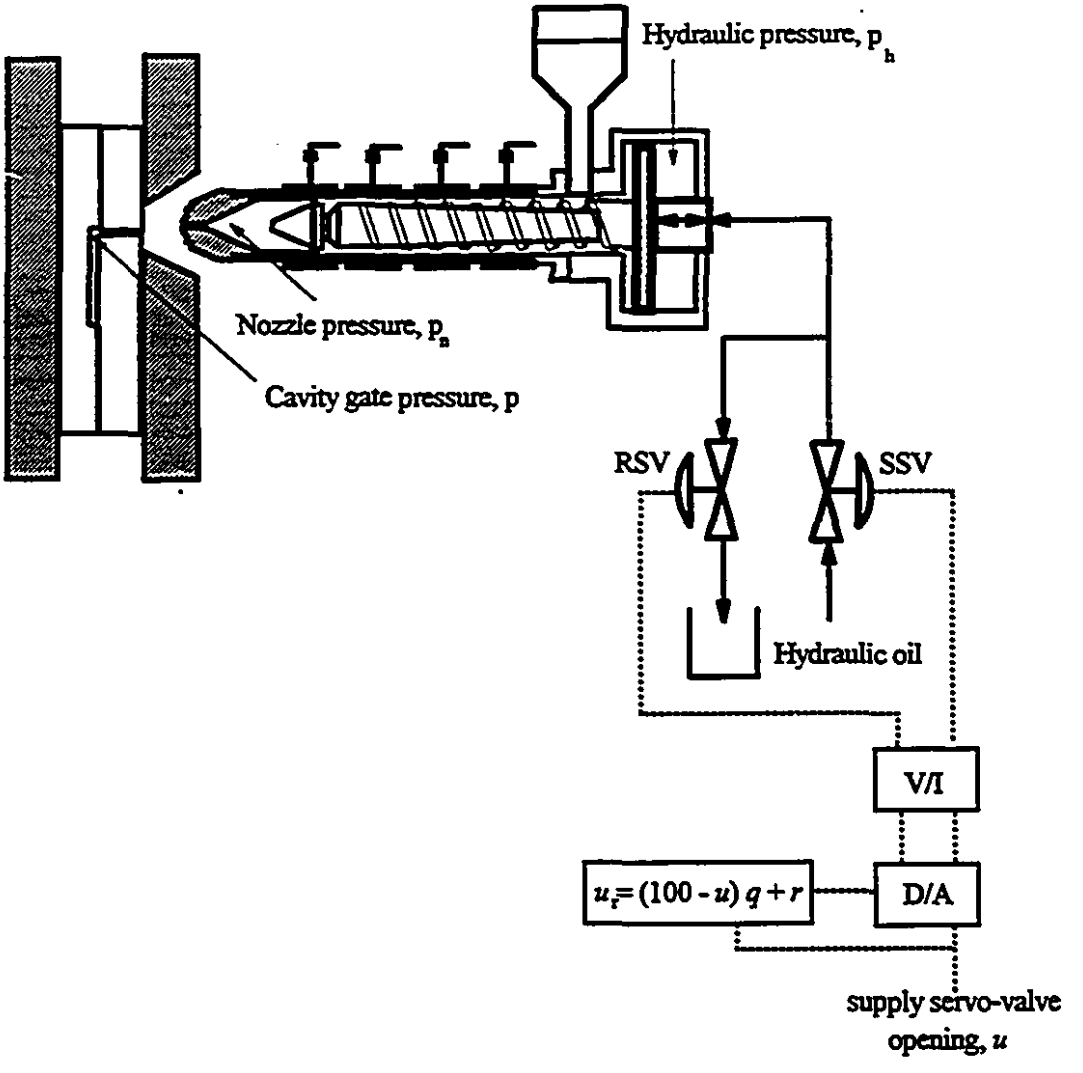

Figure 5.1 Schematic of the injection molding process showing the variables used in the derivation of the cavity pressure model.

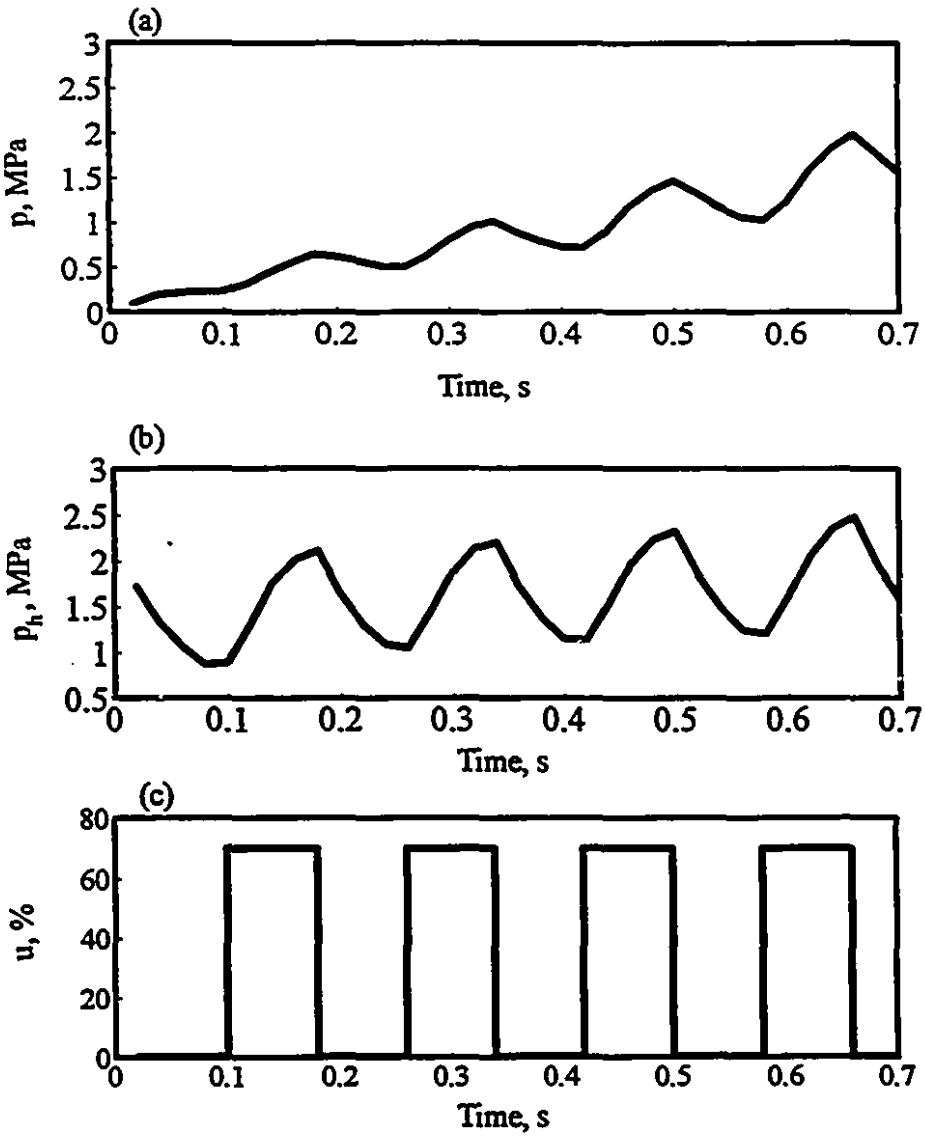

Figure 5.2 Variations in (a) cavity pressure, (b) hydraulic pressure, and (c) servo-valve opening in the filling stage for Experiment D-4 with the conditions shown in Table 5.2.

Assumptions (1) and (2) imply that a force balance for the screw-assembly may be written as

$$A_h p_h - A_n p_n = -ma = -K\frac{dp_h}{dt} \tag{5.2}$$

where A_h and A_n are the effective areas for the hydraulic and nozzle pressure. The flow rate, $Q(t)$, of polymer-melt from the nozzle to the cavity is related to the pressure drop in the runner by

$$Q(t) = \frac{\pi R^4}{8\eta}\frac{(p_n - p)}{L} \tag{5.3}$$

A change in polymer mass in the cavity equals the mass flowing through the runner, so a mass balance for the cavity may be expressed as

$$V_c\left(\frac{\partial \rho}{\partial t}\right) = \rho_n Q(t) = \rho_n\left|\frac{p_n - p}{R_r}\right| \tag{5.4}$$

where R_r is the flow resistance from the nozzle to the cavity gate. The variation in density with time is expressed as a function of the cavity gate pressure and bulk temperature variations as

$$\frac{\partial \rho}{\partial t} = \left(\frac{\partial \rho}{\partial P}\right)_T \frac{\partial p}{\partial t} + \left(\frac{\partial \rho}{\partial T}\right)_P \frac{\partial T}{\partial t} \tag{5.5}$$

Assuming isothermal filling, supposition (4), and substituting the density variation from Equation 5.5 into Equation 5.4 gives

$$\frac{1}{c}\frac{dp}{dt} = p_n - p \tag{5.6}$$

where

$$c = \left[\left(\frac{\partial \rho}{\partial P}\right)_T\right]^{-1} \frac{\rho_n}{V_c R_r} \tag{5.7}$$

Considering constant τ_h, K_h, A_n, K, and c, which is valid for short periods only, and solving Equations 5.1, 5.2, and 5.6 using Laplace transformation, the following expression results for the cavity pressure dynamic:

$$\frac{p(s)}{u(s)} = \frac{K_p(\tau_a s + 1)}{(1 + \tau_1 s)(1 + \tau_2 s)} \tag{5.8}$$

where $\tau_1 = \tau_h$, $\tau_2 = 1/c$, $K_p = A_h/A_n$, and $\tau_a = mK/A_h$. The discrete transfer function with zero-order hold is

$$G_p = \frac{y(k)}{u(k)} = \frac{b_1 z^{-1} + b_2 z^{-2}}{1 + a_1 z^{-1} + a_2 z^{-2}}, \tag{5.9}$$

whose parameters are related to the parameters of the continuous model by (Seborg et al., 1989):

$$\begin{aligned}
a_1 &= -e^{-\Delta t/\tau_1} - e^{-\Delta t/\tau_2} \\
a_2 &= e^{-\Delta t/\tau_1} e^{-\Delta t/\tau_2} \\
b_1 &= K_p\left(1 + \frac{\tau_a - \tau_1}{\tau_1 - \tau_2} e^{-\Delta t/\tau_1} + \frac{\tau_2 - \tau_a}{\tau_1 - \tau_2} e^{-\Delta t/\tau_2}\right) \\
b_2 &= K_p\left(e^{-\Delta t(1/\tau_1 + 1/\tau_2)} + \frac{\tau_a - \tau_1}{\tau_1 - \tau_2} e^{-\Delta t/\tau_2} + \frac{\tau_2 - \tau_a}{\tau_1 - \tau_2} e^{-\Delta t/\tau_1}\right)
\end{aligned} \tag{5.10}$$

where Δt is the sample interval, and the corresponding difference equation for a constant input is

$$y(k) + a_1 y(k-1) + a_2 y(k-2) = b_1 u(k-1) + b_2 u(k-2). \tag{5.11}$$

Equation 5.8 shows a second-order model for the cavity pressure response. However, according to Figure 5.2, a first-order or an overdamped second-order model may give similar results. Abu Fara (1988) used a second-order model for the filling stage (see Equation 2.7), and a first order-model for the packing stage. Gao (1993) employed a second-order model in both stages. In this work, the selection of the model order is based on the analysis of experimental data. The discrete transfer function with zero-order hold for the first-order model is:

$$G_p = \frac{y(k)}{u(k)} = \frac{b_1 z^{-1}}{1 + a_1 z^{-1}} \tag{5.12}$$

where

$$\begin{aligned} a_1 &= -e^{-\Delta t/\tau} \\ b_1 &= \frac{K}{\tau}(1 + a_1) \end{aligned} \tag{5.13}$$

In the discrete-time domain, Equation 5.12 is expressed as

$$y(k) + a_1 y(k-1) = b_1 u(k-1) \tag{5.14}$$

The parameters in Equations 5.11 and 5.14 should be estimated on-line using input/output process data, as they vary with time during the filling and packing stages.

5.2.2 Recursive Identification

For low-order systems with time-varying parameters, an appropriate estimation technique (Åström & Wittenmark, 1995) is the least-squares algorithm with an exponential forgetting factor. This identification algorithm

is briefly described below.

Assume a process is described by the following linear difference equation with constant parameters:

$$A(z^{-1})y(k) = B(z^{-1})u(k-1) + e(k) \tag{5.15}$$

where

$$\begin{aligned} A(z^{-1}) &= 1 + a_1 z^{-1} + \ldots\ldots\ldots + a_{n_a} z^{-n_a} \\ B(z^{-1}) &= b_1 + b_2 z^{-1} + \ldots\ldots\ldots + b_{n_b} z^{-n_b}. \end{aligned} \tag{5.16}$$

To find coefficients of the polynomials in Equation 5.16, Equation 5.15 is conveniently written in the matrix form

$$y(k) = \varphi^T(k)\theta + e(k) \tag{5.17}$$

where $\varphi^T(k)$ is the vector of measured input/output variables

$$\varphi^T(k) = [\, -y(k-1) \ldots\ldots -y(k-n_a)\; u(k-1) \ldots\ldots u(k-n_b-1)\,] \tag{5.18}$$

and θ is the parameter vector

$$\theta^T = [\, a_1 \ldots\ldots a_{n_a}\; b_1 \ldots\ldots b_{n_b}\,] \tag{5.19}$$

The parameters are calculated by finding the minimum of the function $J(\theta,k)$, defined as

$$J(\theta,k) = \frac{1}{2}\sum_{i=1}^{k} \lambda^{k-i}\left[y(k) - \varphi^T(k)\theta\right]^2 \tag{5.20}$$

where λ is the forgetting factor. The least-squares solution is obtained with (Åström and Wittenmark, 1990):

$$\begin{aligned} \theta(k) &= \theta(k-1) + K(k)\left[y(k) - \varphi^T(k)\theta(k-1)\right] \\ K(k) &= P(k-1)\varphi(k)\left(\lambda + \varphi^T(k)P(k-1)\varphi(k)\right)^{-1} \\ P(k) &= \left[I - K(k)\varphi^T(k)\right]P(k-1)/\lambda . \end{aligned} \tag{5.21}$$

To satisfy this equation, the covariance matrix $P(k)$ should be positive-definite. This is accomplished by choosing a large $P(0)$.

Values between 0 and 1 are given to the forgetting factor (λ). For slowly changing processes, λ values close to 1 are normally used, for example 0.99. In injection molding, λ should be appropriately selected to reflect the cavity pressure dynamics during the filling and packing stages.

5.3 CAVITY PRESSURE CONTROL

The main control objective is to maintain a desired peak pressure in a cycle-to-cycle sequence. For this purpose, the cavity pressure profile is regulated at a reference profile, $r(k)$. An adaptive feedback strategy is used to take into account changes in process dynamics. The pole placement approach was used to design the self-tuning control.

5.3.1 Controller Design

Controller parameters are calculated using the pole assignment approach. The algorithm is presented in detail in the text of Wellstead and Zarrop (1991). A block diagram for the self-tuning control is shown in Figure 5.3a. Neglecting model errors, $e(k)$, in Equation 5.15, this can be written in

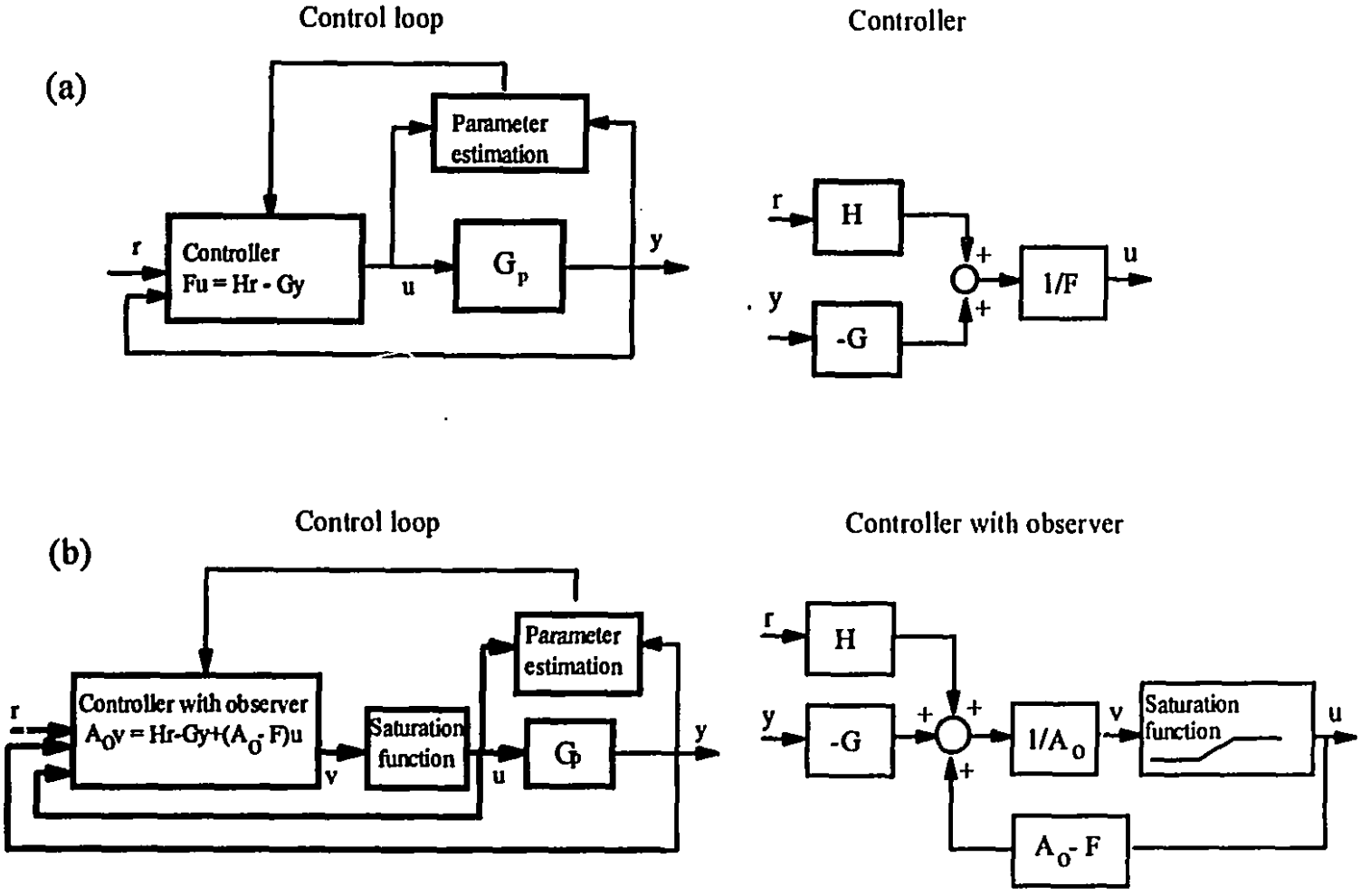

Figure 5.3 (a) Block diagram of the self-tuning control control and the controller.
(b) Block diagram of the self-tuning control loop and the controller with observer.

polynomial form as

$$A(z^{-1})y(k) = B(z^{-1})z^{-1}u(k)\ , \tag{5.22}$$

and the feedback controller is of the form

$$Fu(k) = Hr(k) - Gy(k) \tag{5.23}$$

where $r(k)$ and $y(k)$ denote the reference and the measured controlled variable, respectively. F, H, and G are polynomials which are selected so that the system output tracks the reference signal r(k). Substituting u(k) from Equation 5.23 into Equation 5.22 yields the closed loop form

$$y(k) = \frac{BHz^{-1}}{FA + z^{-1}BG}r(k) = \frac{BHz^{-1}}{T}r(k)\ . \tag{5.24}$$

The desired response is obtained by assigning zeroes to the polynomial:

$$T(z^{-1}) = 1 + t_1 z^{-1} + ... + t_{n_t} z^{-n_t}\ . \tag{5.25}$$

Then, F and G polynomials are found by solving the polynomial identity

$$FA + z^{-1}BG = T(z^{-1}) \tag{5.26}$$

Requirements for a unique solution of Equation 5.26 are given by Wellstead and Zarrop (1991). The polynomial H is calculated to achieve the desired output, which is:

$$\frac{y(k)}{r(k)} = \left[\frac{BH}{K}\right]_{z=1} = 1\ . \tag{5.27}$$

For a desired closed-loop response based upon a first-order model, the

polynomial $T(z^{-1})$ is written as

$$T(z^{-1}) = 1 - t_1 z^{-1}$$
$$t_1 = e^{-\Delta t/\beta}. \tag{5.28}$$

Using the second-order model given by Equation 5.11, if the response is required to follow a first-order model (Eq. 5.28) the control parameters using the pole assignment criterion are

$$g_o = -\frac{(t_1 + a_1)(b_1 a_2/b_2 - a_1) + a_2}{b_2 + b_1(b_1 a_2/b_2 - a_1)}$$
$$f_1 = \frac{a_2 + b_2 g_o}{b_1 a_2/b_2 - a_1}$$
$$g_1 = -\frac{f_1 a_2}{b_2} \tag{5.29}$$
$$h = \frac{1 - t_1}{b_1 + b_2},$$

and the controller is implemented using the expression

$$u(k) = -f_1 u(k-1) - g_o y(k) - g_1 y(k-1) + hr(k). \tag{5.30}$$

Applying the pole location design procedure with the first-order model given by Equation 5.14, the controller parameters are found as

$$g_o = -\frac{t_1 + a_1}{b_1}$$
$$h = \frac{1 - t_1}{b_1}, \tag{5.31}$$

and the controller output is generated as

$$u(k) = -g_o y(k) + hr(k). \tag{5.32}$$

The closed-loop model parameters are estimated using the cavity pressure response, $y(k)$, as output and the servo-valve opening, $u(k)$, as input. Therefore, the controller parameters are adjusted on-line with the feedback signals from the cavity pressure measurements. For on-line estimation, the requirement of persistent excitation increases with the number of unknown parameters; using their minimum number is thus convenient. Thus, only first-order and second-order models were used in this work.

5.3.2 Self-Tuning Control with Observer

Controller saturation is a problem encountered in the control of the cavity pressure. This is attributed chiefly to measurement and model errors. To reduce this problem, Åström and Wittenmark (1991) suggest using a controller with observer and state feedback. The block diagram of the control system with the new structure is shown in Figure 5.3b. The controller equation is obtained from Equation 5.23 in observer form as

$$A_o(z^{-1})\,v(k) = H(z^{-1})r(k) - G(z^{-1})y(k) + [A_o(z^{-1}) - F(z^{-1})]\,u(k) \qquad (5.33)$$

where $A_o(z^{-1})$ is the observer polynomial. The controller can be described by the saturation function $f(v(k))$

$$u(k) = \begin{cases} u_{max}, \text{ if } v(k) > u_{max} \\ v(k), \text{ if } u_{min} \le v(k) \le u_{max} \\ u_{min}, \text{ if } v(k) < u_{min} \end{cases} \qquad (5.34)$$

where u_{max} and u_{min} are the upper and lower bounds of the control variable. A_o=1 denotes a deadbeat observer. An observer with first-order dynamic is written as

$$A_o(z^{-1}) = 1 - a_o z^{-1}$$
$$a_o = e^{-\Delta t/\tau_o} \tag{5.35}$$

where τ_o is the observer time constant. Therefore, to reduce saturation of the controller given by Equations 5.30 and 5.31, this is implemented as

$$v(k) = -a_o v(k-1) + \frac{1-t_1}{b_1}[r(k) + a_o r(k-1)] - g_o y(k) + (a_o - h)u(k-1)\,. \tag{5.36}$$

The control output $u(k)$ is determined using Equations 5.34 and 5.36.

5.3.3 Set-Point Profile

A model for the cavity pressure as a function of time should be used to generate a set-point trajectory. During the filling stage for an open-loop operation and with a fixed servo-valve opening, the cavity pressure profile is nearly linear for a simple rectangular cavity. The cavity pressure is then described as

$$p_{sp}(t) = p_{of} + \frac{p_{ef} - p_{of}}{\tau_f} t = p_{of} + \left(\frac{dp}{dt}\right)_{sp} t \tag{5.37}$$

where p_{of} = initial pressure, p_{ef} = pressure at the end of filling, and $(dp/dt)_{sp}$ is the desired slope of the cavity pressure curve during filling.

To determine if the control variable tracks the set-point at short intervals during the filling stage, the set-point can be calculated in stepwise or incremental form. This is obtained by writing Equation 5.37 as

$$p_{sp}(k) = p(k-1) + \left(\frac{dp}{dt}\right)_{sp} \Delta t, \tag{5.38}$$

where $p(k\text{-}1)$ denotes the pressure measured at the beginning of each sampling interval.

The model for the set-point in the packing stage is derived as follows. The nozzle pressure assumes nearly constant values during packing (see Figure 2.2). This pressure is assumed to be proportional to u; thus, Equation 5.6 can be integrated with $\tau_p = 1/c$ and $p_n = K_p u$ to obtain an expression for the packing pressure with time:

$$p_{sp}(t) = p_{op} + (\pi - p_{op})(1 - e^{-t/\tau_{sp}}) \tag{5.39}$$

where p_{op} is the initial packing pressure and π is the maximum pressure. The initial packing pressure measured at the end of filling, $p_o = p_{ef}$, and the final pressure is the peak pressure, so that $\pi = p_p$. The desired packing pressure profile may then be written as

$$p_{sp}(t) = p_{ef} + (p_{psp} - p_{ef})[1 - \exp(-t/\tau_{sp})] \tag{5.40}$$

where τ_{sp} is the time constant for the packing stage and p_{psp} the peak pressure. The packing pressure curve fits the following four-parameter formula, which is made up of two straight-line segments as a limiting case:

$$p_{sp}(t) = a + b - \left[(c + 0.00689bt)^2 + d^2\right]^{1/2} \tag{5.41}$$

Although this equation adapts to the curvature of the packing pressure profile, Equation 5.40 is easier to use, and parameter τ_{sp} can be interpreted as a "time constant". However, the coefficients of Equation 5.41 do not have physical significance. The time profile given by Equation 5.40 was selected for controlling the packing stage.

5.4 EXPERIMENTAL PROCEDURE

Before describing the experimental procedure, a brief review of the equipment described in Chapter 3 is given. The supply (SSV) and return (RSV) servo-valves permit the continuous flow of hydraulic oil during filling and packing. Computer outputs range from 0 to 5 Vdc, corresponding to 0% and 100% servo-valve opening, respectively. The barrel reaches the set-point temperatures in about 45 minutes. Before starting each experiment, sufficient material is purged to clear the barrel and about 15 samples are molded.

The supply servo-valve opening is the manipulated variable. The relationship between the relative size of the supply servo-valve opening (u) and the return servo-valve opening (u_r), both expressed as a percent of the corresponding full opening, was

$$u_r = (100 - u)q + 0.5 \tag{5.42}$$

where q is a proportionality factor which is assigned a value between 0 and 1. According to Equation 5.41, as u decreases, u_r increases, thereby increasing the flow through the return servo-valve. This structure provides greater response to the pressure in the injection cylinder during the packing stage. Consequently, the polymer melt in the barrel can be compressed and decompressed more easily.

In the experiments for cavity pressure control, the coolant temperature and barrel temperatures are controlled using sampling intervals of 0.200 s and 1 s, respectively. The experiments were divided into three groups: (1) static open-loop experiment, (2) dynamic open-loop experiments, and (3) closed-loop control experiments.

5.4.1 Static Open-Loop Experiment

An open-loop experiment with constant (static) servo-valve opening during each cycle was used to find the range of the control variable, so that the molding operations could be carried out without causing short-shots or over-packed parts. The controlled coolant temperature and barrel temperature near the nozzle were set at 40°C and 250 ℃, respectively. Table 5.1 summarizes the experimental conditions.

The experiment was conducted by increasing the servo-valve opening from 10% to 80% every 5 cycles. Servo-valve openings lower than 10% caused short shots, and values higher than 80% produced over-packed parts (flashing). The file structure used to carry out this experiment is shown in Figure 3.8. In this Figure, the executable file *pcontrol* is used to output the required voltage for each servo-valve and collect the cavity, nozzle, and hydraulic pressure data.

5.4.2 Dynamic Open-Loop Experiments

A second group of experiment was conducted to record input/response data which could be used in selecting the process model structure. A square-wave signal with various amplitudes and periods T_u of 0.08 s and 0.16 s was employed to obtain data for the model identification. Preliminary experiments showed that the cavity pressure response to changes in servo-valve opening decreases during the packing stage. This is due to the rapid solidification of the polymer in the sprue and runner. Several experiments were done to find the conditions at which the cavity pressure presents the greatest sensitivity to changes in servo-valve opening during molding.

Table 5.1 Conditions for the static open-loop experiment.

Time settings:	Injection	13 s
	Decompression	2 s
	Cooling	10 s
	Open	10 s
Coolant temperature set-point		40°C
Barrel temperature set-points		250/220/200/190 °C

Data acquisition and servo-valve manipulation

Sampling interval, Δt =0.040 s

Factor of valve openings (Eq. 5.41) q = 0.2

Servo-valve openings, u (staircase function):

u(%)	Cycles
10	1-5
20	6-10
40	11-15
60	16-20

Table 5.2 summarizes the conditions of the various experiments to study the dynamic of the cavity pressure. Three values of q (see Equation 5.41) and three amplitudes were used.

5.4.3 Closed-Loop Control Experiments

The self-tuning control of the cavity pressure was implemented in two modes: (1) employing the normal algorithm from the beginning of the filling stage (STC), and (2) using the algorithm with an observer, which is started at a predefined screw position (STCO-SP). Starting the control action after the polymer has filled part of the cavity avoids errors in measurements of the cavity pressure at the beginning of the filling stage.

In the STCO-SP mode, the filling stage is carried out with a fixed servo-valve opening of 40% until the screw has reached a specific position (0.75 cm). The filling stage is then completed under self-tuning control with a linear set-point trajectory (see Equation 5.45) until the transition from filling to packing occurs. This is detected by the sudden increase in slope of the cavity pressure curve in the sampling interval (0.020 s).

Two sets of control experiments were performed:

(1) Control of the cavity pressure during filling with a constant slope. The purpose of these experiments was to determine appropriate parameters and conditions to be used in the control of the cavity pressure during filling and packing. Experimental conditions are summarized in Table 5.3

Table 5.2 Conditions for the dynamic open-loop experiments

Time settings:	Injection	13 s
	Decompression	2 s
	Cooling	10 s
	Open	10 s
Coolant temperature set-point		40°C
Barrel temperature set-points		250/220/200/190 °C

Cavity pressure control (open-loop)
Sampling interval Δt=0.020 s
Input u: square-wave pulse trains of amplitude A_u

Conditions	Experiment			
	D-1	D-2	D-3	D-4
A_u, %	20-80	0.5-90	0.5-70	0.5-70
Period T_u, s	0.08	0.08	0.16	0.16
q (Eq. 5.41)	0.20	0.5	0.5	0.6

Table 5.3 Conditions for the control of the cavity pressure during filling

Time settings:	Injection	13 s
	Cooling	10 s
	Decompression	2 s
	Plasticating/open	10 s
Coolant temperature set-point		40°C
Barrel temperature set-points		250/220/200/190°C
Cavity pressure control		
	Factor q in Eq. 5.42	q=0.5
	Sampling Interval	Δt=0.020 s
	Desired pole location	t_1=0.7

Conditions	Experiments			
	CP-1	CP-2	CP-3	CP-4
Model order	2	1	1	1
Forgetting factor λ	0.90	0.95	0.95	0.75
Input range u, %	0.5-99.5	0.5-80	0.5-90	0.5-90
Set-points				
Filling, $(dp/dt)_{sp}$, MPa/s	3.86	4.98	3.10	3.10
Control mode	STC	STC	STCO-SP	STCO-SP

(2) Control of the cavity pressure during filling and packing. These experiments were intended to control the peak pressure at a reference value by following a set-point trajectory. The STCO-SP control strategy was used in these experiments. The packing stage is controlled until the pressure is equal to or higher than the desired peak pressure. Table 5.4 summarizes the experimental conditions.

5.5 RESULTS AND DISCUSSION

The discussion below is focused on the following aspects: (1) range of the control variable in static open-loop experiments, (2) cavity pressure responsiveness, (3) model order selection from the dynamic open-loop experiments, (4) parameters of the set-point profile model, (5) Control of the cavity pressure during filling, and (6) control of the cavity pressure during filling and packing.

5.5.1 Range of Control Variable (Static Open-Loop Experiment)

The traces shown in Figure 5.4 were obtained with the experimental conditions shown in Table 5.1. These show the cavity-pressure curves for supply servo-valve openings varying between 10% and 80%. With the increase in the supply servo-valve opening, the peak pressure increases from about 20 MPa to 23 MPa. Figure 5.5 presents the screw position and velocity variations with time. The velocity signal, which is provided by the sensor, does not exactly confirm the derivative of the position data. However, any inaccuracy does not affect this work. At the instant the screw has moved to about 0.2 cm from the end of the screw stroke, as seen in Figure 5.5a, the

Table 5.4 Conditions for the control of the cavity pressure during filling and packing (STCO-SP mode).

Time settings:	Injection	13 s
	Decompression	2 s
	Cooling	10 s
	Open	10 s
Coolant temperature set-point		40°C
Barrel temperature set-points		240/220/200/190°C
Cavity pressure control		
. Factor q in Eq. 5.42		q= 0.5
Sampling Interval		Δt=0.020 s
Desired pole location		t_1= 0.7
Forgetting factor		λ= 0.75
Time-constants		
Cavity-pressure set-point		τ_{sp}=0.16 s
Observer		τ_o=0.04 s (filling)
		τ_o=0.01 s (packing)

Conditions	Experiment	
	CP-5	CP-6
Pressure set-points		
$(dp/dt)_{sp}$, MPa/s	1.74	5.19
p_{psp}, MPa	19.99	22.06

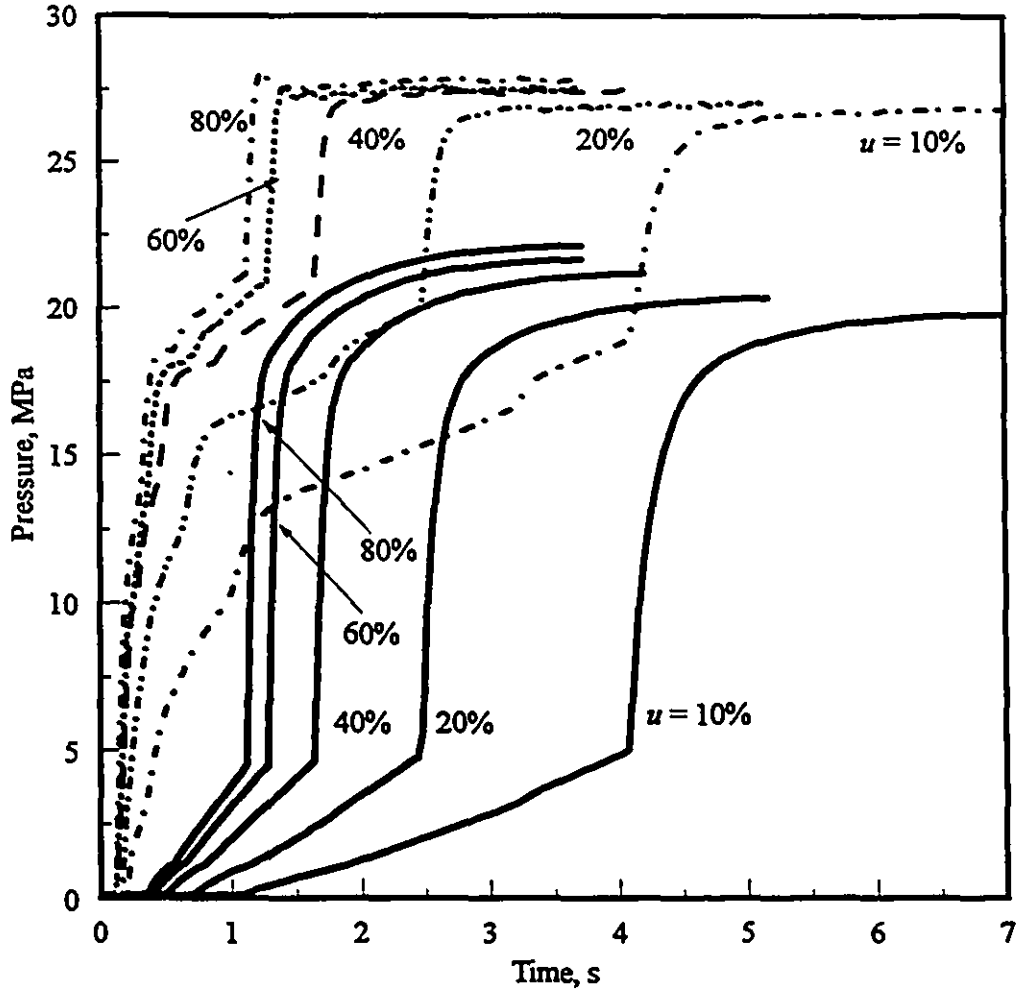

Figure 5.4 Variations in nozzle and cavity pressures (-) with time using the conditions given in Table 5.1.

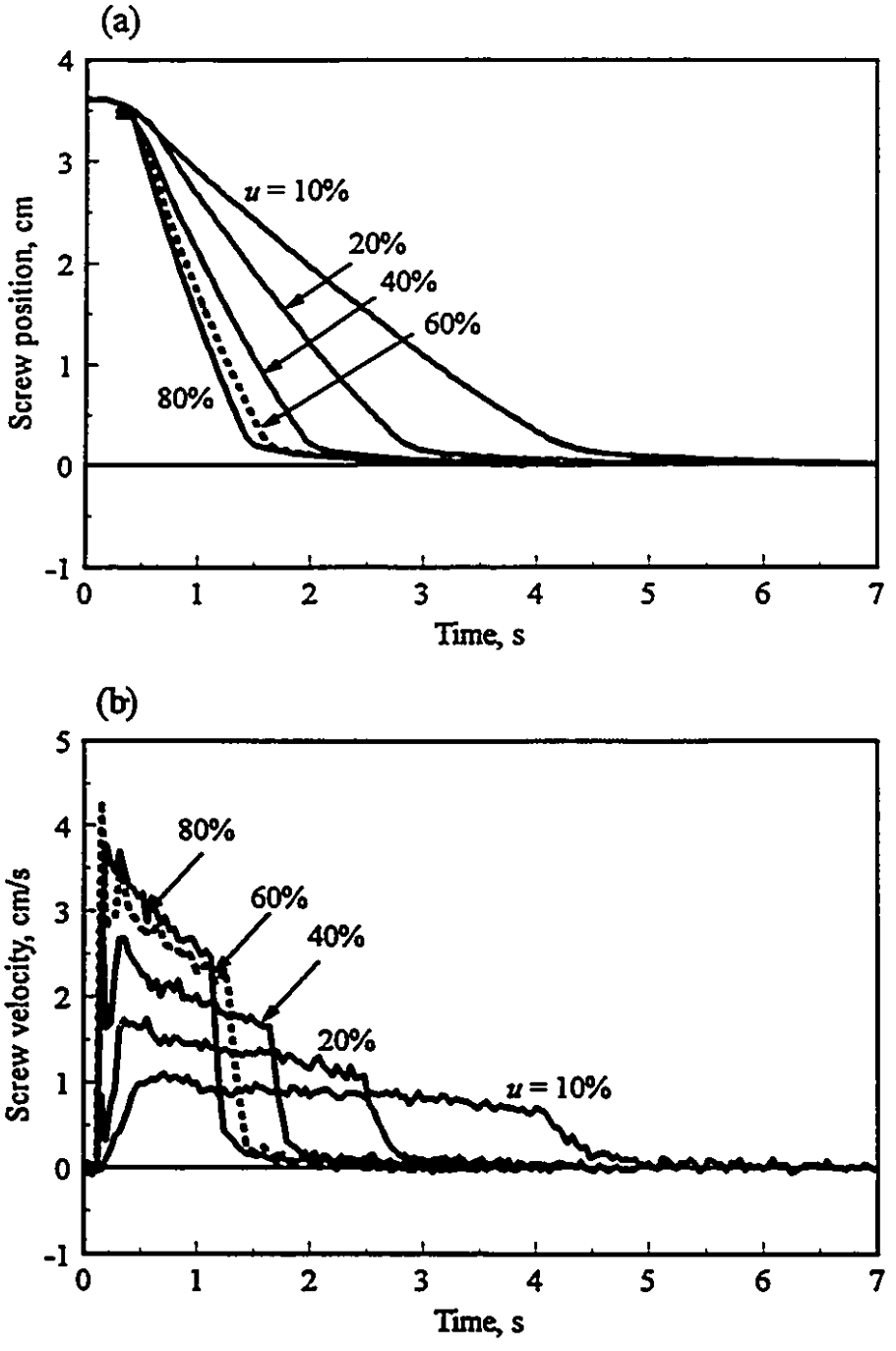

Figure 5.5 Variations in screw position (a) and screw velocity (b) with time using the conditions given in Table 5.1.

screw velocity is near zero (Figure 5.5b); and the cavity pressure is close to, but not yet at, its peak value, as seen in Figure 5.4. The cavity pressure then starts to increase very slowly to its peak value until the gate seals.

Figure 5.6 shows the nozzle and cavity pressure variations for five consecutive cycles operated at 10% servo-valve opening. The nozzle and cavity pressures increase with time until they reach their maximum values, but the cavity pressure shows a greater difference between cycles.

5.5.2 Cavity-Pressure Responsiveness

Table 5.2 summarizes the conditions used during the experiments designed to study the cavity pressure response to a sequence of square-wave pulses of different periods and magnitudes, and for the model order selection.

Experiment D-1 showed small variations in the response in the filling stage for a period of 0.08s and amplitude 20%-80%, but the packing pressure remains insensitive. This is seen in Figure 5.7, and occurs because at the end of filling the screw moves slowly and attains its lowest position, which implies that little polymer flows into the cavity during the packing stage. The low compressibility of the semi-solidified polymer causes a fast pressure rise and makes the process difficult to control. The packing pressure builds up in less than 0.5 seconds.

To elicit a larger response during the packing stage, the conditions were changed to those of Experiment D-2 (see Table 5.2) with an amplitude of 0.5%-90% and q=0.5. The response increased in the filling stage only, as seen in Figure 5.8. Increasing q did not affect the packing pressure response, because a period of 0.8 s was not enough for the cavity to decompress. A

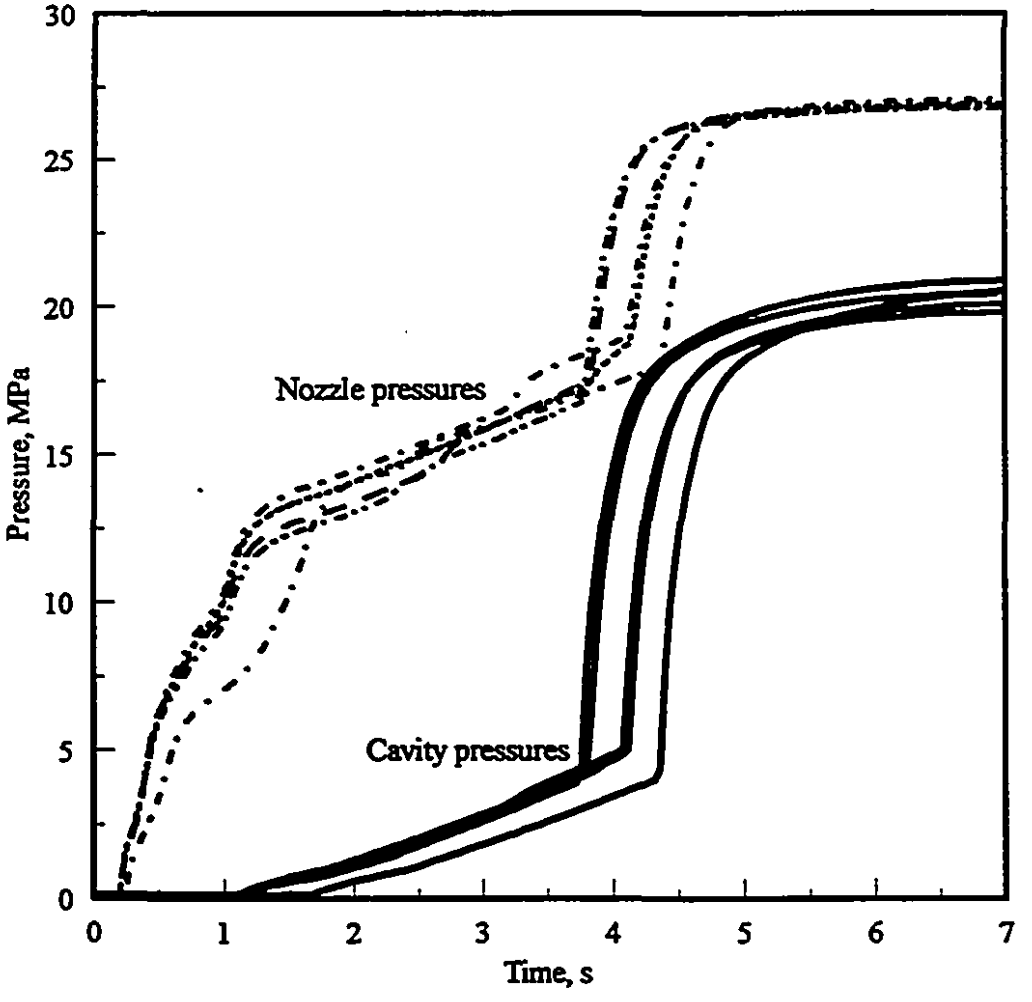

Figure 5.6 Variations in nozzle and cavity pressures with time for five consecutive cycles using the conditions given in Table 5.1 ($u = 10\%$).

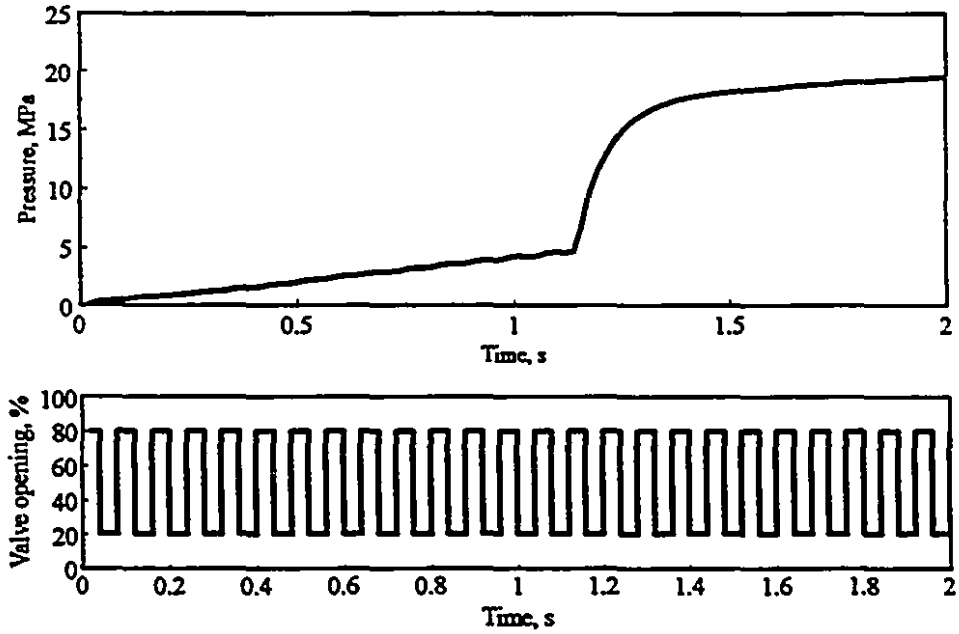

Figure 5.7 Cavity pressure response to a square-wave variations in servo-valve opening for Experiment D-1 (Table 5.2).

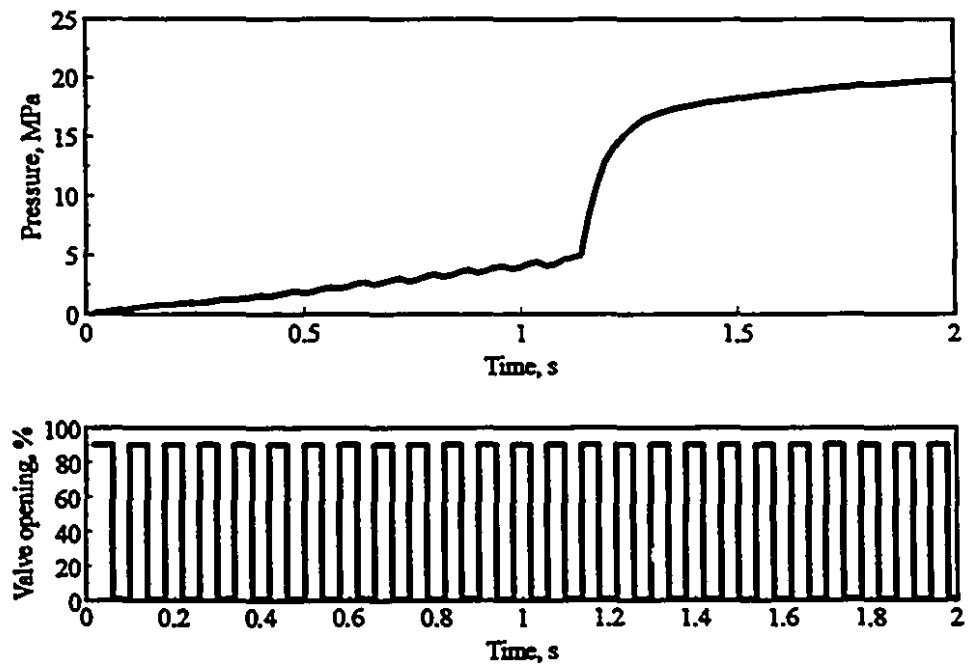

Figure 5.8 Cavity pressure response to a square-wave variations in servo-valve opening for Experiment D-2 (Table 5.2).

period of 0.16 s was used in Experiment D-3 with q=0.5 and amplitude of 0.5%-70%. Figure 5.9 shows that with these conditions the cavity pressure during the filling and packing stages is more sensitive than in the previous experiments. A value of q=0.6 slightly improves the response over that of Experiment D-3, as seen in Figure 5.10 for Experiment D-4. Nevertheless, the difference is not significant, and therefore the value q=0.5 was selected for the control experiments.

5.5.3 Model-Order Selection

The recursive identification algorithm described by Ljung (1991) was used to fit the cavity pressure data of Experiment D-3 with the first-order model (Equation 5.14) and the second-order model (Equation 5.11). Two performance criteria were used for model structure selection: the minimum values of the summation of square error V_N (Ljung, 1987), given by

$$V_N = \frac{1}{N}\sum_{k=1}^{N}\frac{1}{2}[y(k) - \hat{y}(k,\theta)]^2 \tag{5.43}$$

and the final prediction error (FPE)

$$FPE = \frac{1 + n/N}{1 - n/N} V_N \tag{5.44}$$

where n=total number of estimated parameters and N=length of the data record. The models are compared with respect to their performance criteria in Table 5.5, using different forgetting factors. The first-order model showed prediction errors lower than those of the second-order model. This is seen in Figure 5.11, which shows the measured and calculated cavity pressures for a forgetting factor of λ=0.75.

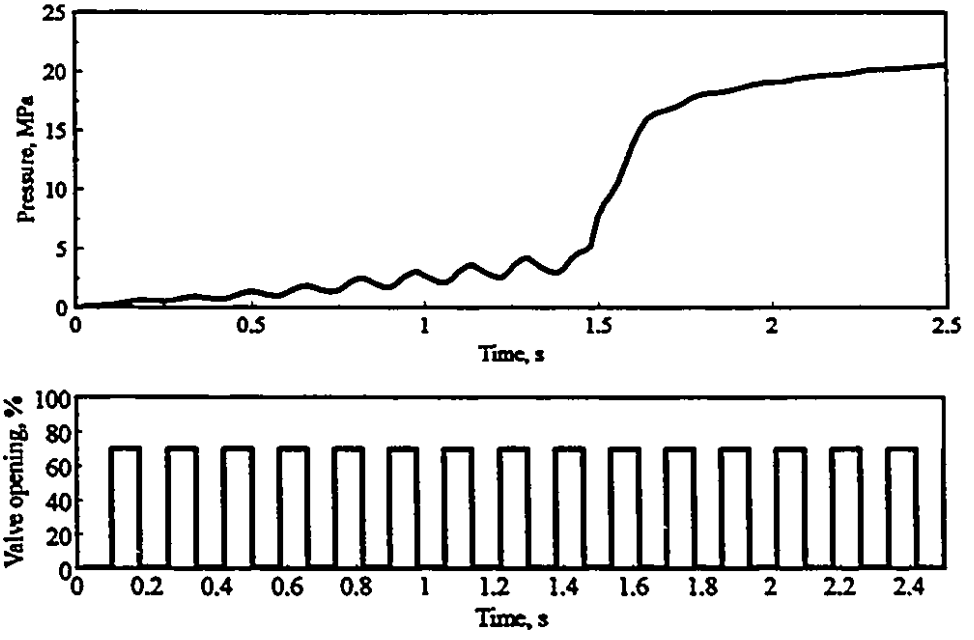

Figure 5.9 Cavity pressure response to a square-wave variations in servo-valve opening for Experiment D-3 (Table 5.2).

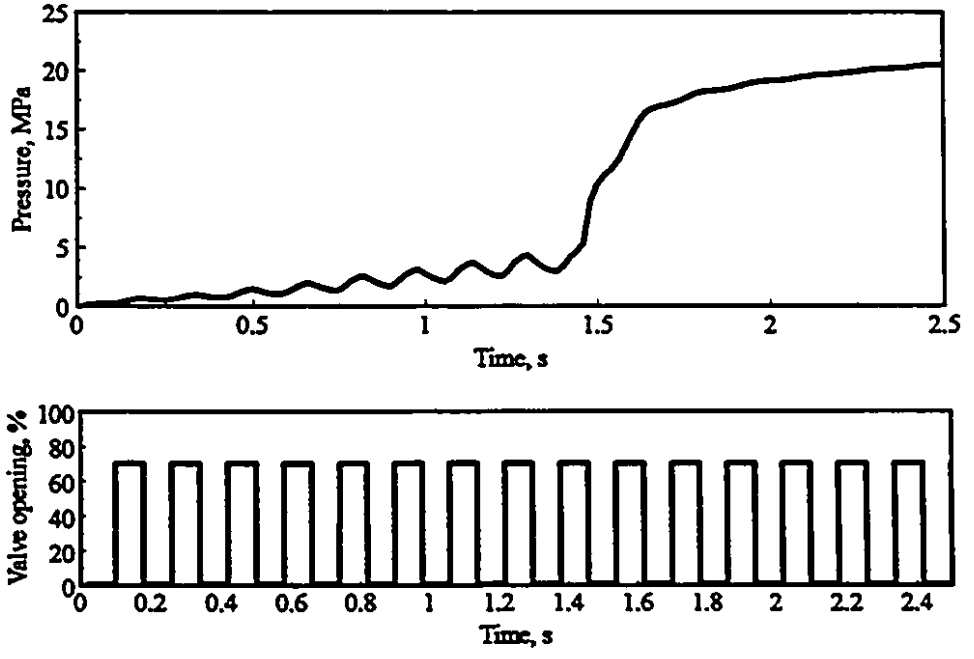

Figure 5.10 Cavity pressure response to a square-wave variations in servo-valve opening for Experiment D-4 (Table 5.2).

Table 5.5 Comparison between prediction errors for different forgetting factors using data of Experiment D-3

First-order model, Equation 5.14		
λ	V_N(MPa^2)	FPE(MPa^2)
0.75	0.1470	0.1530
0.90	0.1541	0.1604
0.95	0.1611	0.1677
0.99	0.1683	0.1751
Second-order model, Equation 5.11		
λ	V_N(MPa^2)	FPE(MPa^2)
0.75	2.4539	2.6584
0.90	2.4241	2.6261
0.95	2.3617	2.4002
0.99	2.2996	2.4983

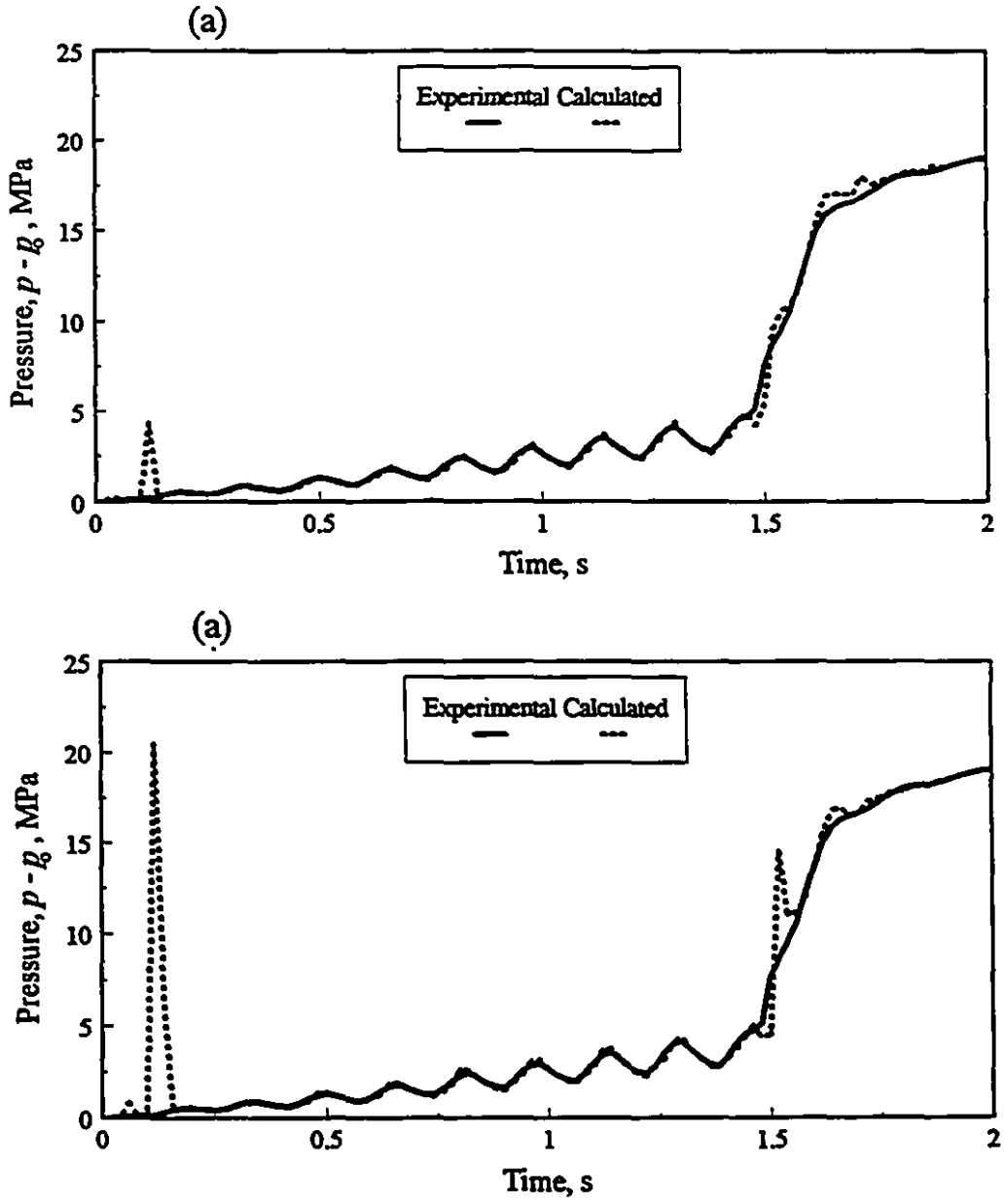

Figure 5.11 Experimental and calculated cavity pressure for (a) first-order model and (b) second-order model, with λ=0.75.

5.5.4 Parameters of the Set-Point Profile Model

Equation 5.37 is used to generate the set-point profiles in the filling stage. The ability of this Equation to reproduce cavity pressure profiles is shown in Figure 5.12, which presents the measured and calculated values for cycle 15 at conditions given in Table 5.1. Measured values agree with those calculated by Equation 5.37, and the slope determined by least-squares calculation is dp/dt=3.86 MPa/s (559 psi/s).

Figure 5.13 presents the measured and fitted packing pressures, using Equation 5.40 with τ_p=0.16 s. The peak pressure given by the model agrees with the experimental value. As can be seen in the Figure, Equation 5.41 fits the packing pressure, with a=184.7 MPa, b=2381.1 MPa/s, c=1.27MPa, and d=0.53MPa^2. However, this model is more difficult to implement than Equation 5.40. Values of τ_p ranging from 0.05s to 0.20s can be used to reproduce all the packing profiles shown in Figure 5.4.

5.5.5 Control of the Cavity Pressure during Filling

The pole location, t_1 (see Equation 5.28), was selected based on the values of the time constant, τ_{sp}, in Equation 5.40, used for calculation of the set-point trajectory in the packing stage. After fitting different data of packing pressure profiles, values of τ_{sp} were found to be between 0.05s and 0.16s. By considering $\beta=\tau_{sp}$, the desired pole location, t_1, for the set-point profile (according to Equation 5.28 for Δt=0.02 s) should be between 0.88 and 0.67. A value of t_1=0.7 was chosen for the control experiments.

An observer with first-order dynamic was implemented to reduce controller saturation. The time constant for the observer during filling was

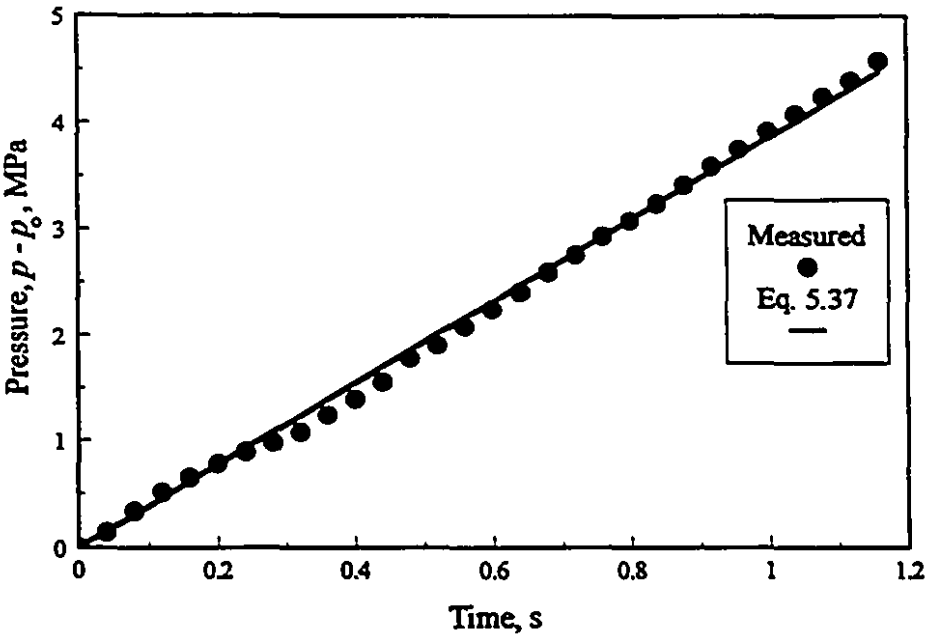

Figure 5.12 Measured and calculated cavity pressures in the filling stage using the conditions given in Table 5.1. p_o is the initial cavity pressure.

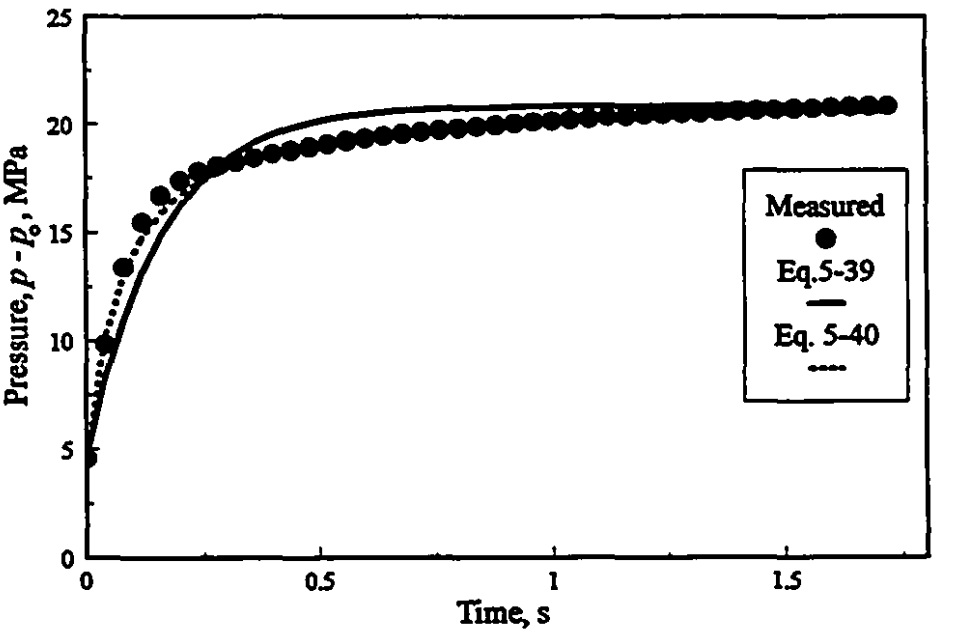

Figure 5.13 Measured and calculated cavity pressures in the packing stage using the conditions given in Table 5.1. p_o is the initial cavity pressure.

selected as two sampling intervals; thus, τ_o = 0.04s, which correspond to a_o = 0.39s (see Equation 5.35).

The second-order model was tested in Experiment CP-1, and the results are shown in Figure 5.14. The servo-valve saturates during most of filling as seen in Figure 5.14b, and remains switched off for long intervals. Because of the model inadequacy, the controller signal is deficient, and the process output does not follow the set-point profile. In addition, the process gains are almost null as seen in Figure 5.14d. From these results and Figure 5.11, it can be concluded that the first-order model is more appropriate.

Figures 5.15 illustrates the process output, manipulated variable, and estimated parameters for Experiment CP-2 using the first-order model with λ=0.95. In order to reduce controller saturation, Equation 5.38 was employed for the set-point profile. It can be seen that the cavity pressure follows the slope set-point, $(dp/dt)_{sp}$=4.98 MPa/s (722 psi/s), but the pressure fluctuates significantly. This suggests that this equation is not suitable for calculation of the set-point profile.

Starting the control action when the polymer starts to fill the cavity leads to rough changes in pressure (see Figure 5.15a). The algorithm was then implemented to start after a certain screw position. The problem of controller saturation and oscillations that produce ripples in the cavity pressure may be attributed to measurement and model errors. A solution to this problem was found by using the controller with a first-order observer. Thus, to reduce oscillations of the control variable and improve the control performance, the experimental procedure was set introducing the following changes:

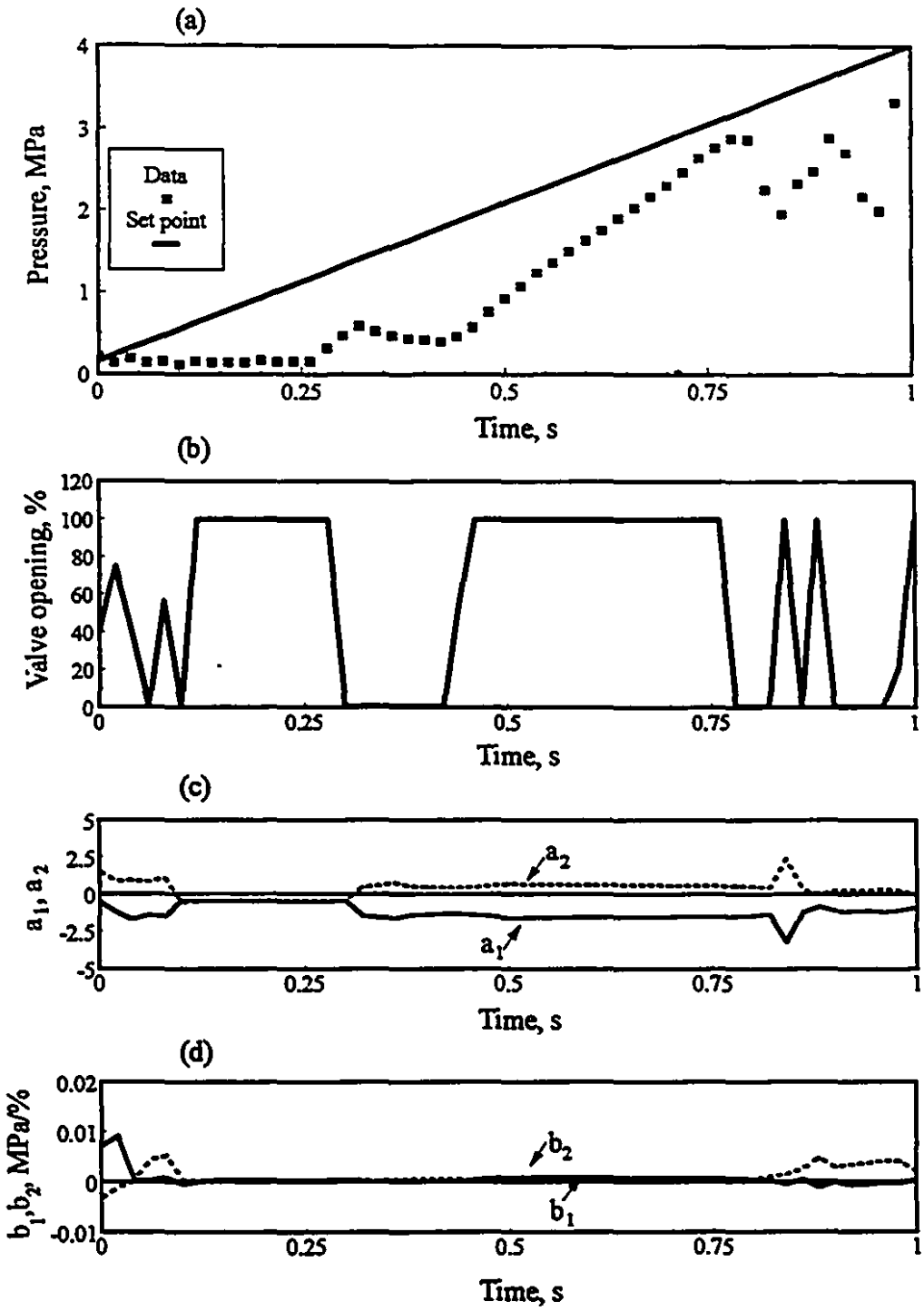

Figure 5.14 System response for a second order model using the STC control strategy in Experiment CP-1, Table 5.3. (a) Cavity pressure and set-point. (b) Servo-valve opening, (c) and (d) Estimated parameters.

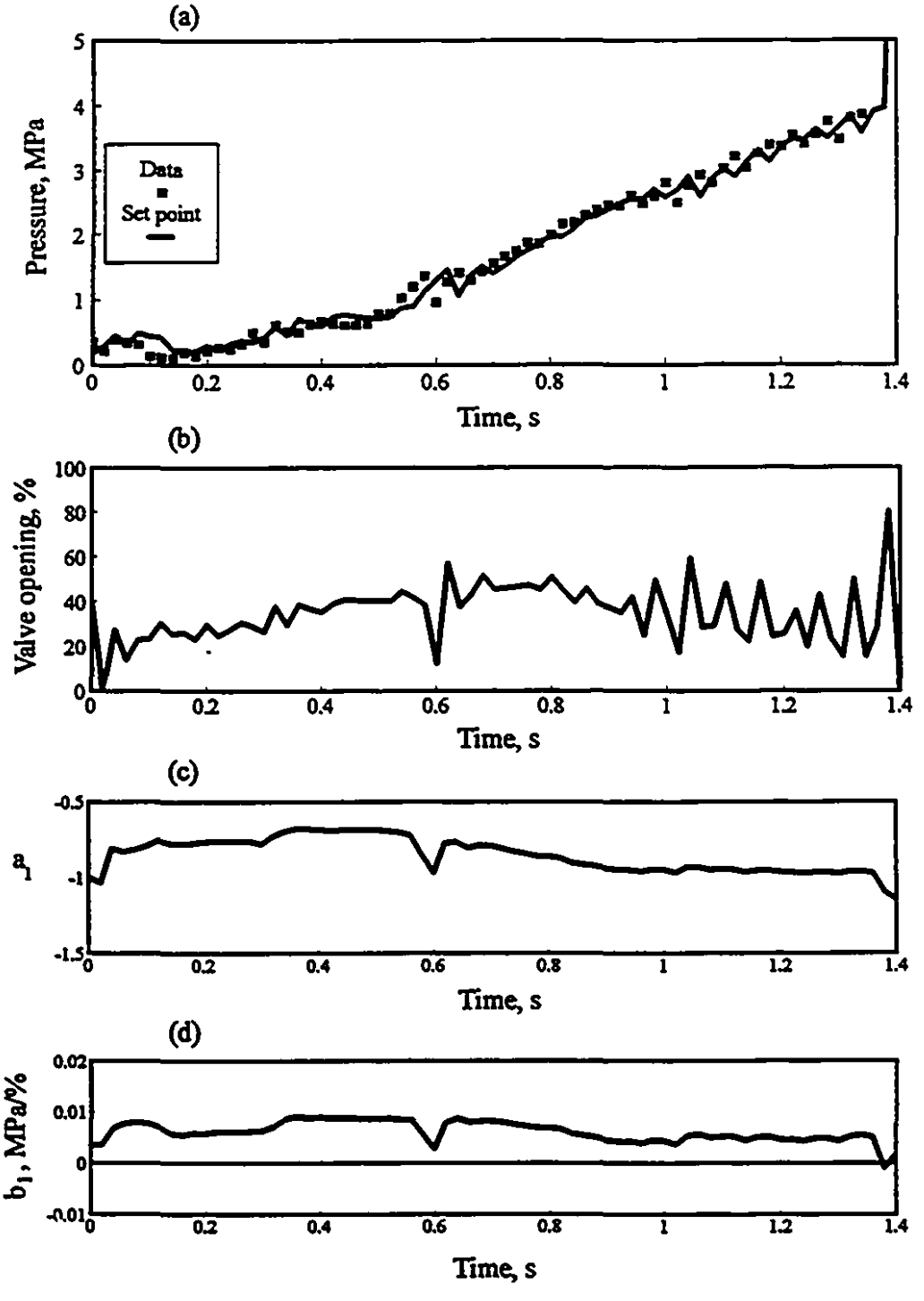

Figure 5.15 System response during the filling stage using the STC control strategy in Experiment CP-2, Table 5.3. (a) Cavity pressure and set-point, (b) Servo-valve opening, (c) and (d) Estimated parameters.

(1) The control valve is set to a constant opening until the screw moved approximately 0.75 cm, before starting the control action.

(2) A self-tuning control with a first-order observer and state feedback is implemented (Figure 5.3b).

The positive effect of using this strategy is seen in Figure 5.16, which illustrates variations in pressure, servo-valve opening, and screw position with time. For 10% of initial value of the control signal and λ=0.95, the cavity pressure tracks the slope set-point (3.10 MPa/s). A delay is observed because the controller does not have integral action. The oscillations have diminished noticeably when compared to Figure 5.15.

Forgetting factors close to one are normally used for a system with slowly varying parameters. A high value of λ averages parameters in the estimation period as seen in Figures 5.15c and 5.15d. Parameter variations have been found to be quite rapid during the filling stage. A value of λ=0.75 was used, as suggested by Gao (1993), for the filling stage. Figure 5.17 shows the results of Experiment CP-4 with a set-point profile of 3.10 MPa/s. In this case, the controller performs better, although more oscillations occur. This is due to the lower forgetting factor which weights the most recent measurements.

5.5.6 Control of the Cavity Pressure during Filling and Packing

The experimental conditions used for the control of the cavity pressure during filling and packing are given in Table 5.4 The time constant for the observer dynamic during the packing stage was selected as half-sampling intervals; thus, τ_o = 0.01s, which correspond to a_o = 0.87 (see Equation

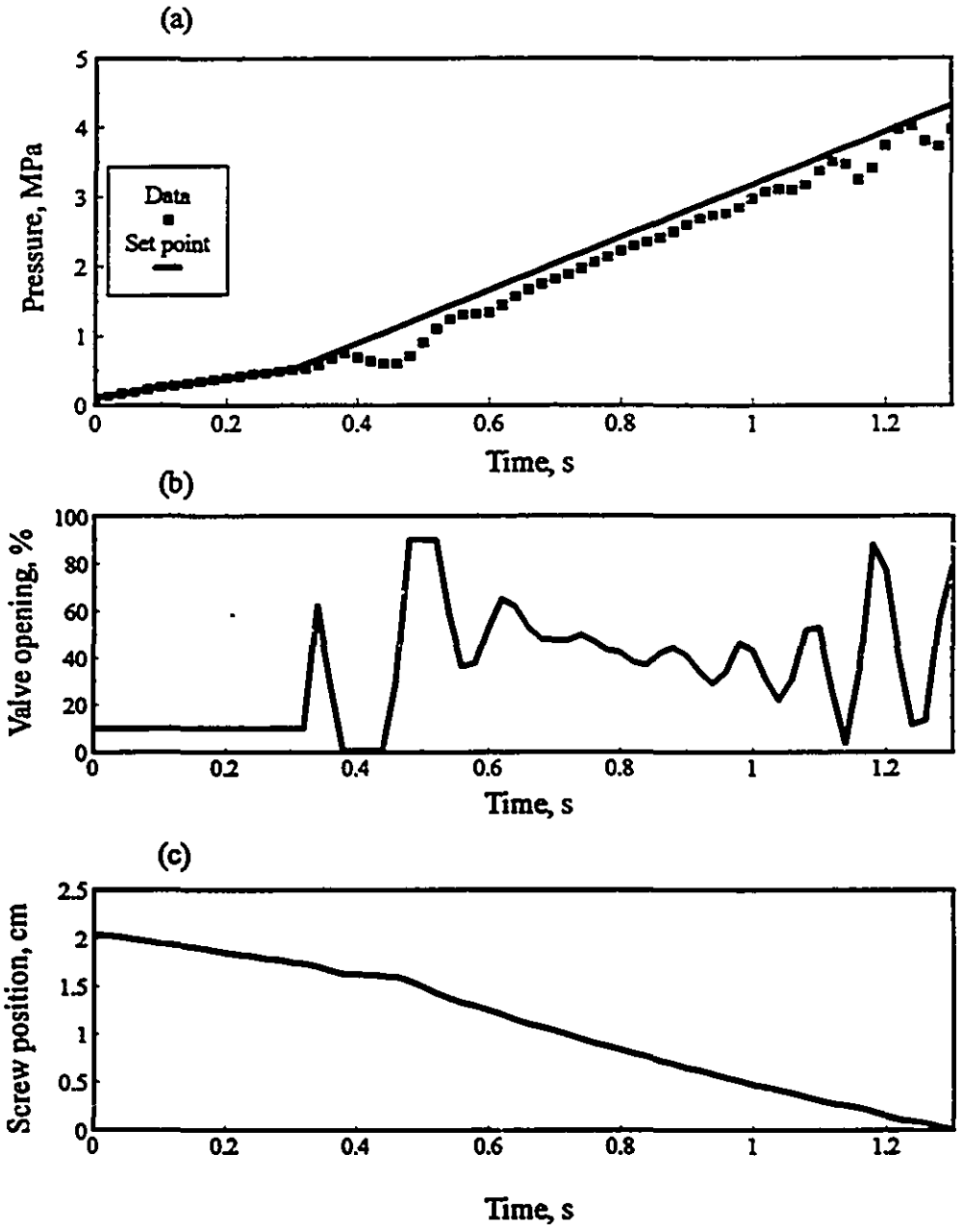

Figure 5.16 System response during the filling stage using the STCO-SP strategy in Experiment CP-3 (λ=0.95), Table 5.3. (a) Cavity pressure and set-point, (b) servo-valve opening, and (c) screw position.

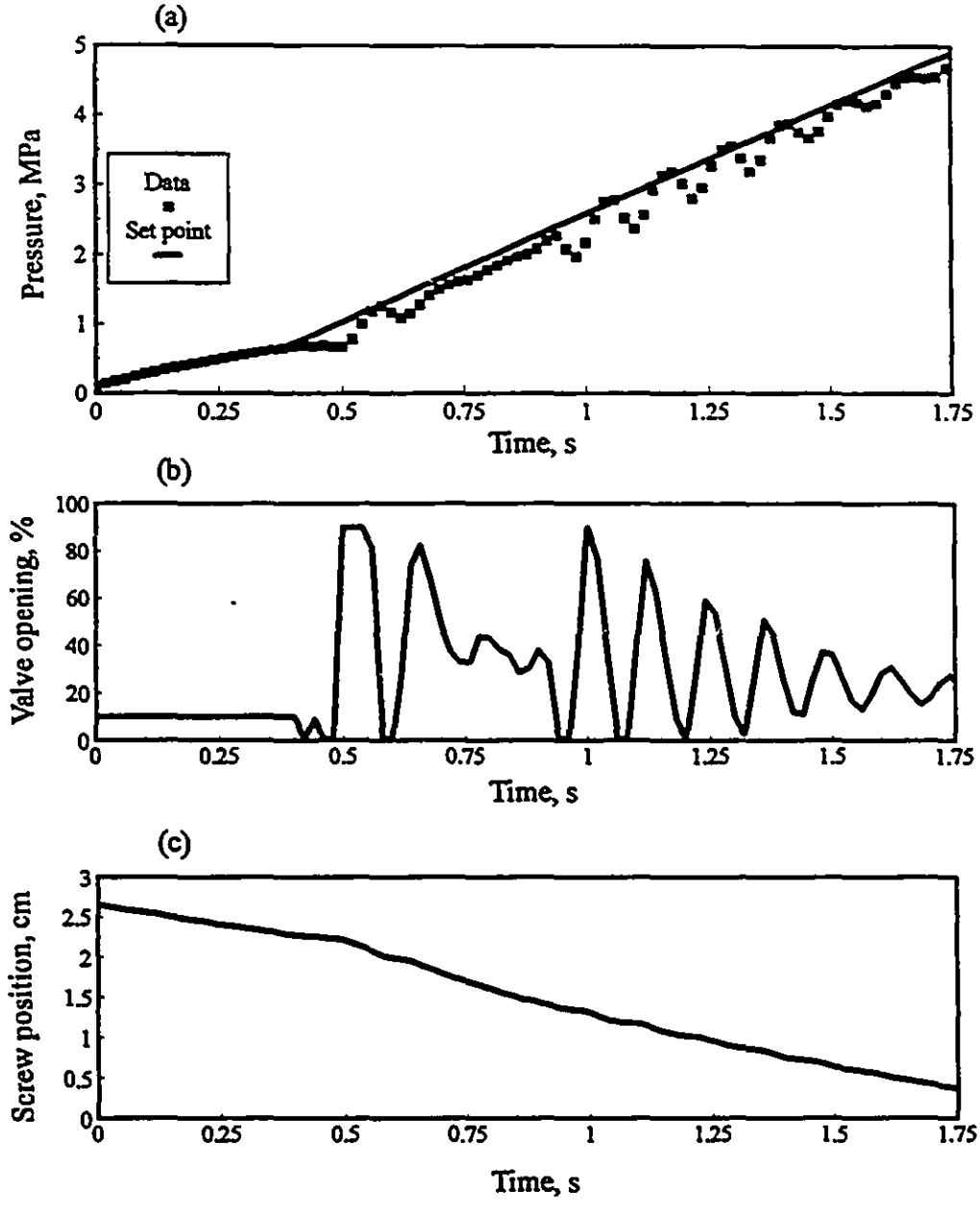

Figure 5.17 System response during the filling stage using the STCO-SP strategy in Experiment CP-4 (λ=0.75), Table 5.3. (a) Cavity pressure and set-point, (b) servo-valve opening, and (c) screw position.

5.35). The forgetting factor was fixed at 0.75. The transition from filling to packing is detected by the change in the slope of the cavity pressure.

The slope set-point during filling, $(dp/dt)_{sp}$, and the desired peak pressure, p_{psp}, cannot be defined independently. Figure 5.4 shows that the filling slopes do not affect the cavity pressure at the end of filling, but they determine the peak pressure. The filling pressure was controlled at constant slopes in the range from 1.72 MPa/s (250 psi/s) to 4.83 MPa/s (700 psi/s), in an experiment with the conditions given in Table 5.4 for Experiment D-4. After filling, the servo-valve opening was maintained at a low value of 0.5%. From the results, a relationship between the peak pressure and filling slope set-points was defined as

$$\left(\frac{dp}{dt}\right)_{sp} = (p_{psp} - 18.95)/0.6 \qquad (5.45)$$

Figure 5.18 shows that the response follows the set-point trajectory in Experiment CP-5, and that the control signal remains within the bounds ($0.5\% < u < 80\%$) during most of the filling stage. Figure 5.19 shows the system-response of Experiment CP-6 with the peak pressure set at 22.06 MPa (3200 psi). The control signal shows a few oscillations, and reaches the controller's bounds several times; however, the peak pressure remains close to the set-point. Both temperature and pressure change very rapidly during filling and packing, thereby affecting the polystyrene since it is amorphous and its viscosity is very sensitive to temperature near the glass transition temperature (Cowie, 1991). In addition, the high bulk modulus of polystyrene makes the cavity pressure difficult to control during the fastest section of packing. However, reasonable results on the control of the peak pressure were obtained.

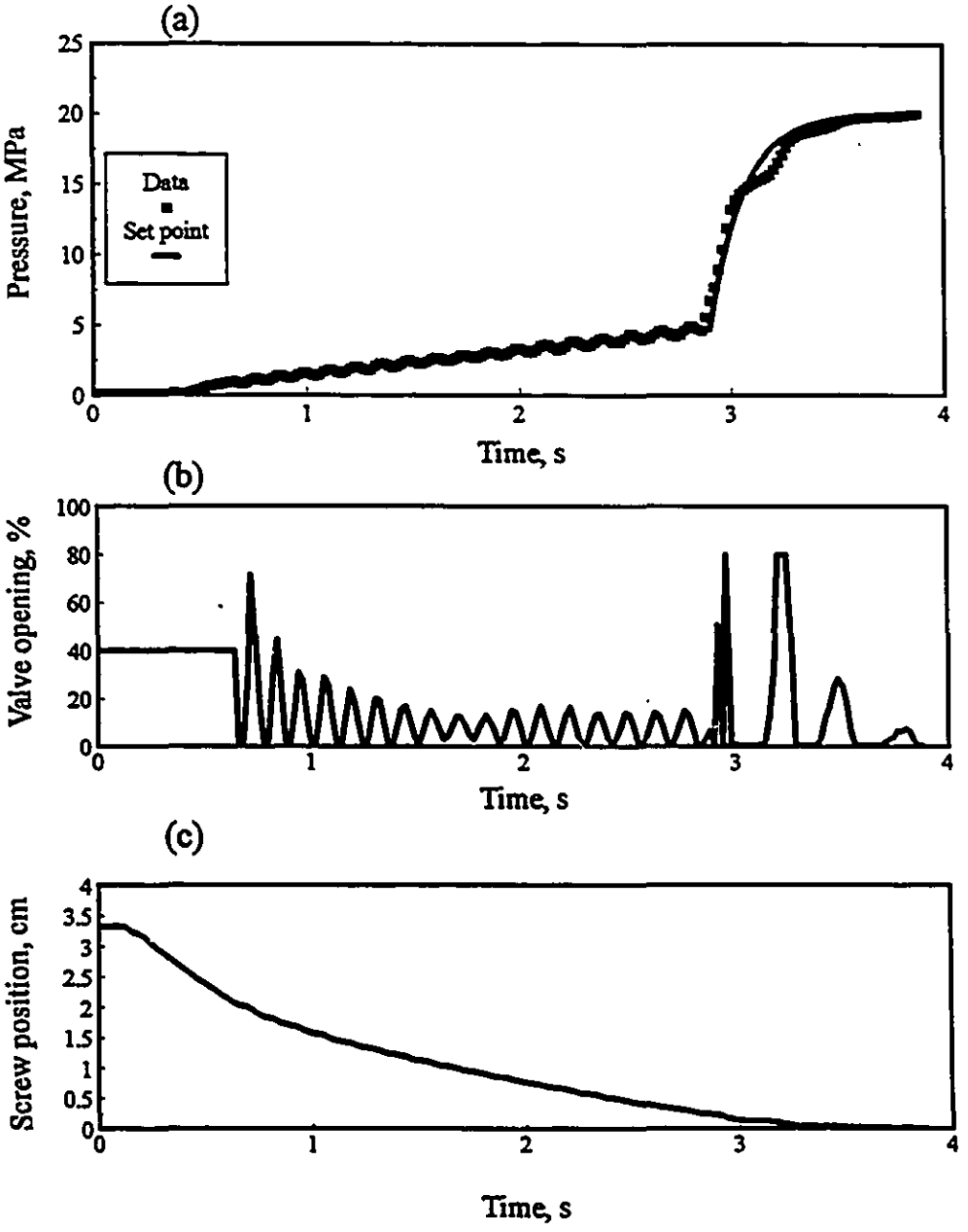

Figure 5.18 System response during filling and packing using the STCO-SP strategy in Experiment CP-5, Table 5.4. (a) Cavity pressure and set-point, (b) servo-valve opening, and (c) screw position.

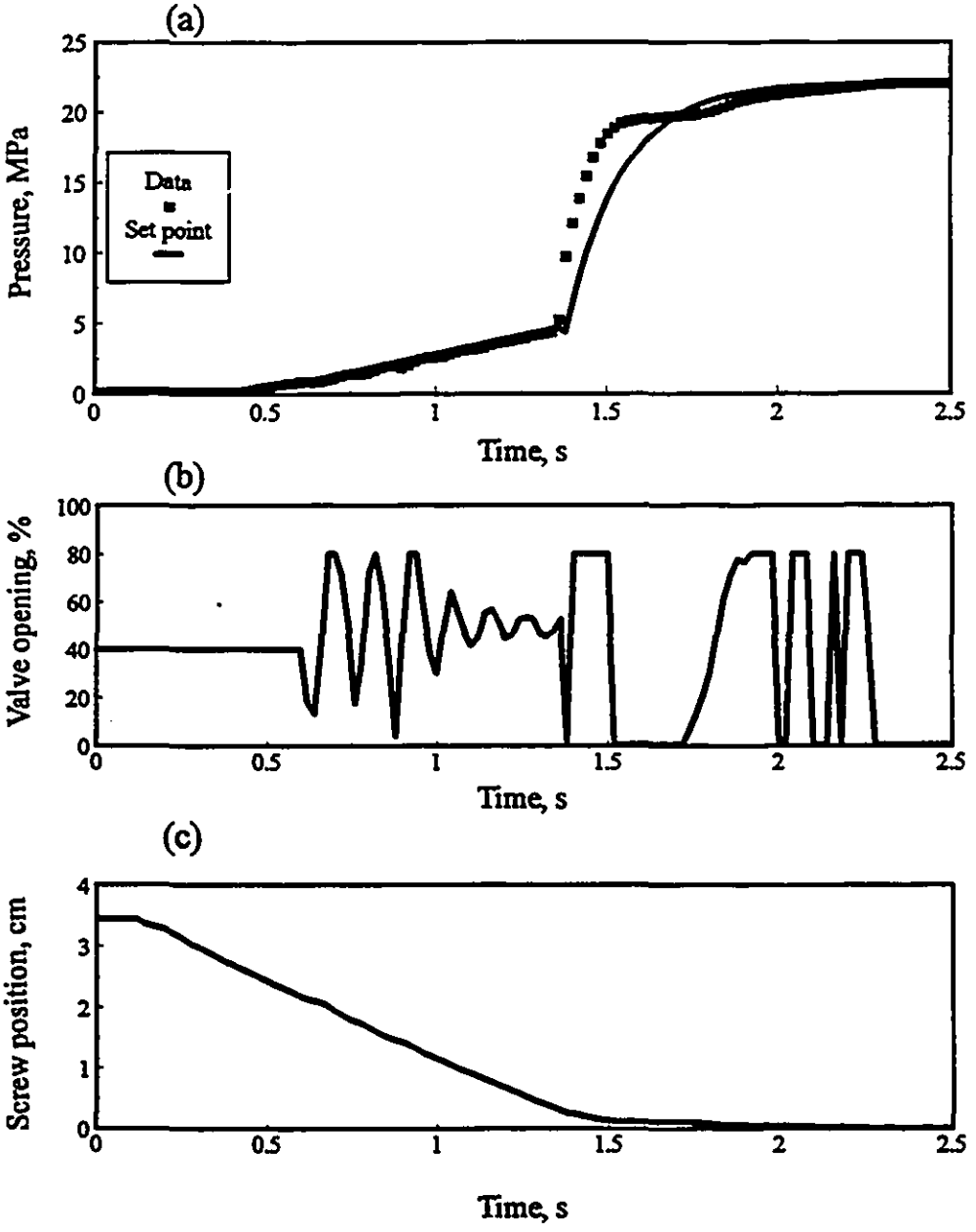

Figure 5.19 System response during filling and packing using the STCO-SP strategy in Experiment CP-6, Table 5.4. (a) Cavity pressure and set-point, (b) servo-valve opening, and (c) Screw position.

5.6 SUMMARY

A self-tuning approach started at a certain screw position has proven to be effective in controlling the cavity pressure profile during the filling and packing stages.

The packing pressure loses controllability as it approaches its peak value. This is due to polymer solidification in the sprue and runner and at the cavity walls, which causes the low cavity pressure responsiveness in the packing phase. To improve the cavity pressure sensitivity, the relation between openings of the supply servo-valve and return servo-valve should be q=0.5 (Equation 5.41).

A solution to the problem of control saturation has been presented. Controller saturation is reduced using a self-tuning control with first-order observer and state feedback. The time constants used for the observer, $\tau_o = 0.04s$ during filling and $\tau_o = 0.04s$ during packing, along with a forgetting factor of λ=0.75 and a pole location $t_1 = 0.7$ of, for the desired output response, allowed for the control of the cavity pressure at different profiles during filling and packing.

CHAPTER 6
BULK TEMPERATURE CONTROL

This chapter deals with cycle-to-cycle control of the bulk temperature. A cascade control scheme is implemented using a secondary control loop for the coolant temperature. The outer loop regulates the cycle bulk polymer temperature by adjusting the coolant temperature set-point. On-line estimates of the bulk polymer temperature are obtained from measurements of pressure and temperature at the cavity surface, as discussed in Chapter 4.

6.1 COOLANT TEMPERATURE CONTROL

The coolant temperature is regulated by manipulating the cold and hot water valves. Figure 6.1 presents a schematic of the coolant control system, where T_{hot} and T_{cold} denote the temperatures of the hot and cold water, respectively. The opening of the hot water valve u_1, expressed in percent, is the manipulated variable and is also used to set the opening of the cold water valve with the relationship: $u_{cold} = 100 - u_1$.

For the dimensionless coolant temperature which is defined as

$$y_1 = \frac{T_c - T_{cold}}{T_{hot} - T_{cold}}, \tag{6.1}$$

Gao (1989) determined a dynamic model using step changes in the opening of the hot water valve for this system. The model is first-order and, including the zero-order hold and a dead time of N sampling intervals, is expressed by

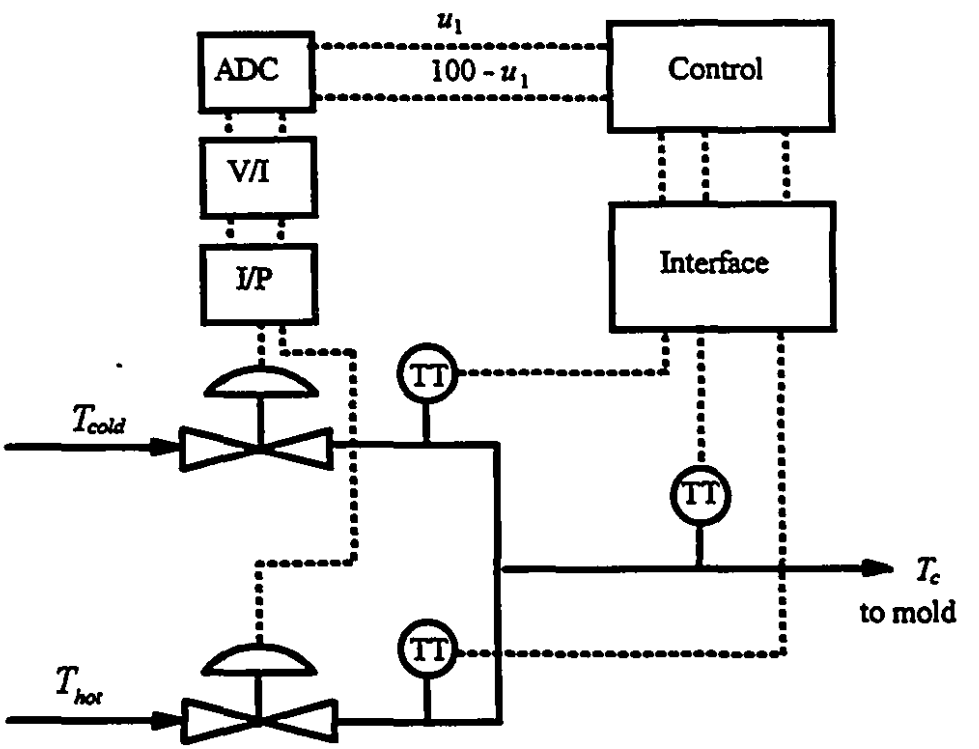

Figure 6.1 Schematic diagram of the feedback control for the coolant temperature.

$$HG_1 = \frac{y_1(z)}{u_1(z)} = \frac{K_1(1-a_1)z^{-N-1}}{1-a_1z^{-1}} \qquad (6.2)$$

$$a_1 = \exp(-\Delta t/\tau_c)$$

A time delay of about 1.2 s was observed, and thus N=6 for a sampling interval of $\Delta t = 0.2s$. The model parameters suggested are: $K_c = 0.009\ (\%)^{-1}$ and $\tau_c = 1.8$ s. Combining Equations 6.1 and 6.2 and inverting the result gives the discrete-time model for the coolant temperature

$$T_c(k) = a_1 T_c(k-1) + (1-a_1)T_{cold} + K_c(1-a_1)(T_{hot} - T_{cold})u(k-7) \qquad (6.3)$$

Figure 6.2a shows a block diagram of the coolant control system. The digital controller was implemented using the Dahlin algorithm which is based on the transfer function (Seborg et al., 1989):

$$D_1(z) = \frac{(1-A)z^{-N-1}}{1-Az^{-1}-(1-A)z^{-N-1}} \frac{1}{HG(z)} \qquad (6.4)$$

Substituting Equation 6.2 into 6.4 with $A=A_1$ and $N=6$ yields the controller transfer function

$$D_1(z) = \frac{u_1(z)}{e_1(z)} = \frac{1-A_1}{1-A_1z^{-1}-(1-A_1)z^{-7}} \frac{(1-a_1z^{-1})}{K_1(1-a_1)} \qquad (6.5)$$

$$A_1 = \exp(-\Delta t/\lambda_1)$$

where λ_1 is the time constant for the desired closed-loop response. The error e_1 may be written as

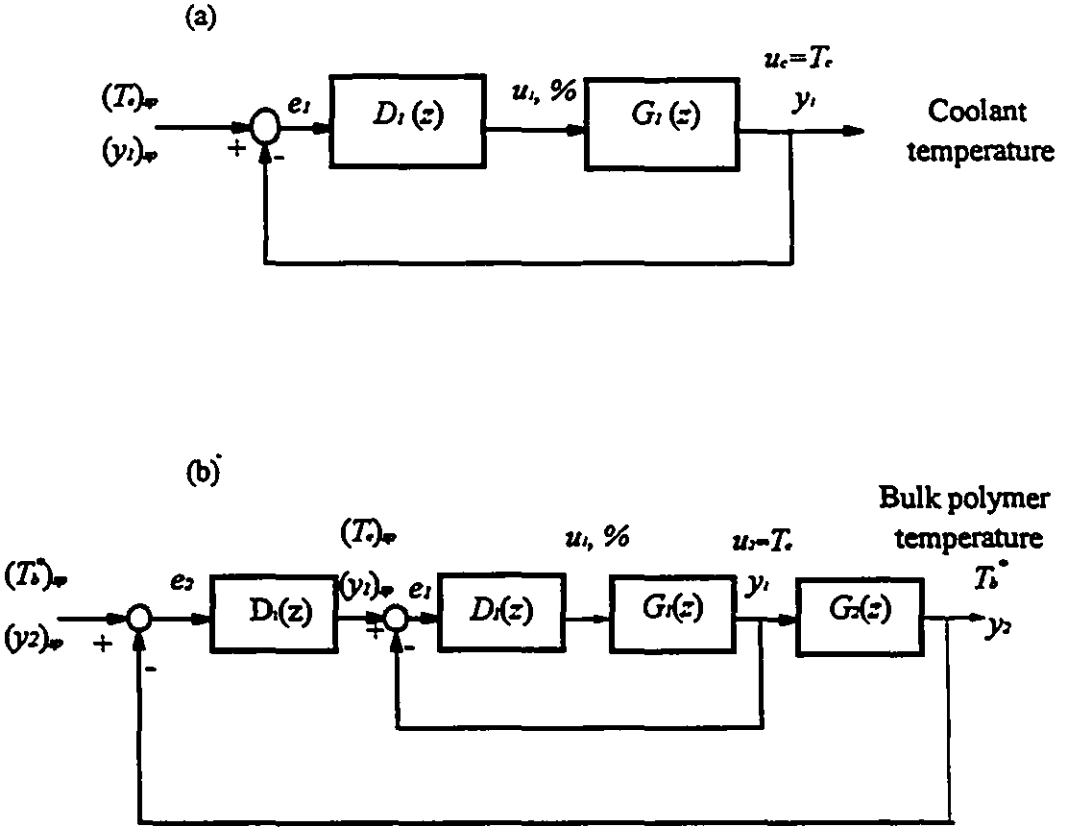

Figure 6.2 Block diagrams of (a) the coolant temperature control system, and (b) the cascade control system for the bulk temperature.

$$e_1(z) = (y_1)_{sp} - y_1(z) = \frac{T_c - (T_c)_{sp}}{T_{hot} - T_{cold}} \tag{6.6}$$

Substituting Equation 6.6 into 6.5 and inverting to the time domain leads to an equation for the opening of the hot water valve in T_c, the process output, which is given by

$$u_1(k) = A_1 u_1(k-1) + (1-A_1)u_1(k-7) + \frac{1-A_1}{K_1(1-a_1)} \frac{T_c(k) - a_1 T_c(k-1) - (1-a_1)(T_c)_{sp}}{T_{hot} - T_{cold}} . \tag{6.7}$$

Results of a simulation of the coolant temperature response for three step-changes in set-points are shown in Figure 6.3. The coolant temperatures settle at each set-point in about 2s.

6.2 BULK TEMPERATURE CONTROL

Temperatures of the polymer in the cavity are affected by the conditions of the melt at the nozzle and different machine parameters. Injection temperature, holding pressure, and coolant temperature are the variables that have the greatest influence on the bulk temperature. A dynamic model is determined from the bulk temperature response to a step change in the controlled coolant temperature. The main problem encountered in determining this model is that the melt nozzle temperature is not constant.

6.2.1 Empirical Modeling

Under the assumption that the temperature of the melt injected into the cavity is constant during a cycle sequence, the use of a simple parametric model is possible. An empirical model can be obtained from the step-

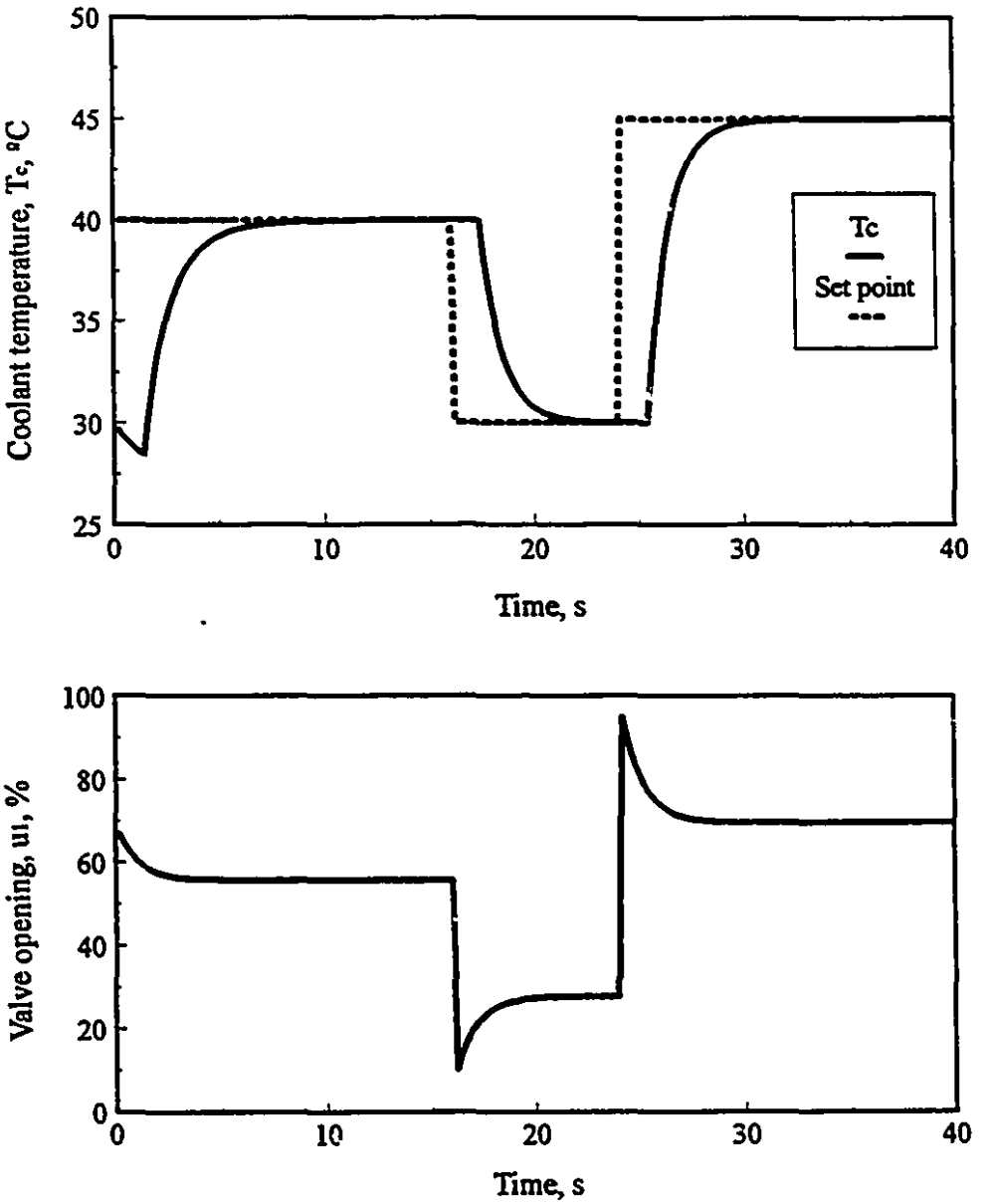

Figure 6.3 Simulated coolant temperature response and opening of the hot water valve for three step changes in set-point. The value of λ is 1.

response data of the bulk temperature to the coolant temperature. This is described by a first-order model as

$$HG_2(z) = \frac{y_2(z)}{u_2(z)} = \frac{b_2 z^{-1}}{1 - a_2 z^{-1}} \tag{6.8}$$

where y_2, the process output, is the bulk temperature (T_b^*), and u_2 is the coolant temperature (T_c). This equation in discrete form is

$$y_2(k) = a_2 y_2(k-1) + b_2 u_2(k-1). \tag{6.9}$$

6.2.2 Control Selection and Design

To control the bulk temperature, the cascade strategy shown in Figure 6.2b was implemented. In the primary control loop, the output y_2 is controlled by setting the coolant temperature $(y_1)_{sp}$ with the controller D_1. The inner loop controls the coolant temperature by manipulating the cold and hot water control valves (see Figure 6.1). The bulk temperature is determined in about 7 s after initiating the injection state (time t_{sf} in Figure 4.4), and the coolant temperature is regulated in less than 5 s. Therefore, the coolant temperature settles to a desired set-point in about 30 s before a new injection starts. Thus, the dynamic of the primary control loop is not affected by the dynamic of the inner control loop.

The discrete control is designed using a time-domain approach (Ogunnaike and Ray, 1994), which consists of assigning the controller a specified form such as

$$u_2(k) = u_2(k-1) + K_o e_2(k) + K_1 e_2(k-1). \tag{6.10}$$

In this equation, k denotes the cycle number. Combining and rearranging Equations 6.9 and 6.10, along with the error determined by $e_2(t) = (y_2)_{sp} - y_2(t)$, yields the desired discrete-closed-loop response which can be written as

$$y_2(k) = (1 + a_2 - b_2K_o)y_2(k-1) - (a_2 + b_2K_1)y_2(k-1) + b_2(K_o + K_1)(y_2)_{sp} \qquad (6.11)$$

The closed-loop response to a set-point change of value $(y_2)_{sp}$ is assumed to be given by a first-order model which may be written as

$$\frac{y_2(k)}{(y_2)_{sp}} = \frac{(1 - A_2)z^{-1}}{1 - A_2z^{-1}} \qquad (6.12)$$

Taking into consideration the fact that the sampling time is 1 cycle, A_2 may be determined using the equation

$$A_2 = \exp(-1/\lambda_2) \qquad (6.13)$$

where λ_2 is the desired time constant for the cavity-polymer-temperature response. In discrete-time form, Equation 6.12 may be written as

$$y_2(k) = A_2y_2(k-1) + (1 - A_2)(y_2)_{sp}. \qquad (6.14)$$

Controller parameters K_o and K_1 can be obtained by comparing Equations 6.10 and 6.14, so the following expressions result

$$K_o = \frac{1 + a_2 - A_2}{b_2}, \quad K_1 = -\frac{a_2}{b_2} \qquad (6.15)$$

6.3 EXPERIMENTAL PROCEDURE

Two sets of experiments were conducted:

(1) Dynamic open-loop experiments which were intended to determine the dynamic relationship between the bulk temperature and the controlled coolant temperature.

(2) Closed-loop control experiments (PT control) for the cycle-to-cycle control of the peak cavity pressure as well as the bulk temperature. The peak pressure is controlled in each cycle through controlling the cavity pressure profile using the self-tuning algorithm (STCO-SP) described in Section 5.4.3.

6.3.1 Dynamic Open-Loop Experiments

To determine an approximate dynamic model of the bulk temperature, experiments were conducted using step changes in the controlled coolant temperature with magnitudes ± 10 °C. The experimental conditions are shown in Table 6.1. The file structure described in Section 3.3 was used to carry out the experiments (see Figure 3.8). File *pcontrol* (*p_tav_tc.c*) sends the coolant temperature set-point to task *moldtemp.control* (*mt_tavg.c*) after a specified cycle in the cycle sequence. Task *tavg* (*tavg.c*) uses the algorithm discussed in Chapter 4 to estimate the bulk temperature (T_b^*) from collected data of cavity pressure and surface temperatures.

6.3.2 Closed-Loop Control Experiments (PT Control)

The cavity pressure and the bulk temperature vary within ranges that depend on the molding conditions. This is seen in Figure 6.4, obtained with

Table 6.1 Conditions of experiments for step tests in coolant temperature

Servo-valve opening 40 %				
Sampling period 0.020 s				
Barrel temperature set-points:	Nozzle zone	240 °C		
	Front zone	220 °C		
	Rear zone	200 °C		
	Feed zone	190 °C		
Cycle times:	Injection	13 s		
	Decompression	2 s		
	Cooling	10 s		
	open	10 s		
Experiment	DT1	DT2	DT3	DT4
T_c change	40–30	40–30	35–45	30–40

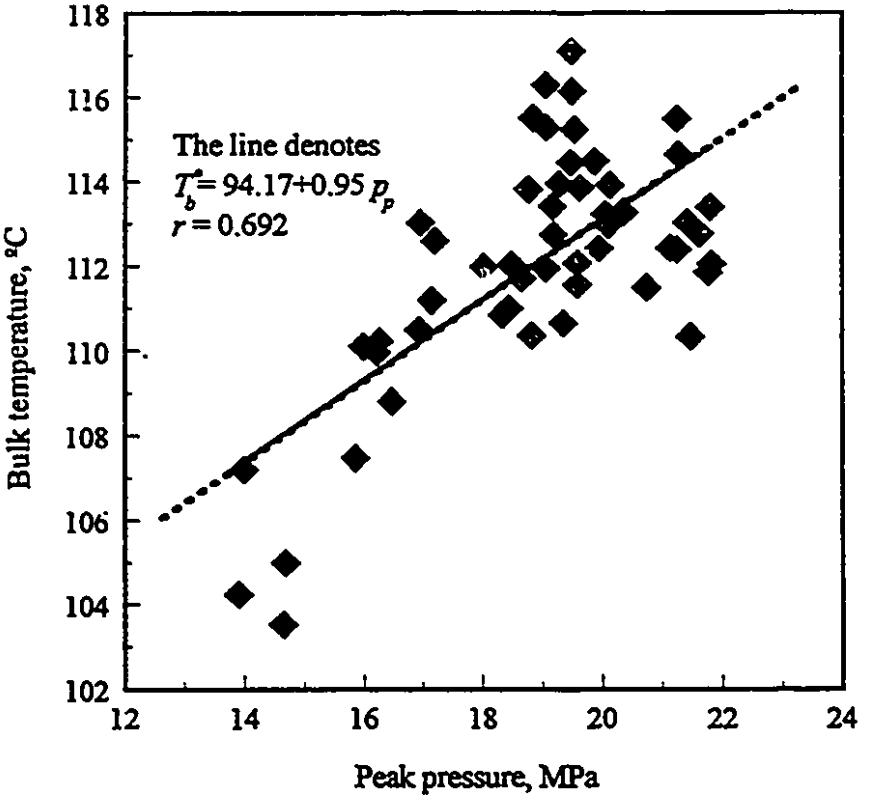

Figure 6.4 Variation of the bulk temperature with peak pressure for Experiments P-1 and P-2 (see Table 4.2). The fitted regression has a coefficient of correlation of 0.692.

data of Experiments P-1 and P-2 at conditions given in Table 4.2, which shows that the bulk temperature increases with the peak cavity pressure in a limited range of operating conditions. The experimental conditions for the PT control strategy are shown in Table 6.2, in which the set-points for the bulk temperature were selected using the fitted line shown in Figure 6.4 according to the desired peak pressure. Therefore, these variables are controlled at selected values in this region. This procedure is called PT control and is shown in Figure 6.5

The structure given in Figure 3.8 was used to control the polymer temperature, as well as the cavity pressure. In the Figure, file *pcontrol* (*pcontrol.c*) is used to regulate the cavity pressure by the self-tuning algorithm described in Chapter 5. The file *tcontrol* (*tcontrol.c*) records the pressure and surface temperature profiles in the cycle, which are used in file *tavg* (*tavg.c*) to determine the instant at which the gate seals and estimate the bulk temperature. The bulk polymer temperature is controlled with file *moldtemp.control* (*mt_pt.c*). In the inner loop, the sampling time was 0.2 s.

6.5 RESULTS AND DISCUSSION

Figure 6.6 shows the step change in coolant temperature used in Experiment DT-2 to determine the dynamic of the bulk temperature. It is seen that the coolant temperature settles in about 2 s for a step change in the set-point from 40 °C to 30 °C. The cycle time is 35s, so the coolant temperature settles about 33 seconds before the beginning of the next cycle.

The dynamic experiments were carried out at conditions in which variations in the nozzle melt and barrel temperatures were less than 5 °C after

Table 6.2 Conditions of experiments used to control the peak cavity pressure and bulk temperature (PT control).

Initial servo-valve opening = 40 %
Pole location of desired response, $t_1 = 0.7$
Sampling period, $\Delta t = 0.02$ s.
Time constant for the set-point profile model in packing
τ_{sp}=0.16s (see Equation 5.40)
Range in opening of the supply servo-valve, $0.5 \leq u \leq 80$.
Time constant for the observer dynamics,
$\tau_o = 0.04$ (filling), $\tau_o = 0.01$ s (packing)
Forgetting factor, $\lambda = 0.75$
Barrel temperature set-points (°C) = 240/220/200/190
Initial controlled coolant temperature = 30 °C

Experiment	PT-1	PT-2
Set-points		
p_{psp}, MPa	20.00	22.06
$(\bar{T}_b^{\circ})_{sp}$, °C	115	120

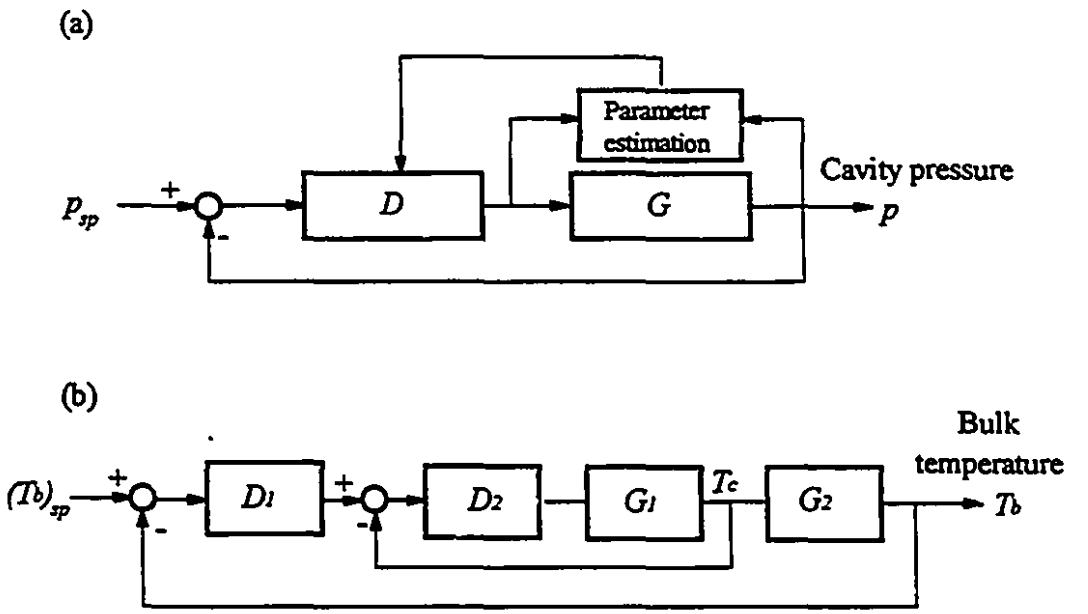

Figure 6.5 Block diagrams for the PT control strategy. (a) Self-tuning control of the cavity pressure, and (b) cascade control of the bulk temperature .

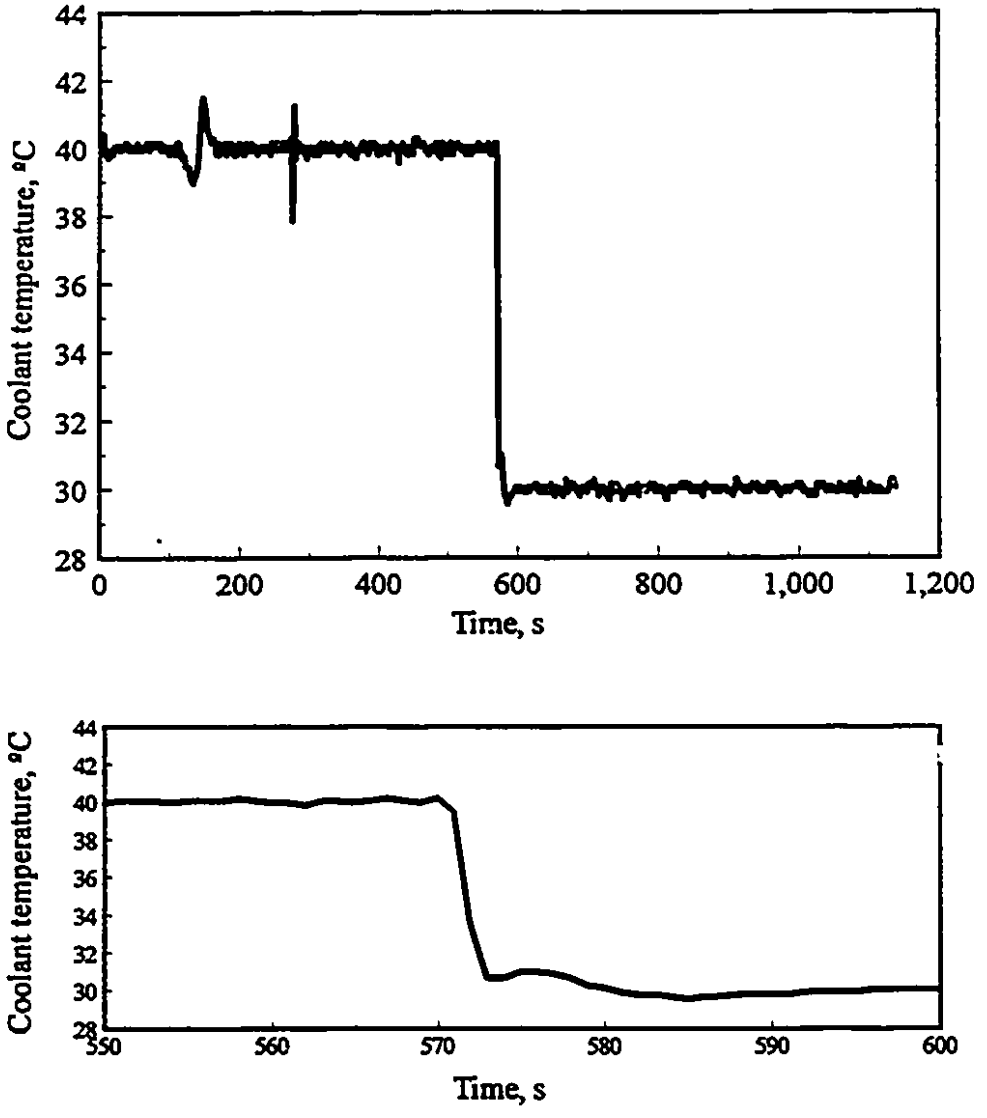

Figure 6.6 Variations in the controlled coolant temperature with time in Experiment DT-2.

the step test. Therefore, the melt temperature may be assumed constant which suggests that the polymer temperature be controlled by the heat transfer process in the cavity. The melt injected into the cavity cools very quickly as no band heater is installed on the nozzle, and takes about 15 cycles to reach stable conditions.

Figure 6.7 illustrates the variations of the bulk and coolant temperatures in the cycle sequence in Experiment DT-2. The bulk temperature increased when the coolant temperature changed from 40° to 30 °C. The reason for this is that when the temperatures of the cavity walls decrease, the polymer viscosity and flow resistance increase. As a result, the polymer temperature rises due to viscous dissipation. The opposite effect was observed in Experiment DT-4, as seen in Figure 6.8.

The above results can also be explained by analysing cooling rates at the cavity surface in Experiment DT-2. The measurements at sensor TS1 (see Figure 3.4), in the interval (t_{peak}, t_{ef}), are fitted by linear regression, and the results give the gradients plotted in Figure 6.9 for each cycle. The cooling rates are about 1.25 °C/s for T_c = 40° C and 1.3° C for T_c = 30 °C. This suggests that the heat flow when T_c = 40°C is higher than when T_c = 30 °C . A lower cooling rate is attributed to higher polymer temperatures, since the driving temperature difference between the coolant and the melt becomes smaller. In summary, the step-test experiments showed that with a constant injection temperature, for a negative change in coolant temperature (40°C to 30 °C), the cooling rates decrease and the bulk temperatures increase. The opposite effect is observed for a positive change coolant temperature (40° to 45 °C). These observations are valid for the coolant and bulk temperature conditions evaluated in this study. They may be different outside this range.

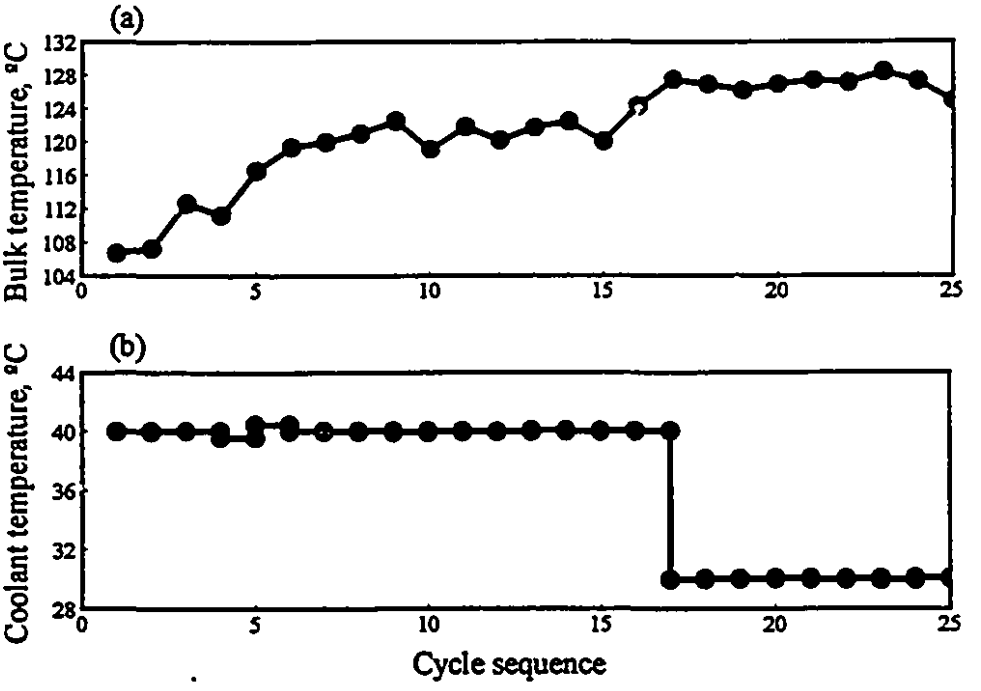

Figure 6.7 Temperature variations in Experiment DT-2. (a) Bulk temperature, and (b) coolant temperature.

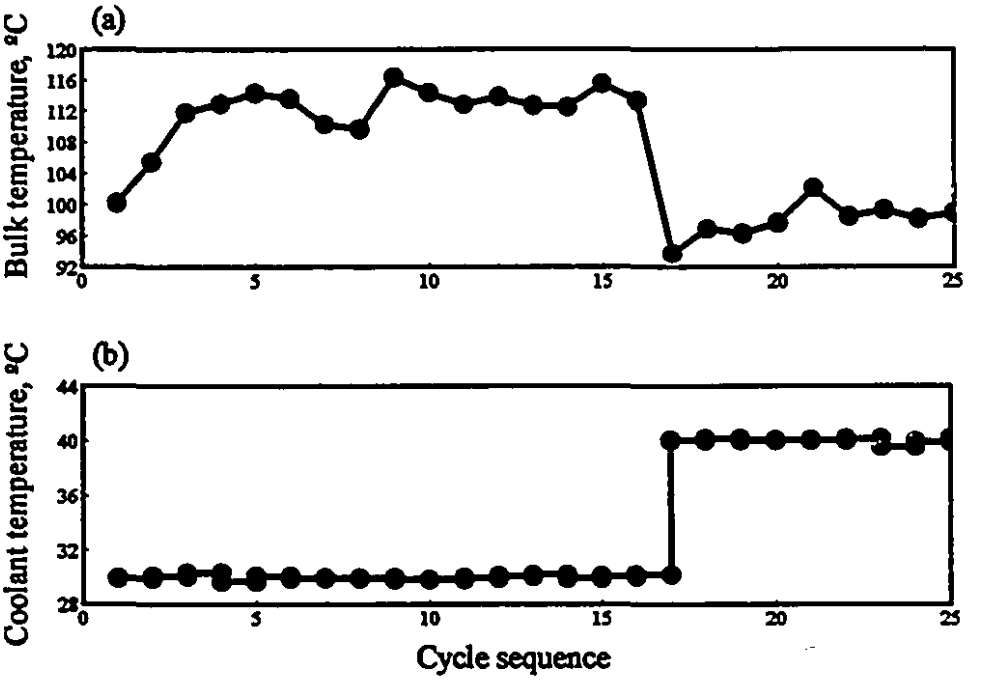

Figure 6.8 Temperature variations in Experiment DT-4. (a) Bulk temperature, and (b) coolant temperature.

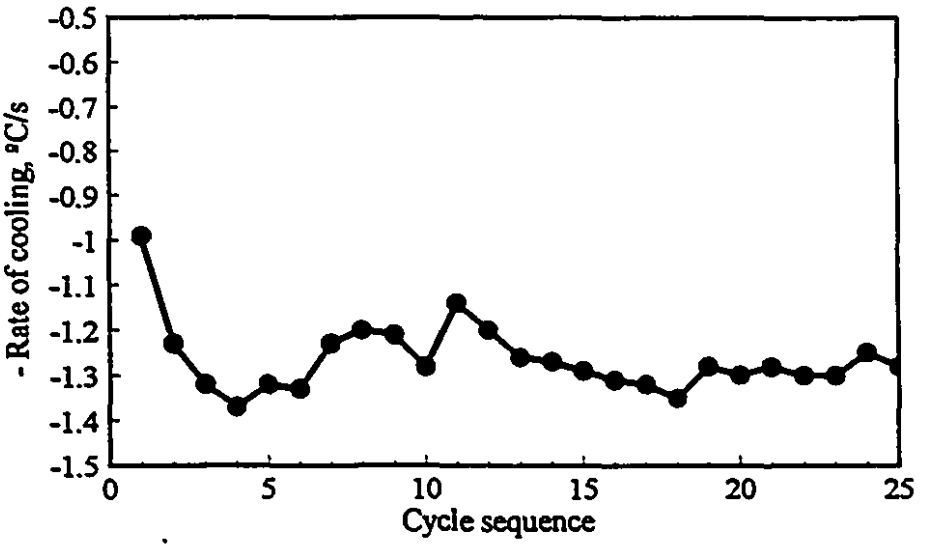

Figure 6.9 Variations in cooling rate at sensor TS1 in Experiment DT-2.

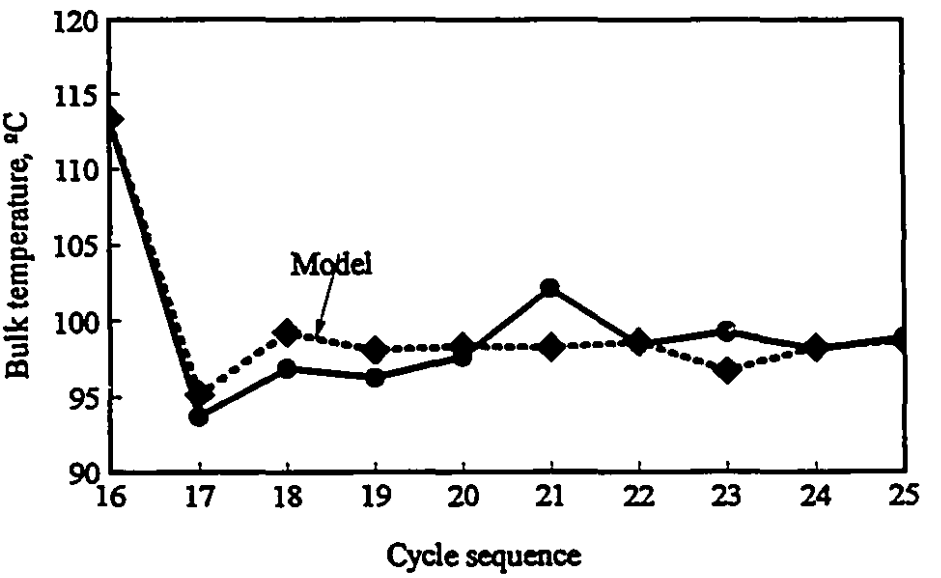

Figure 6.10 Bulk temperature variations in Experiment DT-4.

Table 6.3 summarizes the results of parameter identification for the first-order model given in Equation 6.9, where $u_2=T_c$ and $y_2=T_b^*$. Model parameters were estimated using the MATLAB ID-Toolbox (Ljung, 1991) with the data obtained in Experiments DT-1 to DT-4. Average parameter values are a_2=0.2010 and b_2=2.9263. Calculated polymer temperatures are close to the data values, as seen in Figure 6.10 for Experiment DT-4.

Figure 6.11 illustrates the system response for experiment PT-1 in which the polymer temperature set-point was 115 °C, and the peak pressure was controlled at 20 MPa (2900 psi). The observed increase in bulk temperature is due to viscous heating caused by drifts in the front barrel and melt temperatures, as seen in Figure 6.11d. Fluctuations in the nozzle-melt temperature retard the controller action, so the bulk temperature takes several cycles to settle at the desired set-point.

Figure 6.12 presents the results of Experiment PT-2 with the polymer temperature regulated at 120 °C and the peak pressure at 22.06 MPa (3200 psi). Steady-state values of the bulk temperatures are about 5 °C higher than the desired response. The Figure shows that the control over the peak cavity pressure was effective.

6.5 SUMMARY

This chapter presents a cascade control scheme for the temperature of the polymer in the cavity at the time the gate seals or bulk temperature. The strategy has been implemented experimentally using first-order models.

Table 6.3 Results of parameter identification for the first-order model of the bulk temperature (Equation 6.9)

Experiment	DT-1	DT-2	DT-3	DT-4
Tc change	40-30	40-30	35-45	30-40
a	0.3187	0.2241	0.0552	0.2060
σ	0.2180	0.1599	0.0552	0.1249
b	2.9329	3.2935	2.5195	2.9592
σ	0.9286	0.6761	0.1432	0.3111
V_N (Eq. 5.43)	6.746	0.418	1.176	4.017
FPE (Eq. 5.44)	10.6	0.653	1.764	6.026

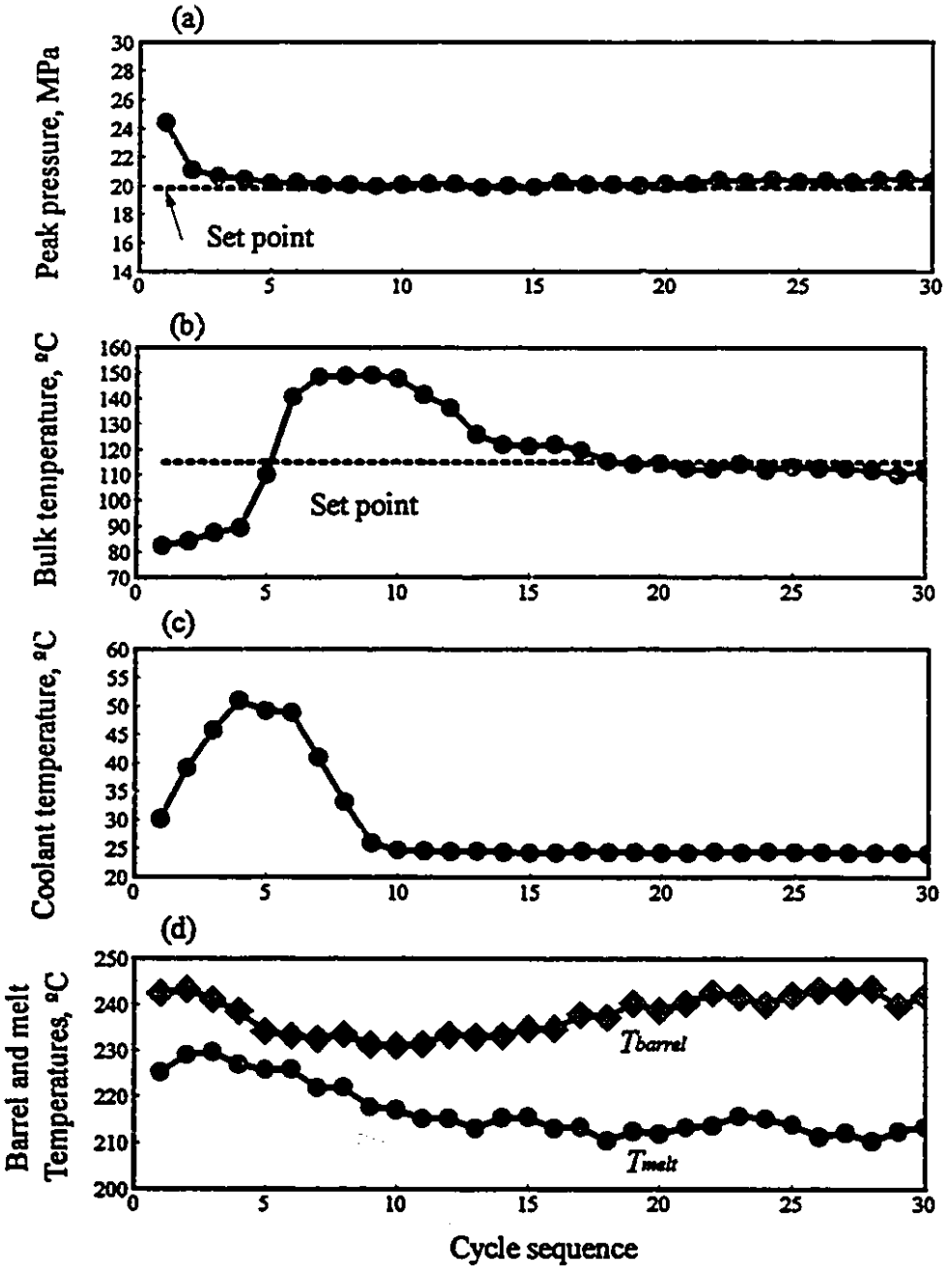

Figure 6.11 Peak pressure and temperature variations in Experiment PT-1, Table 6.2. (a) Peak pressure, (b) bulk temperature, (b) coolant temperature, and (c) front barrel and melt temperatures.

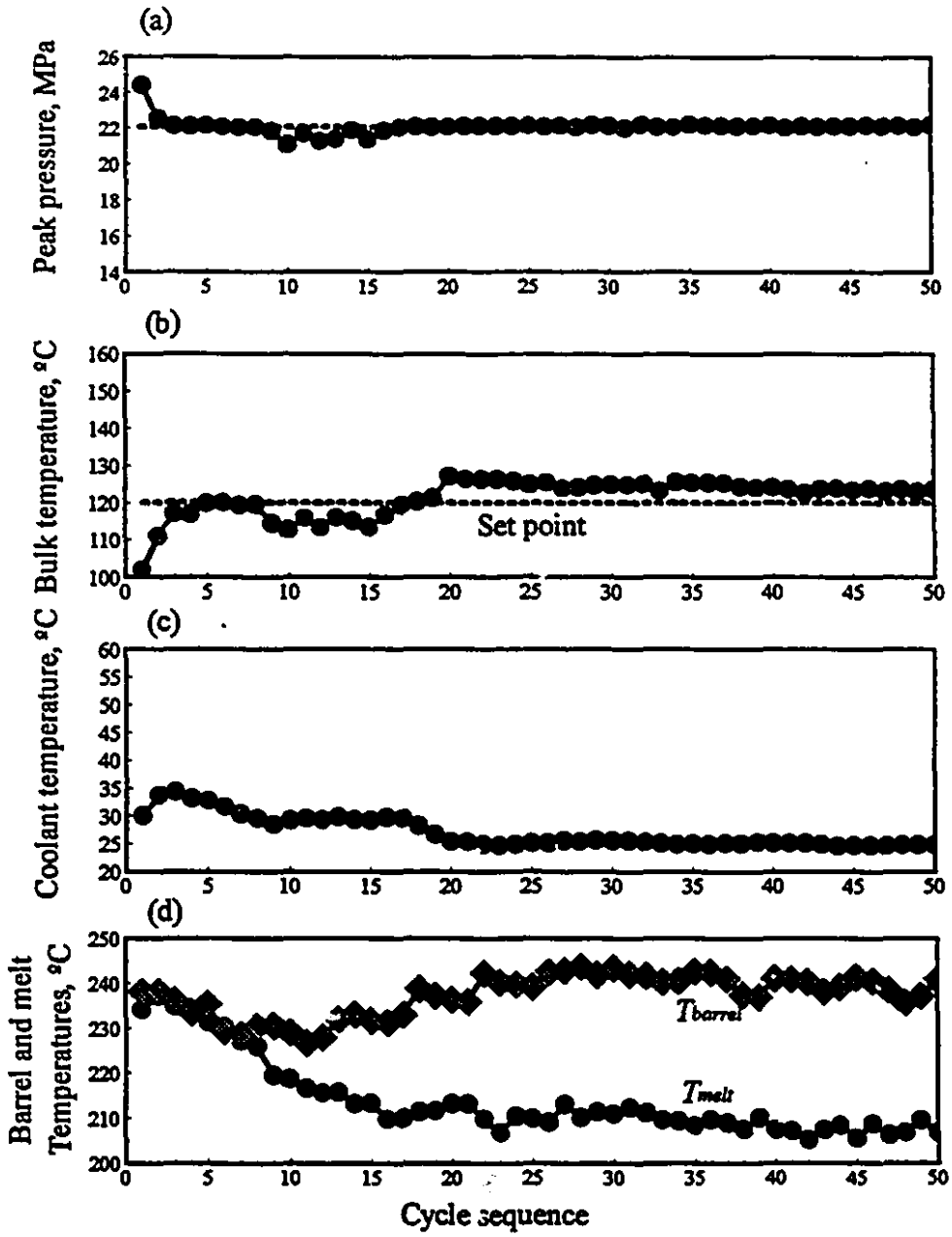

Figure 6.12 Peak pressure and temperature variations in Experiment PT-2, Table 6.2. (a) Peak pressure, (b) bulk temperature, (b) coolant temperature, and (c) front barrel and melt temperatures.

The inner loop controls the coolant temperature by a Dahlin algorithm. An expression based on the desired response of the bulk temperature was found appropriate for synthesis of the controllers in the primary loop.

Control of the bulk temperature was observed during cycle sequences where the melt temperatures were approximately constant. The average nozzle-melt temperature changes during the cycle sequence, so the bulk temperature takes about 10 cycles to settle at the set-point. Therefore, installing a band heater in the nozzle and setting up a control system for the temperature of the polymer melt injected into the cavity is advisable.

CHAPTER 7
CONTROL OF PART WEIGHT

7.1 INTRODUCTION

Shot-to-shot variations of product quality in the injection molding process may occur for several reasons. Major factors are defects in the check valve of the injection screw (worn or bad seating), poor barrel temperature distribution, and variations in melt density caused by alterations in the hydraulic pressure, barrel temperature distribution, and in the cavity pressure and temperature. Apart from this natural variability of the molding process, changes in the temperature of the hydraulic oil, and alterations in the servo-valves and heater control system may also affect the weight.

The part weight is determined when the gate seals because the polymer in the cavity is then isolated and the melt cannot flow back out of the cavity at the end of the holding stage. Normally, the gate seal time is found by increasing the injection time (includes filling, packing, and holding) until the weight of fully packed parts does not change significantly. However, this procedure does not guarantee part consistency from cycle to-cycle.

7.2 ANALYSIS OF CONTROL STRATEGIES

Two approaches are possible to control the part weight: direct control and indirect control. The term "weight control" will be used to mean the control of the part weight.

7.2.1 Direct Control of Weight

This method involves on-line measurement of the weight, and requires either an automatic weighing scheme or an operator to weigh the parts and then enter the result in the control loop. Figure 7.1 shows a block diagram of this strategy. A relationship between the weight and a manipulated variable, such as the opening of the hydraulic valve, is required to carry out the control action. Because this model is not general, and a rapid weighing method may not be reliable, direct control is not convenient.

Figure 7.2 shows a block diagram of weight control using a model to infer the weight from cavity pressure and temperature measurements. The model can be approximated by the linear form of the weight model around a reference $W(T_{ref},p_{ref})$, where T_{ref} and P_{ref} can be taken as the characteristic bulk temperature and pressure for a reference shot. A linear model is

$$W=W_{ref}+\left(\frac{\partial W}{\partial p_p}\right)_{T_b}(p_p-P_{ref})+\left(\frac{\partial W}{\partial T}\right)_{P_p}(T_b^*-T_{ref}) \tag{7.1}$$

In deviation variables, this equation may be expressed by

$$\bar{W}=\beta_T\bar{P}+\beta_p\bar{T}$$

$$\beta_T=\left(\frac{\partial W}{\partial p_p}\right)_{T_b},\quad \beta_P=\left(\frac{\partial W}{\partial T}\right)_{P_p} \tag{7.2}$$

To carry out a control algorithm based on the estimation of the weight, the model must be very accurate.

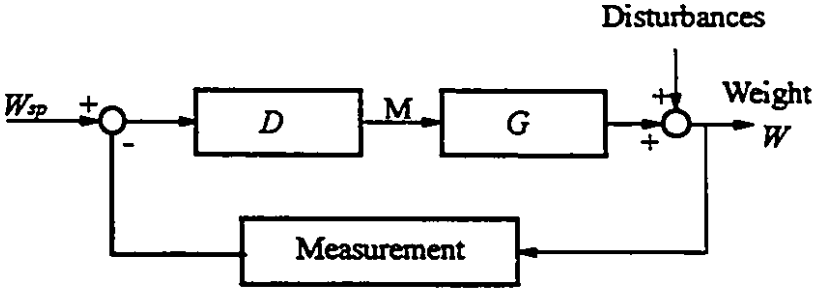

Figure 7.1 Direct control of part weight

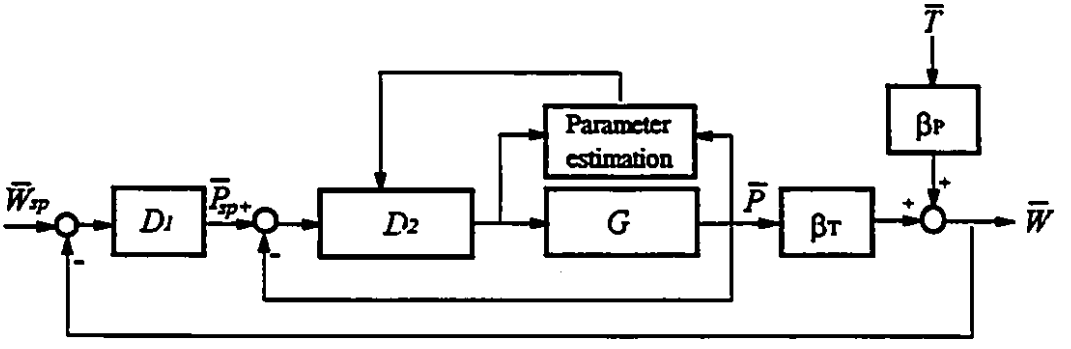

Figure 7.2 Block diagram for inferred control of weight using a linearized part weight model.

7.2.2 Indirect Control of Weight

Indirect weight control consists of controlling the properties which determine the weight at the time the gate freezes, the pressure and bulk temperature.

One procedure is to control both the peak pressure and bulk temperature with separate control loops as was discussed in Section 6.4.2, using the PT control scheme (see Figure 6.5).

Another procedure consists of measuring one of these properties and using a model to estimate at what level should the other property be controlled in order to keep the weight constant. One way to do this is by adjusting the peak pressure to compensate for variations in the bulk temperature. Then, if no deviations from a reference shot, $W = W_{ref}$, are expected to occur in next the cycle, k+1, the peak pressure is obtained from Equation 7.2, and is given by

$$\bar{P}(k+1) = -\left(\frac{\beta_T}{\beta_P}\right)_k \bar{T}(k) \tag{7.3}$$

β_P and β_T are determined from the cavity temperature and pressure of the previous cycle k. Substituting the deviation variables, Equation 7.3 becomes

$$p_p(k+1) = P_{ref} - \left(\frac{\beta_T}{\beta_P}\right)_k (T_b^*(k) - T_{ref}) \; . \tag{7.4}$$

This method is called PWT control and is illustrated with the simplified flow diagram shown in Figure 7.3. β_T and β_P, given by Equation 7.2, can be

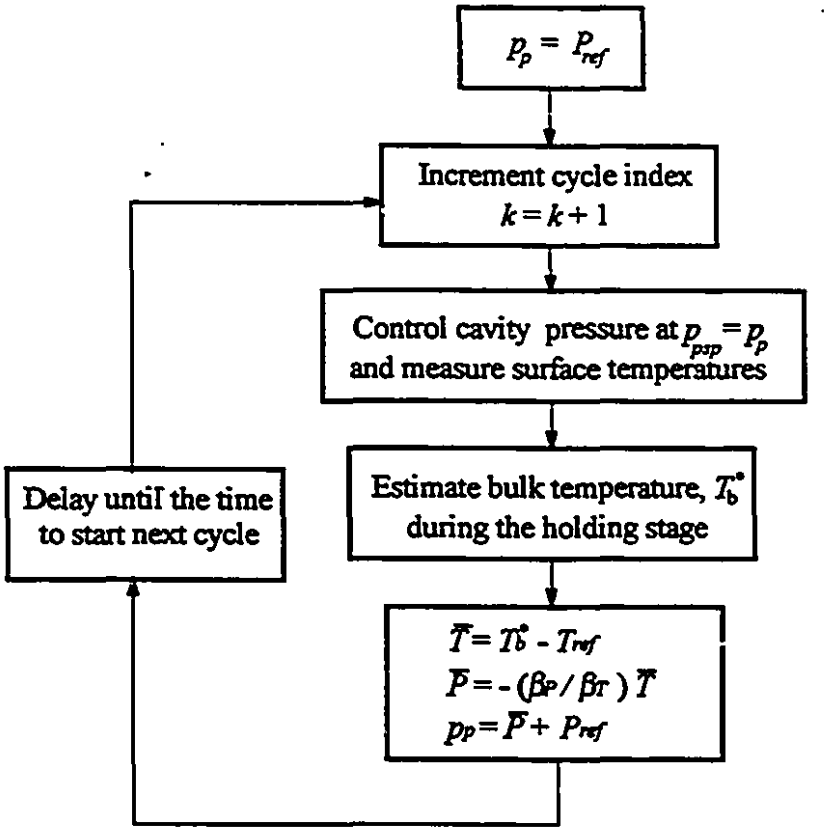

Figure 7.3 Flow diagram of the PWT control algorithm.

evaluated for each cycle using the part weight model discussed in Section 4.4.

7.3 EXPERIMENTAL PROCEDURE

The following experiments were conducted: (1) open-loop, to find the effect of certain operating variables on weight, and (2) ciosed-loop, to implement the PT and PWT control strategies. The cycle times were set as follows: injection 13 s. decompression 2s, cooling 10s, and open time 10s.

7.3.1 Open-Loop Experiments

Experiments were conducted to determine the variations in weight with different barrel temperature profiles and servo-valve openings. Table 7.1 summarizes the experimental conditions. The file structure employed to operate the injection molding machine is given in Figure 3.8. Files ***moldtemp.control*** (***mt_const.c***) and ***heater*** (***heater.c***) are used to control the coolant temperature and barrel temperatures, respectively. The command to maintain the supply servo-valve at a fixed opening is given by file ***pcontrol*** (***p_const.c***)

Preliminary experiments showed that the front barrel wall temperature exceeds the nozzle melt temperature by a minimum of 20 °C. An injection temperature of 218 °C is recommended for polystyrene (Rosato and Rosato, 1990). Therefore, the set-points for the barrel temperature profiles (see Figure 3.3a) should be selected so as to ensure no solidification occurs in the nozzle during the cooling stage.

Table 7.1 Experimental conditions used to determine the effects of machine variables on part weight

Experiment	Barrel temperature set-points, °C	Coolant temperature, °C	Servo-valve opening, %
W-1	290/260/230/190	40	16
W-2	280/260/230/190	40	16
W-3	280/260/230/190	40	12
W-4	230/220/200/190	40	10
W-5	280/220/200/190	40	50
W-6	290/220/200/190	40	50

7.3.2 Control Experiments

The program structure used to carry out the weight control is shown in Figure 3.8. Program *pcon_pwt.c* (*pcontrol*), described in Table 3.6, is used to control the cavity pressure profile with the same parameters of the TP control. The bulk temperature is estimated with files *tcon_pwt.c* (*tcontrol*) and *tavg_pt.c* (*tavg*). The cavity pressure is controlled using the self-tuning control with an observer implemented after a certain degree of filling (STCO-SP), as was discussed in 5.4.3, but in this case the set-point for the peak pressure is predicted with Equation 7.4, that is $p_{psp} = p_p(k+1)$. Table 7.2 summarizes the conditions of the experiments conducted to control the part weight.

7.4 RESULTS AND DISCUSSION

The discussion concerning the open-loop experiments considers only a few factors of part weight variations. Other variables, such as ram velocity, oil temperature, and clamp pressure are not included.

7.4.1 Open-Loop Experiments

Once a cycle sequence is initiated, the front barrel temperature drifts from the set-point as shown in Figure 7.4 for the first 20 cycles in Experiment W-3 and W-4. The melt temperatures decrease to 210 °C in the first case, and to about 185 in the second. The differences between temperature of the barrel and of the melt are due to the low thermal conductivity of the melt, which does not allow a thermal equilibrium in a short cycle time. The molten polymer cools quickly because the nozzle does not have a heating element.

Table 7.2 Experimental conditions used to control the weight

Initial servo-valve opening = 40 %
Pole location of desired response, $t_1 = 0.7$
Sampling period, $\Delta t = 0.02$ s.
Time constant for the set-point profile model in packing
τ_{sp}=0.16s (see Equation 5.40)
Range in opening of the supply servo-valve, $0.5 \leq u \leq 80$.
Time constant for the observer dynamics,
τ_o = 0.04 s (filling), τ_o = 0.01 s (packing)
Proportionality factor, Eq. 5.42, q=0.5
Forgetting factor, $\lambda = 0.75$
Barrel temperature set-points (°C) = 240/220/200/190
Initial controlled coolant temperature = 30 °C

Experiment	WC-1	WC-2	WC-3	WC-4
Set-points				
P_{ref}, MPa	20	22.06	20.00	22.06
T_{ref}, °C	115	120	115	120
Control method	PT	PT	PWT	PWT

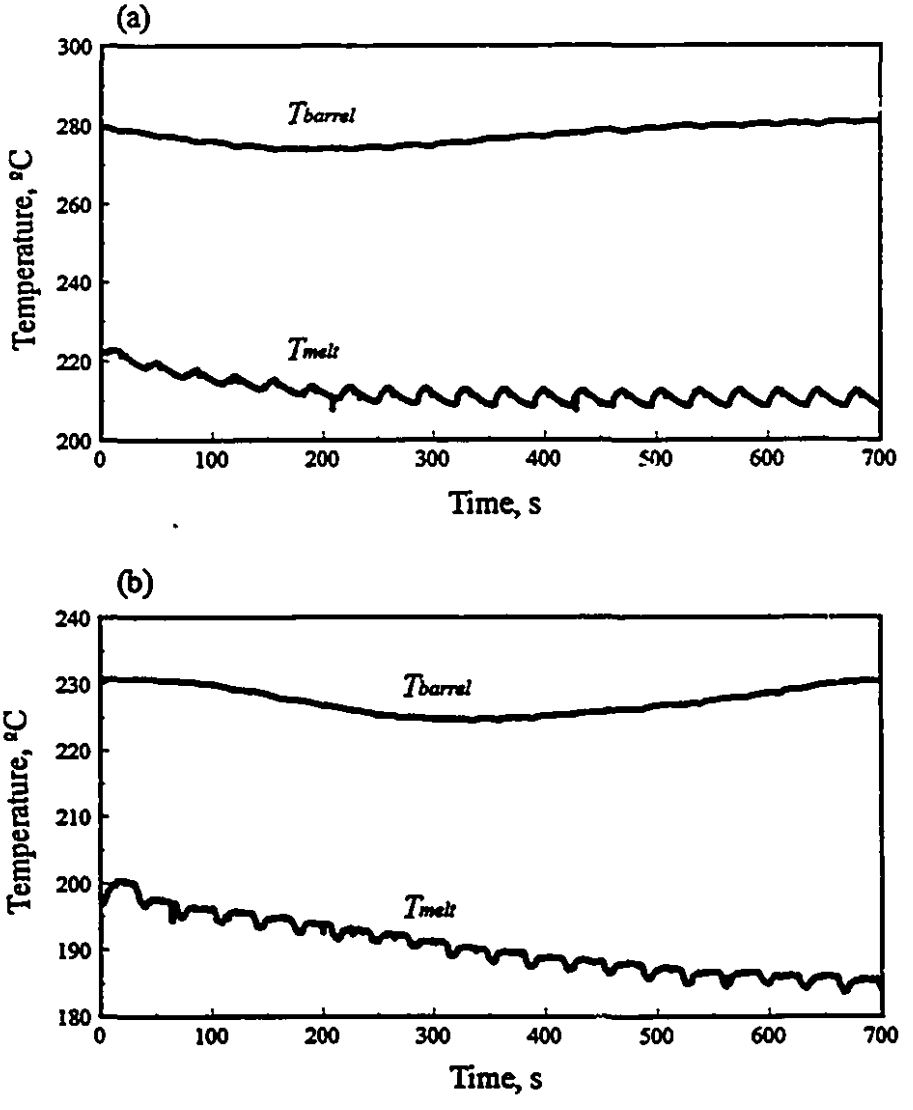

Figure 7.4 Front barrel and melt nozzle temperatues in: (a) Experiment W-3 and (b) Experiment W-4, using the conditions given in Table 7.1.

The effects of the barrel temperature profile and opening of the supply servo-valve on part weight are illustrated in Figure 7.5. For the same set-points in the barrel temperature profile (Experiments W-2 and W-3), the weight increases as the servo-valve opening is increased. This is because the hydraulic pressure in the injection cylinder increases. Figure 7.6 shows the effect of the front barrel temperature on weight, for moderate temperatures in the middle and rear section. The effect is quite appreciable, as a difference of 10 °C in the front barrel temperature causes an increase of about 0.2 g in weight. A significant variation in weight was always observed during the start up period, typically the first 25 cycles, after which the variations are as high as 0.05 g. A comparison between Figures 7.5 and 7.6 shows the effect of the barrel temperature distribution. With moderate temperatures in the middle and rear zones and for the same servo-valve opening, the parts weigh less than the parts obtained at higher temperatures (Experiments W-1, W-2, and W-3).

Standard deviations up to 0.04g, or 0.2% deviation from the mean values, can be seen in part weights in the open-loop operations. These fluctuations are associated with changes in cavity pressure and bulk temperatures.

7.4.2 Closed-Loop Control Experiments

The results of PT control strategy for Experiment WC-1 and WC-2 with the conditions given in Table 7.2, are shown in Figure 7.7. It is seen that the weight starts to settle after sample 10, indicating the positive effect of controlling the peak pressure and bulk temperature in maintaining low cycle-to-cycle fluctuations. Figures 7.8 and 7.9 illustrate the variation in weight and in peak pressure and bulk temperature, respectively, obtained using the

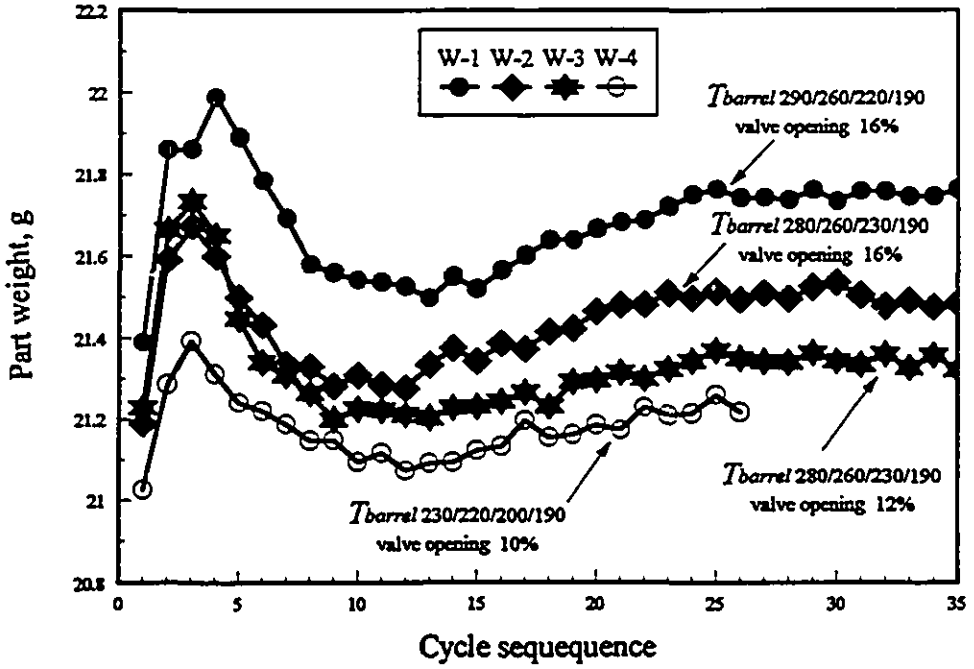

Figure 7.5 Effect of the barrel temperature profile and servo-valve opening on part weight in Experiments W-1, W-2, W-3, and W-4, using the conditions given in Table 7.1.

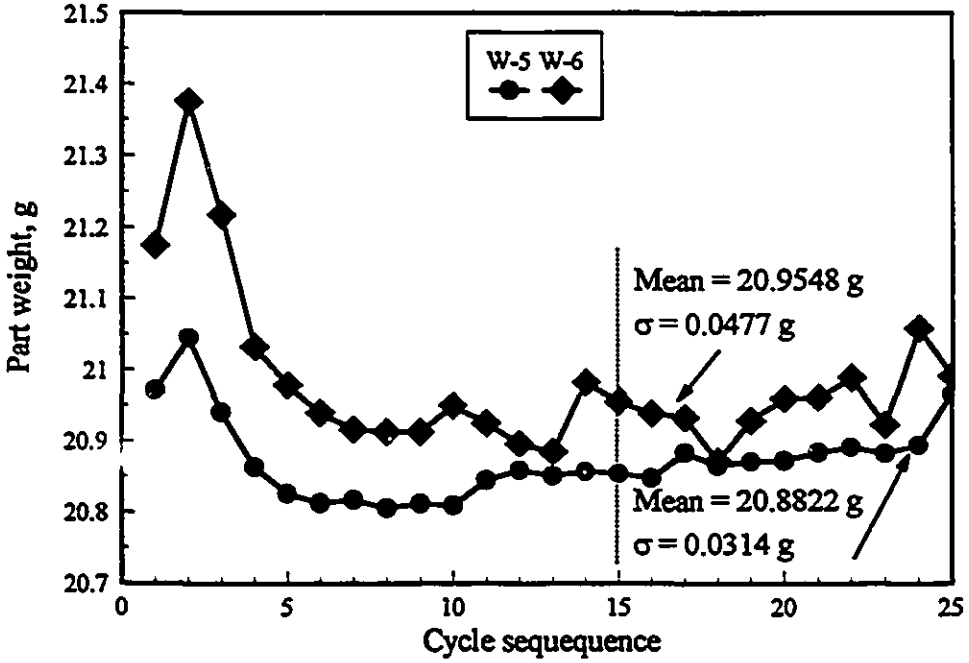

Figure 7.6 Effect of the front barrel temperature on part weight for 50% servo-valve opening in Experiments W-5 and W-6, using the conditions given in Table 7.1.

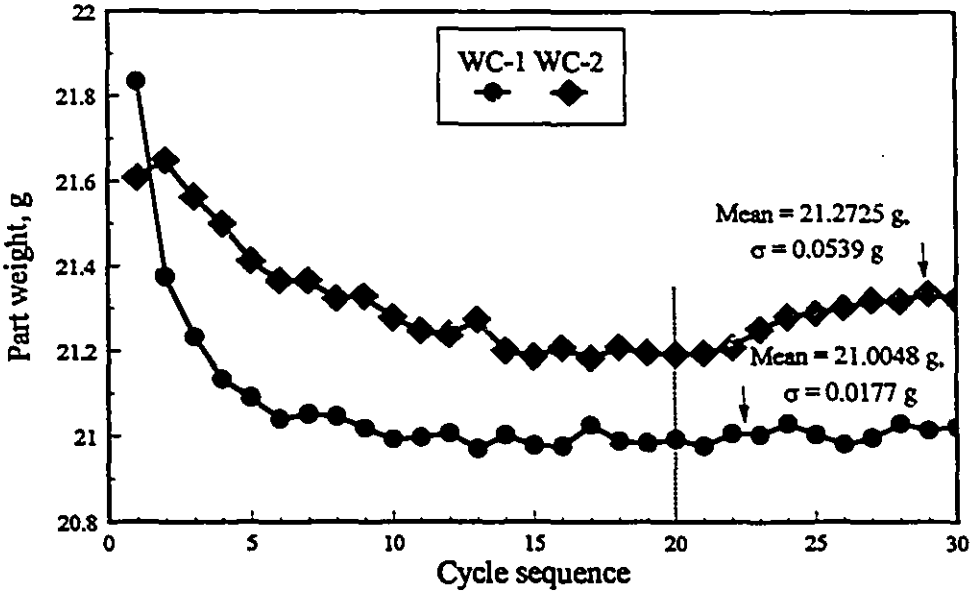

Figure 7.7 Part weight variations in Experiments WC-1 and WC-2, using the conditions given in Table 7.2.

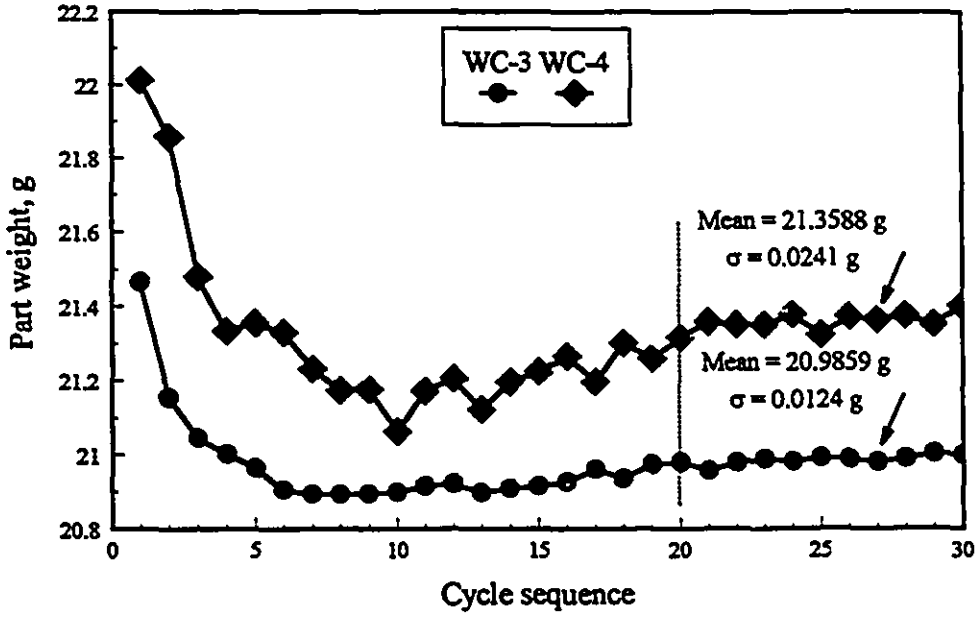

Figure 7.8 Part weight variations in Experiments WC-3 and WC-4, using the conditions given in Table 7.2.

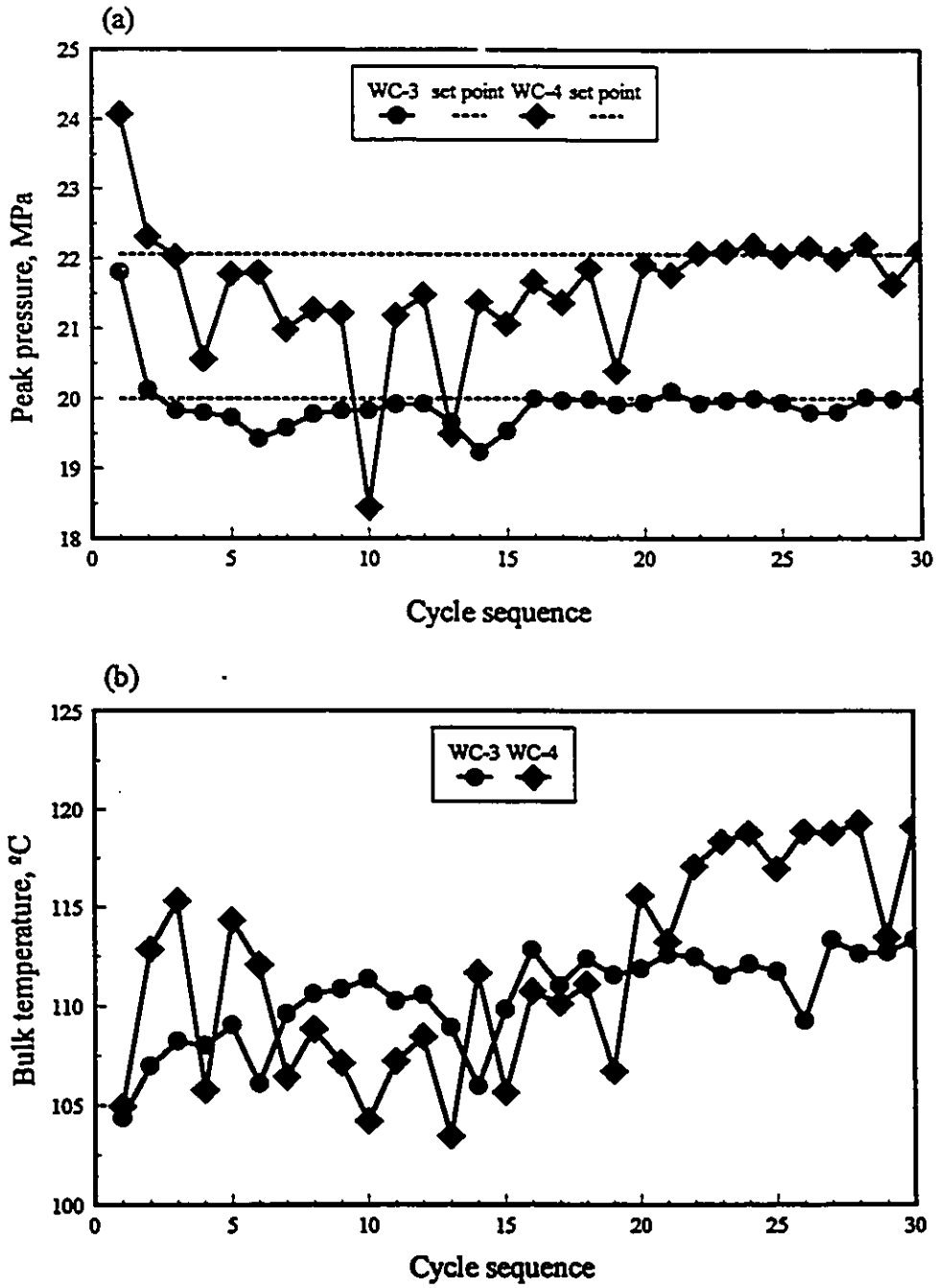

Figure 7.9 Variations in (a) cavity peak pressure and (b) bulk temperature in Experiments WC-3 and WC-4, using the conditions given in Table 7.2.

PWT control strategy in Experiments WC-3 and WC-4. The bulk temperature was not controlled, but it approaches the desired reference temperatures of 115°C and 120 °C, as shown in Figure 7.9a. The peak pressure also settles at the reference values, 20 MPa and 22 MPa, after sample 20 (see Figure 7.9b).

7.5 SUMMARY

Two procedures have been tested for the indirect control of part weight. In the first, called PT control, the peak cavity pressure is under self-tuning control with the observer (STCO-SP) discussed in Chapter 5, and the bulk temperature is controlled using the cascade strategy described in Chapter 6. The other scheme, PWT control, consists of controlling only the cavity pressure to compensate for bulk temperature fluctuations from cycle-to-cycle.

The PWT control gives the lowest cycle-to-cycle fluctuations in weight with variances as low as 0.0124g. In addition to the improvement in weight control, the control of cavity pressure and bulk temperature will yield better quality parts.

CHAPTER 8
CONCLUSIONS AND RECOMMENDATIONS

The control of part weight is important to ensure quality injection molded parts. The part weight is determined by the state (bulk temperature and pressure) of the polymer at the time the gate freezes. Measuring internal polymer temperature profiles in the injection mold cavity during molding is extremely difficult.

This thesis presents a method which combines measurements of cavity surface temperatures, cavity pressure, and on-line calculations for estimating temperature profiles inside the cavity. These profiles are then used to estimate the bulk polymer temperature. Fitting the cycle-to-cycle values of bulk polymer temperature and peak pressure to a Tait equation of state yields a model for predicting part weights. The weight is controlled through the use of a self-tuning algorithm for controlling the cavity pressure-time profile, together with the on-line estimation and control of the bulk temperature.

8.1 CONCLUSIONS

With respect to the bulk polymer temperature and part weight estimation, a number of conclusions can be made:

- A practical methodology has been presented to estimate internal average polymer temperatures from temperature measurements at the cavity surface.

- The proposed method is based on solving the heat transfer problem for amorphous polymers in the injection molding cavity at the end of the holding stage.
- The proposed approach may be used for on-line estimation of spatial temperature profiles in the cavity and part weight.
- The results of the models used to predict weight are in good agreement with experimental data.

Regarding the control of the cavity pressure, bulk polymer temperature, and part weight, the following conclusions can be made:

- A proportional factor of $q = 0.5$ (Equation 5.42) between the servo-valve openings gives maximum cavity pressure responsiveness for the control of the cavity pressure through manipulation of the supply servo-valve.
- A discrete first-order model with time-varying parameters was found appropriate for the dynamic of the cavity pressure to the supply servo-valve opening.
- The self-tuning algorithm has proven to be effective in controlling the cavity pressure to a constant increasing rate and to an exponential function during the filling and packing stages, respectively. The controller parameters are determined using the parameter identification algorithm with a forgetting factor ($\lambda = 0.75$), along with the pole location procedure.
- A linear relationship was found between the slope of the cavity pressure-time profile during filling and the peak pressure. This relationship was used in selecting the set-point trajectory during filling for the required peak pressure.

- It was found that initiating the control after a certain degree of filling or a specified screw position avoids the errors that occur at the beginning of filling, and thus a better control performance is obtained.

The following conclusions are derived from the study on the control of the bulk polymer temperature and part weight.

- The dynamics of the bulk polymer temperature related to the controlled coolant temperature can be approximated with a discrete first-order model.
- A cascade control scheme gave good control of the bulk polymer temperature. The internal loop controls the coolant temperature.
- The part weight was controlled using a PWT algorithm which consists of controlling the peak pressure at a required value, so that the part weight has zero deviation from a reference state $W_{ref}(T_{ref}, P_{ref})$. The required peak pressure is determined using the part weight model and on-line estimation of the bulk temperature at the instant the gate seals.

8.2 CONTRIBUTIONS

The use of a method developed for on-line estimation of internal polymer temperatures based on measurements at the cavity surface during molding, together with a derived part weight model, in strategies for controlling the part weight are the global contributions of this work.

The methodologies proposed in this work can be used to develop strategies for quality control. Their contributions can be specified as follows:

1. A new method for the on-line estimation of internal polymer temperatures during injection molding has been proposed. The procedure uses surface temperature measurements and an experimentally reported form of the spatial temperature profile, together with an experimentally determined heat transfer coefficient to determine the bulk polymer temperature.
2. Through the additional formulation of a model to estimate the mass of the polymer in the cavity (part weight) using cavity process variables, this work introduces a procedure different from the traditional methods which employ either factorial models or equations of state based on equilibrium data. Thus, the method is useful for practical applications.
3. The successful application of a self-tuning controller with a first-order observer in controlling the cavity pressure is another important contribution of this work. Procedures to deal with the difficulties associated with solidification in the delivery system and cavity walls which reduces the cavity pressure response during the holding stage are also addressed for the first time.
4. A cascade control loop was shown to be able to assure the cycle-to-cycle bulk temperature at the moment the gate freezes.
5. The proposed strategies for control of part weight based on on-line measurements at the cavity surface, specially PWT control, are new approaches to dealing with the problem. They represent an important step towards controlling the part weight in injection molding.

6.3 RECOMMENDATIONS

The following topics are recommended for future work:

- The method for estimating temperature profiles in the mold cavity and part weight can be extended to crystalline polymers using the heat of crystallization and numerical solutions to the heat conduction equations.
- The control of other product characteristics, such as shrinkage and residual stresses, can be carried out using the procedure proposed in this work for estimating internal temperature profiles in the mold cavity.
- The control of the cavity pressure of amorphous thermoplastics should be studied using the servo-valve opening as control variable in the filling stage, but using another control variable for the packing stage. The clamping force is a potential candidate as the new control variable during packing.
- To improve the control of the internal polymer temperature, the temperature of the melt injected into the cavity should be controlled as well. For this purpose, installing a band heater at the nozzle is required. A multi-variable controller with two inputs is suggested: the coolant temperature and the power supply to a nozzle band heater.

REFERENCES

Abu Fara, D. (1988). "Control of Nozzle and Cavity Pressure During Filling and Packing in Thermoplastic Injection Moulding." PhD Thesis (McGill University, Montreal).

Abu Fara, D., M.R. Kamal, and W.I. Patterson (1990). "Comprehensive Strategies for Sequential Closed-Loop Pressure Control Throughout the Injection Molding Cycle." *SPE ANTEC Technical Papers*, 239-242.

Agrawal, A.R., and I.O. Pandelidis (1988). "Observers for Optimal Anticipatory Control of Ram Velocity in Injection Molding." *Polym. Eng. and Sci.*, 28(3), 157-164.

Agrawal, A.R., I.O. Pandelidis, and M. Pecht (1987). "Injection-Moulding Process Control- A Review." *Polym. Eng. and Sci.*, 27(8), 1345-1357.

ALR POWERPRO/MC VM (1991). *System Configuration* (Advanced Logic Research Inc.).

Analog Devices STB-HL02 (1988). *High-Level Voltage Panel, User's Guide* (Analog Devices).

Analog Devices RTI-217 (1988). *User's Guide* (Analog Devices).

Analog Devices RTI-220/222 (1989). *User's Guide* (Analog Devices).

Armitano, O., J. Edelman, and U. Garcia (1985). *Programación No lineal* (Limusa, Mexico).

Åström, K.J., and B. Wittenmark (1995). *Adaptive Control* (Addison-Wesley, MA).

Åström, K.J. and B. Wittenmark (1990). *Computer Controlled Systems Theory and Practice* (Prentice-Hall, New Jersey).

Baron, L.E. (1994). "Equipment Temperature Influence on Infrared Temperature Measurements." *SPE ANTEC Technical Papers*, 454-461.

Baird, D.G., and D.I. Collias (1995). *Polymer Processing Principles and Design* (Butterworth-Heinemann, MA).

Berins, M.L. Ed. (1991). *Plastic Engineering Handbook of the Society of the Plastic Industry, Inc.; 5th. Ed.* (Van Nostrand Reinhold, New York).

Bird, R.B., W.E. Stewart, and E.N. Lightfoot (1960). *Transport Phenomena* (Wiley, New York).

Bourdon, R. (1991). "Planning and Optimizing Quality in Injection Moulding." *Kunststoffe German Plastics*, **81** (10), 960-965.

Carslaw, H.S., and J.C. Jaeger (1959).*Conduction of Heat in Solids* (Clarendon-Oxford, New York).

Chen, B.S., and W.H. Liu (1994). " Numerical Simulation of the Post-Filling Stage in Injection Molding with a Two-Phase Model." *Polym. Eng. Sci.*, **34**(10), 835-845.

Chiu, C-P., J-W. Wei, and M-C. Shih (1991). "Adaptive Model Following Control of the Mold-Filling Process in an Injection Molding Machine." *Polym. Eng. Sci.*, **31**(15), 1123-1129.

Chu, E. F-H. (1992). "A Comprehensive Integrated Computer Simulation of the Injection Molding Process for Thermoplastics." Ph.D. Thesis (McGill University, Montreal).

Chu, E., M.R. Kamal, and S. Goyal (1989). "A Computer Simulation of the Injection Molding Process Including Filling, Packing, and Solidification." *SPE ANTEC Technical Papers*, 344-347.

Costin, M.H., D.A. Okonski, and J.C. Ulicny (1987). "Control of An Injection Molding Machine: Adaptive Regulation during Filling." *American Contr. Conf.*, 711-716..

Cowie, J.M.G. (1991). *Polymers: Chemistry and Physics of Modern Materials, 2nd. Ed.* (Chapman & Hall, New York).

Davis, C.C. and J.C. Hudson (1991). "Injection Molding Process Variation Before and After an Interruption." *SPE ANTEC Technical Papers*, 474-476.

Dietz, W., J.L. White, and E.S. Clark (1978). "Orientation Development and Relaxation in Injection Molding of Amorphous Polymers." *Polym.Eng. Sci.*, 18(4), 273-281.

Dupret, F., and L. Vanderschuren (1988). "Calculation of Temperature Field in Injection Moulding." *AIChE J.*, 34, 1959-1972.

Dynisco (1986). *Plastic Melt Pressure Transducer* (Dynisco, MA).

Farag, I.H. and R.L. Curran (1984). "Application of Radiation Pyrometry to Glass- Temperature Measurements." *AIChE Symposium Series on Heat Transfer*, Niagara Falls, 291-296.

Fisher Electro-Pneumatic (1977). *Instruction Manual Transducers Type 546 and 5466.*Fisher Controls Inc.

Fusser, H.B. (1992). "A Man Machine Interface for PC-Controlled Injection Moulding." M. Eng. Thesis (McGill University, Montreal).

Galskoy, A., and K.K. Wang (1978). "Measuring Melt Temperatures: Thermocouples or Pyrometers?" *Plast. Eng.*, 34(11), 42-45.

Gao, F. (1989). "Dynamics and Control of Surface and Mould Temperatures in Injection Molding." M. Eng. Thesis (McGill University, Montreal).

Gao, F. (1993). "The Control of Cavity Pressure Throughout the Injection Molding Cycle." Ph.D. Thesis (McGill University, Montreal).

Gao, F., H. Fusser, M.R. Kamal, and W.I. Patterson (1992). "A Versatile System for the Control of Injection Moulding." *SPE ANTEC Technical Papers*, 38, 1887-1890.

Gao, F., W.I. Patterson, and M.R. Kamal (1993). "Dynamic and Control of Surface and Mold Temperatures in Injection Molding." *Int. Polym. Proc.*, (8)147.

Goldstein, R.J. (1976). "Optical Techniques for Temperature Measurement.."*Measurements in Heat Transfer* (Hemisphere, Washington).

Haber, A. (1982). "Microprocessor Control System for the Injection Molding Process." M.Eng. Thesis (McGill University, Montreal).

Haber, A., and M.R. Kamal (1987). "The Dynamics of Peak Cavity Pressure in Injection Molding." *Polym.Eng. Sci.*, 27(18), 1411-1418.

Harry, D.H. (1991). "Injection Molding Machine Control Algorithms." *SPE ANTEC Technical Papers*, 383-385.

Heiman, W., and U. Mester (1975). "Non-contact Determination of Temperatures by Measuring the Infrared Radiation Emitted from the Surface of a Target." *Temperature Measurement Inst. Phys. Conf. Ser.* 26, 219-237.

Hieber, C.A., and S.F. Shen (1980). "A Finite Element/Finite Difference Simulation of the Injection Molding Filling Process." *J. Non-Newtonian Fluid Mech.*, 7, 1-32.

Kamal, M.R., and S. Kening (1972). "The Injection Molding of Thermoplastics. Part I: Theoretical Model." *Polym.Eng. Sci.*, 12, 294-301.

Kamal, M.R., Y. Kuo, and P.H. Doan (1975). "The Injection Molding Behavior of Thermoplastics in Thin Rectangular Cavities." *Polym.Eng. Sci.*, 15(12), 863-868.

Kamal, M.R., and P.G. Lafleur (1982). "Computer Simulation of Injection Molding." *Polym.Eng. Sci.*, 22, 1066-1074.

Kamal, M.R., A.T. Mutel, G. Salloum, and A. García-Rejón (1991). "Heat Transfer Measurement at the Mold Surface During Injection Molding of Thermoplastic Melts." *SPE ANTEC Technical Papers*, 483-487.

Kamal, M.R., W. I. Patterson, N . Conley, D. Abu Fara, and G. Lohfink (1987). "Dynamic and Control of Pressure in the Injection Molding of Thermoplastics." *Polym. Eng. Sci.*, **27(18)**, 1403-1410.

Janeschitz-Kriegel, H. (1977). "Injection Moulding of Plastics: Some Ideas about the Relationship between Mould Filling and Birefringence." *Rheologica Acta*, **16**(4), 327-339.

Jović, F. (1992). *Process Control Systems*, (Chapman & Hall, London).

Langecker, G.R. (1992). "Process Control in Injection Moulding." *Kunststoffe-German Plastics*, **82**(7) 3-6.

Leigh, J.R. (1988). *Temperature Measurement & Control* (Peter Peregrinus Ltd., London).

Ljung, L. (1987). *System Identification, Theory for the User* (Prentice-Hall, New Jersey).

Ljung, L. (1991). *System Identification Toolbox, User's Guide* (The Math Works, Inc., Massachusetts).

Lord, H.A., and G. Williams (1975). "Mold-Filling Studies for the Injection Molding of Thermoplastic Materials. Part II: The Transient Flow of Plastic Materials in the Cavities of Injection-Molding Dies." *Polym. Eng. Sci.*, **15**(8), 569-582.

McGee, T.D. (1988). *Principles and Methods of Temperature Measurement* (Wiley, New York).

Ogata, K. (1995). *Discrete-Time Control Systems* (Prentice-Hall, NJ).

Ogunnaike, B.A., and W.H. Ray (1994). *Process Dynamics, Modeling, and Control* (Oxford, New York).

Pandelidis, I.O., and A.R. Agrawal (1988). "Optimal Anticipatory Control of Ram Velocity in Injection Molding." *Polym. Eng. And Sci.*, **28**(3), 147-156.

Patterson, W.I., M.R. Kamal, and F. Gao (1990). " Mold Temperature Measurement and Control" *SPE Tech. Papers*, 227.

Patterson, W.I., M.R. Kamal, and V.G. Gomes (1985). "Dynamic Modeling and Control of Melt Temperature in Injection Molding." *SPE Tech. Papers*, 31, 754-758.

Powell, M.J.D. (1964). "An Efficient Method for Finding the Minimum of a Function of Several Variables Without Calculating Derivatives." *Comp. J.* 7, 155.

QNX 4.1 Operating System (1992). *System Architecture* (Quantum Software Systems Ltd., Ontario).

Quach., A., and R. Simha (1971). "Pressure-Volume-Temperature Properties and Transitions of Amorphous Polymers: Polystyrene and Poly (orthomethylstyrene)." *J. Appl. Phys.*, 42(12), 4592-4606.

Rafizadeh, M., W.I. Patterson, and M.R. Kamal (1995). "Physically-Based Model of Thermoplastics Injection Molding Dynamics." *SPE ANTEC Technical Papers*, 733-740.

Rietveld, J.X., and G-Y. Lai (1991). "In Situ Measurement of Process Stream Temperatures for a Polymer within a Mold Cavity during the Injection Molding Cycle." *ASME Heat and Mass Transfer in Solidification Processing*, 175(25), 183-197.

Richardson, S.M. (1989), Ch.L. Tucker Ed. *Fundamentals of Computer Modeling for Polymer Processing*, (Hanser, New York).

Richard, C., G. Helps, and B.T. Griffen (1994). "Predicting Mold-Cavity Temperatures With an Artificial Neural Network." *Plastics Engineering*, October, 25-27.

Rosato, D.V., and D.V. Rosato (1990). *Plastic Processing Data Handbook* (Van Nostrand Reinhold, New York).

Rosato, D.V., and D.V. Rosato (1982). *Injection Molding Handbook* (Van Nostrand Reinhold, New York).

Rosenbrock, H.H. (1960). "An Automatic Method for Finding the Greatest or the Least Value of a Function." *Comp. J.* 3, 175.

Rudd, J.F. (1989). "Physical Constants of Poly(styrene)." *Polymer Handbook* v/81. J. Bandrup and E H. Immergat, Eds. (Wiley, New York).

Ruscitti, G. (1992). "The Measurement and Control of Nozzle Melt Temperature in Injection Molding." M. Eng. Thesis (McGill University, Montreal).

Ruscitti, G., W.I. Patterson, and M.R. Kamal (1994), *SPE ANTEC Technical Papers*, 448.

Sanschagrin, B. (1983). "Process Control of Injection Molding." *Polym. Eng. Sci.*, 23(8), 431-438.

Schenker, J.R. (1993). "Using Abductive Induction to Create a Math Model of an Injection Molding Process." *SPE ANTEC Technical Papers*, 2137-2141.

Seborg, D.E., T.F. Edgar, and D.A. Mellichamp (1989). *Process Dynamics and Control* (Wiley, New York).

Seinfeld, J.H., and L. Lapidus (1974). *Mathematical Methods in Chemical Engineering, v.3* (Prentice-Hall., New Jersey).

Shankar, A., and F.W. Paul (1982). "A Mathematical Model for the Evaluation of the Injection Molding Machine Control." *Trans. ASME, J. Dynamic Systems, Measurements, and Control*, 104, 85-92.

Shen, X., R. Malloy and J. Pacini (1992). "An Experimental Evaluation of Melt Temperature Sensors for Thermoplastic Extrusion." *SPE ANTEC Technical Papers*, 918-926.

Smud, S.M., D.O. Harper, and P.B. Deshpande (1991). "Advanced Process Control for Injection Molding." *Polym. Eng. Sci.*, 31(15), 1081-1085.

Spencer, R.S., and G. D. Gilmore, J. Appl. Phys., 20, 502 (1949).

Srinivasan, K., T. Srinivasan, and G.P. Maul (1992). "Part Weight Control in Thermoplastic Injection Molding." , *SPE ANTEC Technical Papers*, 2204-2208.

Tadmor, Z., and C.G. Gogos (1979). *Principles of Polymer Processing* (Wiley, New York).

TemposonicsTH (1989). Linear Displacement Transducer System with Analog Output. *Installation and Instruction Manual* (MTS System Corporation, MN).

Thienel P., and G. Menges (1978). "Mathematical and Experimental Determination of Temperatures, Velocity, and Pressure Fields in Flat Molds during the Filling Process in Injection Molding of Thermoplastics." *Polym. Eng. Sci.*, 18(4), 314-320.

Turng, L.S., H.H. Chiang, and J.F. Stevenson (1995). "Optimizing Molding at Low Injection Pressures." *Plastics Eng.*, October, 33-36.

Vanzetti Infrared Thermal Monitor, Model LTD. Instruction Manual #5070 (Vanzetti Systems, Stoughton, MA).

Varela, A.E., M.R. Kamal, and W.I. Patterson (1996). "A Method for Estimating Bulk Melt Temperature and Part Weight in Injection Molding of Amorphous Thermoplastics." *Adv. Polym. Tech.* 15(1), 17-28.

Varela, A.E., W.I. Patterson, and M.R. Kamal (1995). "Estimation of Melt Temperatures and Part Weight in Injection Molding from Cavity Surface Temperature Measurements." *SPE ANTEC Technical Papers*, v.1, 334-338.

Viskanta, R. (1975). "Infrared Radiation Techniques for Glass Surface and Temperature Distribution Measurements." *IEEE Trans. on Industry Applications*, 1A-11(5), 494-505.

Viskanta, R., and E.E. Anderson (175). J.P. Hartnett and T.F. Irvine Jr., Eds. "Heat Transfer in Semitransparent Solids." *Advances in Heat Transfer, vol. 11* (Academic Press, New York).

Walsh, G. (1975). *Methods of Optimization* (Wiley, New York).

Wellstead, P.E., and M.B. Zarrop (1991). *Self-Tuning Systems: Control and Signal Processing* (Wiley, New York).

Whelan, A. (1984). *Injection Moulding Machines* (Elsevier, London).

Williams, G., and H.A. Lord (1975). "Mold-Filling Studies for the Injection Molding of Thermoplastic Materials. Part I: The Flow of Plastic Materials in Hot- and Cold-Walled Circular Channels." *Polym. Eng. Sci.*, 15(8), 553-568.

Yakemoto, K., T. Sakai, Z. Maekawa, and H. Hamada (1993). "Adaptive Holding Pressure Control Based on the Prediction of Polymer Temperature in a Mold Cavity." *SPE ANTEC Technical Papers* , 2192-2196.

Yokoi, H., Y. Murata, and H. Tsukakoshi 1992). "Measurement of Melt Temperature Profiles during Filling and Packing Process Using a New Integrated Thermocouple Sensor." *SPE ANTEC Technical Papers*, 1875-1881.

Yu, Ch.J., J.E. Sunderland, and C. Poli (1990). "Thermal Contact Resistance in Injection Molding." *Polym. Eng. Sci.*, 30(24), 1599-1606.

Zoller, P. (1989). "PVT Relationships and Equations of State of Polymers." *Polymer Handbook* vi/475, J. Bandrup and E H. Immergat, Eds. (Wiley, New York).

APPENDIX A

ESTIMATION OF CAVITY MELT TEMPERATURE PROFILES FROM INFRARED RADIATION

A simple algorithm is presented for the determination of temperature profiles using the radiance detected by a pyrometer operating in a narrow wavelength band, $\lambda_{min} < \lambda < \lambda_{max}$. The radiance sensed by the pyrometer $(I)_p$ depends on the temperature profile and physical parameters (reflectivity ρ, absorption coefficient κ):

$$Ip = f(T(x,t),\rho,\kappa) \tag{A.1}$$

The following assumptions are considered:

(1) Heat transfer by conduction, convection, and radiation are important only in the x direction, normal to the cavity surfaces, so that the process can be analyzed using a one-dimensional model.

(2) The melt exhibits local thermodynamic equilibrium, therefore, Planck's and Kirchhoff's laws are valid.

(3) The plastic is isotropic, homogeneous, and able to absorb and emit, but not scatter, thermal radiation.

(4) The thickness is much greater than the radiative wave lengths, making coherence effects negligible.

Consider a cavity of thickness $L=2H$, divided into N slices, each of thickness $\Delta x=L/N$. The equation of radiative transfer can be solved with the above assumptions to obtain the following expression for the directional spectral intensity I_x of that slice located a distance x from the front surface (Farag and

Curran, 1984),

$$I_x = \kappa n^2 I_{b\lambda}(T_x) e^{-\kappa x} \Delta x \tag{A.2}$$

where n is the refractive index, κ the spectral absorption coefficient (1/cm), and $I_{b\lambda}$ is the black body directional spectral intensity given by Planck's law:

$$I_b(\lambda) = \frac{C_1 \lambda^{-1}}{e^{C_2/(\lambda T_x)} - 1} \tag{A.3}$$

The normal intensity G_o of direct radiation from all slices reaching the front surface (x=0) is:

$$G_o = \sum_{i=1}^{N} n^2 (\kappa \Delta x_i) I_{b\lambda}(T_{x_i}) e^{-\kappa x_i} \tag{A.4}$$

Similarly, the normal intensity G_L of direct radiation reaching the back surface (x=L) from slices is:

$$G_L = \sum_{i=1}^{N} n^2 (\kappa \Delta x_i) I_{b\lambda_i} e^{-\kappa (L - x_i)} \tag{A.5}$$

Radiations G_o and G_L undergo multiple internal reflections within the cavity, and the total intensity G_{tot} of normal radiation reaching the front surface is:

$$G_{TOT} = \frac{G_o + G_L \rho \tau}{1 - \rho^2 \tau^2} \tag{A.6}$$

where

$$\tau = \exp(-\kappa L), \qquad \rho = \left[\frac{n-1}{n+1}\right]^2 \tag{A.7}$$

To find a temperature profile, assume $G_{tot} = I_p(T(x,t))$, the intensity sensed at

the cavity surface, and apply an inversion procedure. This procedure has non-uniqueness and stability problems. The temperature profile could be calculated by solving the nonlinear optimization problem,

$$\min J = \sum_{k=1}^{K} [I_p(\lambda_k)_{calc} - (I_p)_{meas}]^2 \qquad \lambda_{max} \geq \lambda_k \geq \lambda_{min} \tag{A.8}$$

The function J varies with the unknown temperature distribution, and it is nearly zero when the correct temperature profile is used.

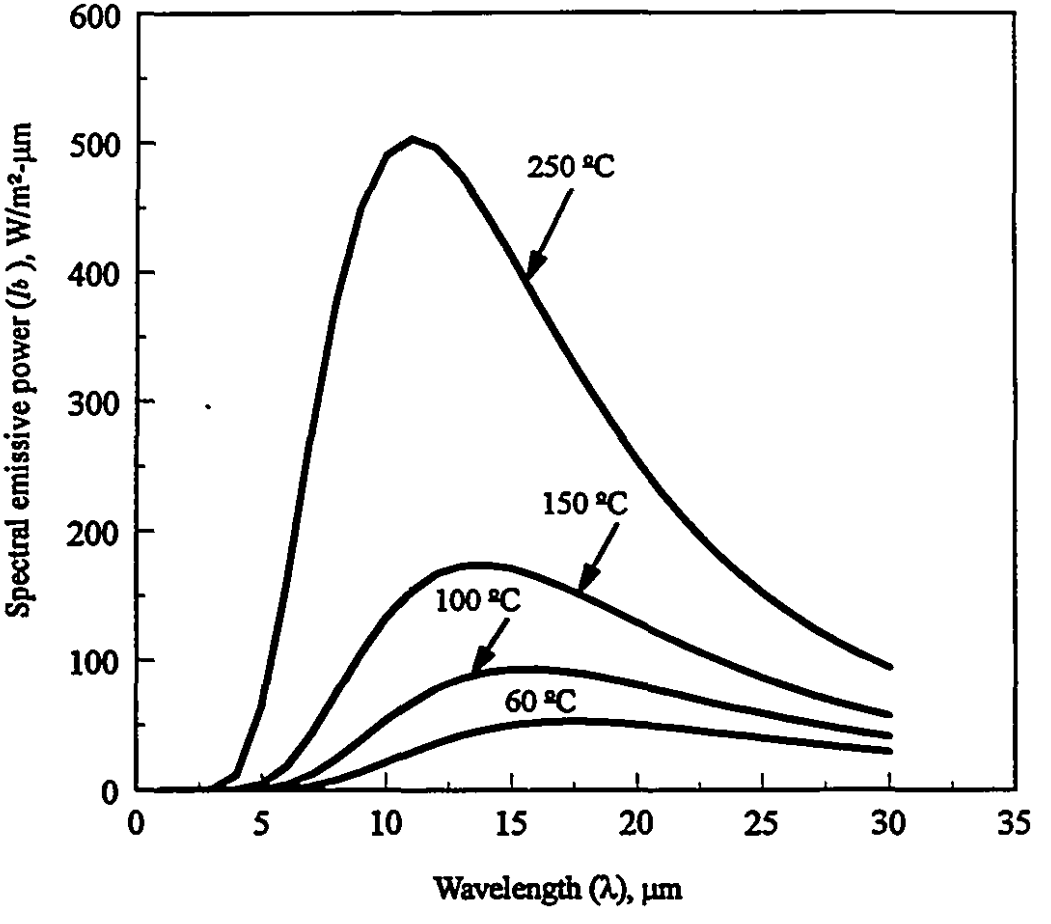

Figure A.1 Black body radiation spectral distribution.

APPENDIX B

CALIBRATION OF THE GATE AND NOZZLE PRESSURE TRANSDUCERS

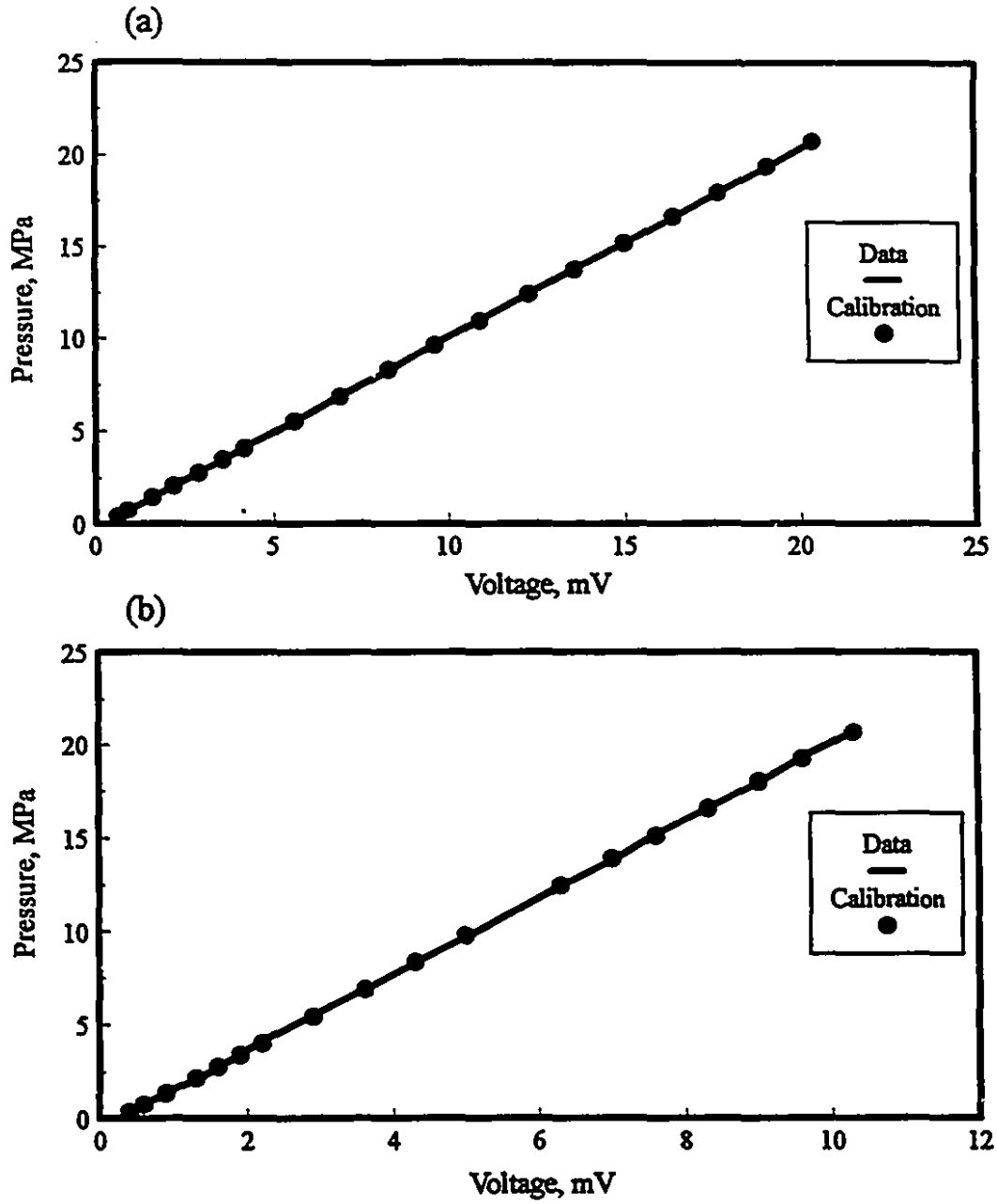

Figure B.1 Calibration of pressure transducers: (a) at the gate (PTG) and (b) at the nozzle. See calibration equations in Table 3.4.

APPENDIX C

CAVITY CENTER TEMPERATURE AND HEAT TRANSFER COEFFICIENT

An open loop experiment was conducted to determine the sensitivity of the estimated cavity center temperature and the heat transfer coefficient to step changes between 10% and 20% in the servo-valve opening. Other experimental conditions were as follows: coolant temperature; T_c=30°C, barrel temperature set-points = 230/220/200/190 °C; cycle times: injection = 13s, decompression = 2s, and cooling = 10 s.

The temperature at the cavity center for each sensor location is estimated by

$$\text{Temperature at the cavity center} = T_c + a \tag{C.1}$$

where T_c is the coolant temperature, and a is the parameter of the heat conduction model used for the temperature profile at the cavity surface (Equation 4.9), which is determined with the algorithm described in Chapter 4, section 4.3.1. The heat transfer coefficient is calculated using the definition of the Biot number:

$$B = \frac{h y_s}{k} \tag{C.2}$$

Figure C.1 shows that the temperature at the cavity center increases with the servo-valve opening for the three sensor locations. As the velocity in the cavity is very low compared to the velocity in the delivery system, conduction is the predominant heat transfer mechanism. Therefore, the cavity

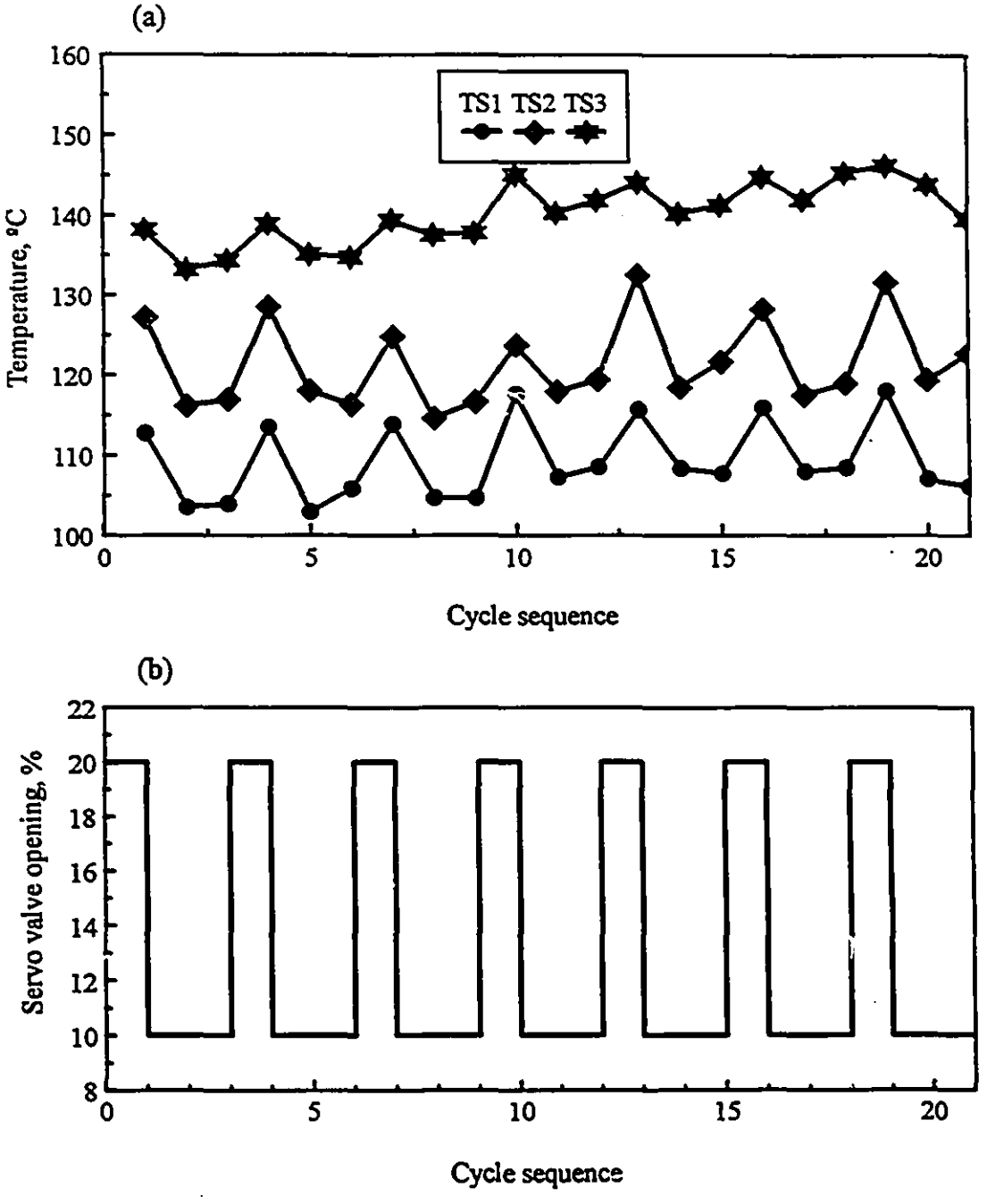

Figure C.1 Variations in (a) estimated cavity center temperature at three sensor locations, and (b) servo-valve opening. Experimental conditions: barrel temperature set-points 230/220/200/190 °C, coolant temperature 30 °C, cycle times: injection 13 s, decompression 2 s, and cooling 10 s.

center temperature is lower in upper part of the cavity which has been cooled for a longer time than the rest of the cavity. This can be seen in Figure C.1a, where the temperature decreases from the nearest cavity gate sensor (TS1) to the end of the cavity (TS3). All temperatures near the gate, which has a longer filling time, are close the glass transition temperature of polystyrene 100 °C.

Values of the cavity center temperature at location TS2 are more representative of the temperature of the whole cavity than those obtained at locations TS1 and TS3. The cavity center temperatures at the location TS2 are approximately the average values of the cavity center temperatures estimated at TS1 and TS3, as shown in Figure C.1. The melt temperatures at the center 6 seconds after the injection starts are in the range of 106 °C to 145 °C. The injection temperature for the used barrel temperature profile is about 190 °C (see Figure 7.4b). The temperature drop from the nozzle to the cavity core was between 84°C and 45 °C. For a similar but not identical experiment, Yokoi et al. (1992) reported measurements of the melt temperature of 150 °C at the cavity center for an injection temperature of 210 °C. These give a temperature difference of 60 °C, which is close to 65 °C the average temperature difference obtained with the methodology used in this work. This suggests that the method gives a reasonable estimation of the temperature at the cavity center.

The heat transfer coefficients were calculated for the thermal conductivity of k=0.166 W/mK for polystyrene (Kamal et al., 1991). Figure C.2 shows that the Biot numbers and the heat transfer coefficients increase with the servo-valve opening. This a reasonable response because the heat transfer coefficients must increase with the injection velocity. This Figure also indicates that the heat transfer coefficient decreases from the cavity gate

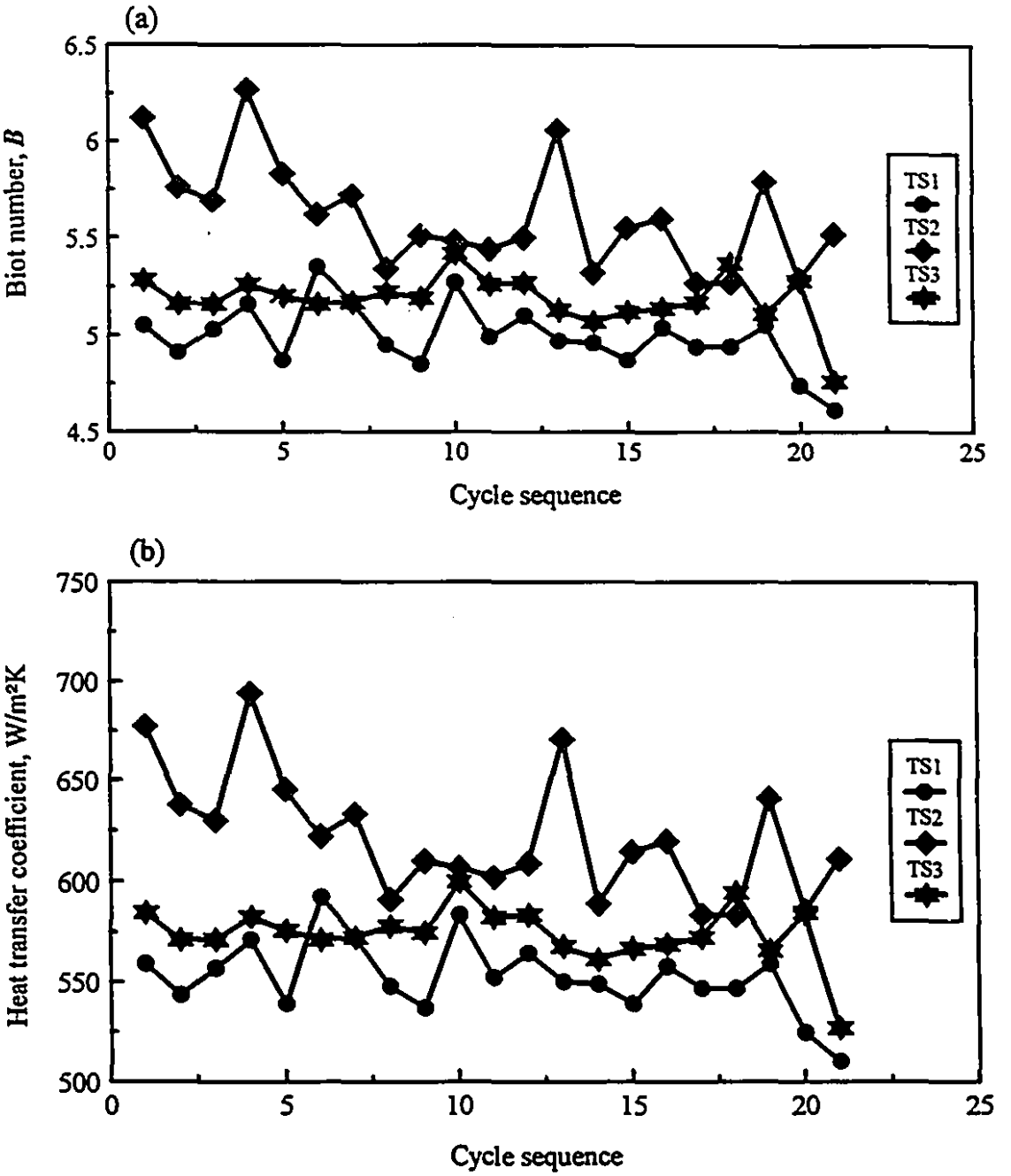

Figure C.2 Variations in (a) Biot number and (b) heat transfer coefficient at three sensor locations with the conditions shown in Figure C.1b.

which is at lower temperatures to the end of the cavity.

Yu et al. (1990) determined the thermal contact resistance (TCR) which is the inverse of the heat transfer coefficient, h = 1/TCR. For injection molding of polystyrene using a 3mm thick cavity, the authors found thermal contact resistance with average values between 1 and 1.16 m^2 °K/W which correspond to 1000 and 862 W/m^2 °K, respectively. These values were obtained using a combination of the numerical of the heat conduction equations and temperature measurements at the cavity surface and of the mold near the surface. Kamal et al. (1991) measured the heat flux at the cavity surface, the melt surface temperature, and the metal wall temperature which allowed the direct calculation of the heat transfer coefficient. These were reported in the range 863 W/m^2 °K (152 Btu/ft^2hr°F) and 1323 W/m^2 °K (233 Btu/ft^2hr°F).

In this experiment, the Biot numbers varied in a range from 4.75 to 6.75, corresponding to 525.7 W/m^2K to 747 W/m^2K, respectively. The values reported by Yu et al. (1990) and Kamal et al. (1991) are higher because they used the difference between the cavity surface temperature and the wall temperature to calculate the heat transfer coefficient, while in this work (see Equation 4.4) the difference between the cavity surface temperature and the coolant temperature was used. Therefore, the thermal resistance is higher, and the heat transfer coefficients are lower.

From the above observation, it can be concluded that for the experiment conducted, the methodology employed to predict the bulk temperatures gives reasonable values of heat transfer coefficients and melt temperatures at the cavity center.